BOUW.GROND.

June, 2026

Towards reproducible compressed earth blocks from Rotterdam excavation soil through material led mix design and the identification of key production parameters influencing mechanical performance.

Delft Technical University

M.Sc Architecture, Urbanism and Building Sciences,
Building Technology Graduation

Moritz Roßdeutscher

Building Technology Graduation Project
M.Sc Architecture, Urbanism and Building Sciences
Technical University of Delft

Figure 01: AI-assisted visualisation of excavated soil in the orange hall of the TU Delft Faculty of Architecture.

This thesis investigates how locally excavated soil from Rotterdam could be translated into reproducible unstabilised compressed earth blocks rather than remaining within low-value fill or disposal pathways.

Instead of treating production as a universal recipe, it examines how the behaviour and characterisation of a local soil inform its processing, mix composition and assessment. To address this, the study combines a literature review with laboratory testing.

The experimental work included geotechnical identification, particle-size analysis, mineralogical and environmental assessment, followed by specimen production, compaction trials, and compressive-strength testing.

On this basis, controlled mixtures were developed to investigate workability, optimise composition and evaluate the influence of key parameters such as compaction moisture, particle-size distribution and press loads.

The study establishes the general suitability of the excavated soil, while identifying main limitations, processing constraints, and the governing parameters for mechanical performance.

Table of contents

List of figures

List of abbreviations

AI	Artificial intelligence
AP04	Dutch soil quality assessment protocol / chemical soil quality analysis
CEB	Compressed earth block
DIN	Deutsches Institut für Normung / German Institute for Standardisation
EN	European Standard
IC	Ion chromatography
ISO	International Organization for Standardization
PSD	Particle-size distribution
SEM	Scanning electron microscopy
TI	Topological interlocking
XRD	X-ray diffraction

1. Introduction

1.1 Background

1.1.1 Transitions in the building sector

At the outset of this work, a simple question was asked: How could we reimagine the brick? Yet why rethink the brick, since it is one of the most widely used and successful building components globally? This question reflects the fundamental transformation underway in the construction sector and our current building practices. Resource and environmental impacts are widely recognized and will remain defining challenges for students like me, soon entering the profession. These challenges are not abstract at all but rooted in measurable material, energy, and emission intensity.

The building sector is among the most resource-intensive and environmentally impactful industries globally, accounting for an estimated 40-60% of total raw material extraction (Schützenhofer et al., 2022). According to the European Commission, the sector was also accountable for roughly 40% of the European Union's total primary energy consumption and contributed about 37% of the EU's greenhouse gas emissions. (Finamore & Oltean-Dumbrava, 2024). Given the substantial resource depletion involved, one would expect the construction industry to prioritize maximizing the value and longevity of these materials. Yet, within the European Union, c&d waste accounts for almost 40% of the total waste generation. The same report underscores that waste generation also impacts wider levels including social, economic, and environmental factors (García et al., 2024). This imbalance between resource consumption and waste volume highlights the sector's responsibility to pursue reduction, material recovery and the development of innovative, economically feasible implementation strategies. Within this framework, conventional linear models based on "take, make, dispose" are just no longer viable (AlJaber et al., 2024). In response to this way of thinking, the European Union has developed a series of regulatory frameworks urging industries to identify and close open material loops. Central to this agenda is the EU Circular Economy Action Plan (CEAP), introduced under the Green Deal. The report also analyses and suggests that adopting circular economy practices across the European Union could yield substantial economic gains, with projections indicating a 0.5% increase in GDP and the creation of roughly 700,000 new jobs by 2030. These figures show that the circular approach is not a marginal or purely ecological concept, but a central pillar of Europe's economic development strategy. For industries, the shift toward closed cycles also carries direct financial benefits as material expenses account for nearly 40% of production costs (European Commission, 2020). Within this broader policy context, the European Commission will develop a comprehensive strategy for a sustainable built environment. This initiative aims to align various policy areas, including climate action, energy and resource efficiency, construction and demolition waste management, and digital innovation, under a unified framework. Among its objectives, the strategy draft gives particular attention to soil management. It is promoting to limit sealing, recover abandoned or contaminated sites, and ensure the circular and environmentally responsible use of excavated soils in construction (European Commission, 2020).

1.1.2 Soil as a resource

Large-scale building and infrastructure projects, including roads, railways, dwellings, and power infrastructure, generate vast amounts of excavated soil, both uncontaminated and polluted. In most cases, this material is still disposed of in landfills rather than recovered or reused. This can be attributed to a combination of regulatory, logistical, and economic barriers. In several European contexts, excavated soil may be classified as waste once removed from its original location, which complicates its transition into reuse pathways. Even where reuse is technically possible, missing testing standards, lengthy approval procedures, limited storage capacity, insufficient financial incentives and variable material quality often prevent its practical implementation (Hale et al., 2021). This practice contradicts the objectives of the Soil Strategy for 2030, which emphasizes that most soils are clean and should be retained within material cycles (European Commission, 2021). The gap between policy ambition and on-site practices reveals a structural challenge in managing these

material streams. Excavated soils and rocks (ESR) represent roughly 20% of all waste generated in the EU. Their significance is even greater in the construction sector, where about 52% of total waste comes from excavation activities (Cristóbal et al., 2024). In absolute terms, this amounts to more than 530 million tonnes of excavated soil generated in the EU in 2018 alone. (European Commission, 2021). To illustrate the scale of this figure, consider that the mass of the Great Pyramid of Giza is about 6.55 million tonnes (Tasellari & Kaiku, 2012). Based on this, the annually excavation in the EU would be enough to construct roughly 81 pyramids of similar size. Therefore, the equivalent mass of one great pyramid is generated every 4.5 days. According to Eurostat data, about 40% of excavated soils are used for backfilling, 35% are recycled, and 25% are disposed of in landfills (Minixhofer et al., 2022). This means that each year, material equal to the mass of about 20 great pyramids is permanently landfilled. At the same time, it must be mentioned, that interpreting these figures remains complicated by the lack of a clear, harmonized definition of ESR in the scientific literature and regulatory frameworks. This further complicates the accurate characterization of their composition and material properties for reuse and management (Minixhofer et al., 2022).

Despite these challenges, reusing excavated soils could offer substantial environmental and systemic benefits. Reintegrating the material into construction can reduce transportation distances and disposal needs, while also lowering demand for new natural resources (Hale et al., 2021). Recent studies show that increasing reuse and recycling rates of ESR could reduce annual greenhouse gas emissions by up to 3.6 million tonnes of CO2-equivalent and save about 12.3 billion euros. (Cristóbal et al., 2024). A Dutch example illustrates how such benefits can materialize at project scale. During the construction of Rotterdam Centraal Station, the entire excavated soil flow was coordinated by a dedicated manager. Instead of disposing of more than one million tonnes of uncontaminated excavated soil in landfill, the material was redirected to nearby urban and private construction projects, resulting in savings of more than 4 million euros and an estimated reduction of 2.4 million kg CO2-equivalent through avoided transport (André Weijenberg, 2012). Within this broader European context, the Netherlands represents a comparatively advanced case of regulated soil reuse. For the year 2021, the Ministerie van Infrastructuur en Waterstaat (2023) reports approximately 59.1 Mton of soil as processed and applied, of which 56.3 Mton was reported as direct application. Only more strongly contaminated excavated soil required industrial treatment. After assessment, directly reusable soil is either transported to a suitable construction site or temporarily stored in a soil bank until an appropriate application becomes available. However, the dominant applications remain largely limited to direct use as soil or waterbed material and large scale earthwork applications, such as noise barriers, road foundations, or backfilling (Ministerie van Infrastructuur en Waterstaat, 2023). While this demonstrates an effective diversion from disposal, it also suggests that excavated soil is still predominantly treated as a bulk material rather than being diversified into higher value applications.

The ministry similarly argues that excavated soil should not only be considered as surplus material, but should increasingly be understood through its individual material fractions, such as sand, soil, and clay. Such a distinction would allow the reuse potential of different soil components to be assessed more specifically. Following this logic, the question arises whether these fractions could also be redirected towards the production of new construction materials. Among circular applications, earth-based construction elements represent a particularly relevant pathway (Reddy, 2022). As (Van Eijk & Breukelman, 2022) show, an efficient circular economy is particularly relevant for a small and densely populated country such as the Netherlands. Resource scarcity and international tensions have further highlighted the dependence on energy, materials, and goods. A potential use of excavated soil as a construction material could therefore not only substitute energy intensive primary raw materials, create new value chains and strengthen local circularity, but also contribute to the broader goal of transforming the Netherlands into a fully circular economy by 2050.

1.1.3 Earth in construction

Exploring such options builds on the long-standing use of earth as a primary construction material, which has served as the basis for many building elements throughout history (Reddy, 2022). Despite technical development in this field, earthen construction materials continue to face a perception barrier, since they are often associated with pre-industrial building practices rather than modern engineered material systems. This view has limited their integration into mainstream building processes. It has also contributed to fragmented regulatory and legislative frameworks, inconsistent testing and application standards, limited professional expertise and persistent technological barriers (Gharbage et al., 2025). That is why, their use must be reconsidered in relation to modern requirements, as articulated by Guillaume Habert, Professor of Sustainable Construction at ETH Zurich:

"If we use earth, (...) within today's economic context and aim to meet users' expectations regarding quality, durability, cost-efficiency, aesthetics, and comfort, these materials can no longer be processed in the same way as they were 200 years ago"(ETH Zürich, 2025)

Within the 20th century, the production of compressed earth blocks emerged as a contemporary, low-emission construction technique. It offers a promising pathway for advancing sustainable building practices (Gharbage et al., 2025). Compressed earth blocks (CEB) are masonry units produced by statically compacting a moist mixture of earth, sand, and when needed, stabilizing agents within a mould. Unlike traditional adobe bricks, which are shaped and left to air-dry without pressure, or fired clay bricks, which gain strength through energy intensive treatment, CEBs derive their mechanical performance mainly from the compaction process (Reddy, 2022). This involves the use of mechanical presses, either hydraulic or manual. The resulting elements achieve higher material density, more consistent dimensional accuracy and often improved strength compared to traditional earthen construction methods. This also enables industrial-scale manufacturing (Hanaor, 2025). Further, this is closely linked to the energy demand and environmental performance of a CEB. Compressed earth blocks have reported energy requirements ranging from about one-fifth to one-fifteenth of those for fired brick manufacturing (Shiferaw, 2025).

Yet, "[...]earth construction is seen as a niche building option in Europe, beloved by architects but neither widely available nor cheap" (Augarde et al., 2016).

1.1.4 Prospective application

In many European cities, a substantial share of excavated materials comes from construction activity. Urban development is increasingly oriented upward, reflecting broader densification and high-rise trends. (Drozdz et al., 2018). A clear example is seen in Industrial-Hub cities such as Rotterdam, where policies promote vertical growth and urban planning frameworks present high-rise visions as central to future development. (Gemeente Rotterdam, 2019). CEBs have shown great potential in interior applications and in hybrid construction systems, for example with lightweight timber structures (Pelicaen et al., 2023). However, their material properties and mass limit their suitability for large-scale vertical densification. Recent developments, including novel design approaches and advanced assessment methods, have enabled contemporary earth masonry in buildings up to four storeys (Wiehle et al., 2025). This raises the question of which low-rise building typologies in today's urban environments, especially in production-oriented cities such as Rotterdam, could enable effective implementation of CEB systems. European cities of this type have a substantial proportion of industrial land use. (Olaf Merk & Theo Notteboom, 2013). In Rotterdam, about one third of the municipal land area is dedicated to industrial functions.

Areas like these are mainly characterized by single-storey industrial buildings, which are representing the most widespread typology (Goncikowski, 2020). Non-residential functions, such as industrial, commercial, and office buildings, tend to have short usage and adaptation cycles. This is largely because the buildings are shaped by economic restructuring, functional shifts, and evolving technological

requirements (Thomsen & Van der Flier, 2011). These dynamics are especially apparent in cities such as Rotterdam, where ongoing transformations are shaped by decarbonization objectives, the integration of digital technologies, and the shift toward circular economic models. These developments are changing spatial demands within industrial areas and introducing new adaptation pressures for production-related buildings. At the same time, they open opportunities for alternative construction approaches (Jansen et al., 2021). Within this, the integration of earth-based industrial complexes would precisely align with the ambitions of the Rotterdam port area. The aim is to be a frontrunner in sustainability, circularity, and innovation. A look at the Port Vision reveals that current development strategies increasingly promote a shift toward "waste-to-value" systems, in which residual materials are reconsidered as productive resources. A key ambition of these strategies is the cut of CO2 emissions, targeting reductions of around 49% by 2030 and climate neutrality by 2050. Importantly, these goals extend beyond maritime operations and address the port as a comprehensive industrial landscape, including its built environment (Port of Rotterdam, 2019). Using earth-based materials could serve as a visible pilot project for sustainable development. At the same time, it is emphasized, that infrastructure must be climate-resilient, especially regarding increasing heat stress and more frequent extreme weather events. (Port of Rotterdam, 2019). Earthen construction offers a wide range of advantages through possible reductions in cooling and energy demand and healthier working environments. In summary, these industrial areas are expected to become cleaner and more environmentally integrated to also reduce conflicts with adjacent residential neighbourhoods. Still, there is the need of remaining attractive places of work. The industrial landscape of Rotterdam could therefore serve as a local application horizon through which the reuse of excavated soil can be connected to broader questions of architectural implementation, circular construction, and industrial transformation.

In 2021 alone, 59.051.000 tonnes of soil moved through Dutch processing and application routes.

Figure 02: Urban excavation works near Rotterdam Central Station, illustrating soil flows generated by inner-city construction activities. Adapted from Chris Mueller, iStock.com/ Chris Mueller, Stock photo ID 45830017, editorial licence.

European industrial-hub cities face a systemic resource paradox:

While vertical densification generates massive volumes of excavated soil effectively lost to low-value fill and disposal routes, the absence of an integrated framework linking soil characterisation, processing, composition and compaction performance limits its transformation into reproducible compressed-earth components for broader architectural applications.

1.2 Problem statement

To address the overarching problem, the research was guided by three interrelated sub-problems:

(1) Excavated soils are highly local and variable, while available material data are often fragmented and not directly connected to earthen-construction suitability criteria. This limits the ability to assess their potential for CEB production.

(2) As a consequence, these soils cannot be treated through a universal CEB recipe. Each earth requires a calibrated processing workflow in which particle-size distribution, water dosing, mixing and compaction are adjusted to its specific material properties.

(3) Within each material system, performance is governed by a complex interaction between material behaviour, processing conditions, and compaction response. Although these relationships have been addressed in broader earthen material research, they are not directly transferable to the locally available materials. Their relative influence must therefore be evaluated experimentally to identify dominant parameters and define reproducible production windows.

1.3 Objectives

The main objective was to investigate how locally excavated soil could be processed into reproducible compressed-earth specimens and to identify the material, composition and production parameters that control compressive strength for future CEB production.

(1) Characterise a locally available excavation-derived soil, assess its material behaviour, geological representativeness and evaluate its suitability for CEB production.

(2) Develop a soil-specific processing workflow that translates the identified material properties into controlled mix compositions and reproducible compressed-earth specimens.

(3) Experimentally evaluate how material composition, processing conditions, and compaction parameters influence CEB performance, including dry density, compressive strength, and dimensional stability.

(4) Determine how key material, composition and production parameters influence compressive strength and define processing windows for reproducible compressed-earth specimens as a basis for CEB production.

(5) Translate the resulting material and process knowledge into an architectural outlook for CEB application, using low-rise industrial buildings as a framework to define performance requirements, construction constraints and possible fields of use.

1.4 Relevance

The project addresses a practical gap between circular ambitions and buildable solutions. Large amounts of excavated soil are produced in European cities, yet they are still mainly used for backfilling, earthworks or disposal because their quality, composition and availability are highly local and variable. In current western architectural and engineering practice, established workflows for upgrading these soils into consistent, construction-grade products remain limited. By working with local material behaviour, composition and processing parameters, this research aims to provide practical evidence for treating excavated soil as a construction resource rather than as surplus bulk material. Material investigation is connected to broader architectural application fields by situating CEB development within production-oriented urban areas. Adaptable low-rise industrial buildings serve as an exemplary context through which the future potential of earthen construction can be discussed. At a societal level, redirecting excavated soils into higher-value construction loops supports circular-economy goals by reducing disposal pressure, transport burdens and demand for newly extracted resources. The relevance of the research therefore lies in moving from the general ambition to reuse excavated soil towards a practical method for assessing when and how it can become a reliable construction material.

How can locally excavated soils from Rotterdam be translated into reproducible compressed-earth blocks by understanding how material behaviour, composition and production parameters influence their mechanical performance?

1.5 Research question

Against this background, the thesis was guided by the adjacent main research question. The following sub-questions were derived from this:

(1) Which physical, mineralogical, and environmental properties characterise the locally excavated soil and how do they determine its suitability for CEB production?

(2) What soil-specific process is required to translate the identified material behaviour into a reproducible CEB mix design and production workflow?

(3) How do material behaviour, composition and production parameters influence the compressive strength of CEB specimens, and which variables are most decisive?

(4) How can the developed material and process knowledge be positioned within broader architectural application fields, with low-rise industrial buildings serving as an exemplary context?

1.6 Scope

This thesis focuses on the translation of locally excavated Rotterdam soil into reproducible compressed-earth specimens as a basis for future CEB production. The work was limited to one representative excavation-derived soil stream from the Rotterdam-Delft region and examines how this material can be characterised, processed, adjusted and compacted under laboratory conditions. The material scope included physical, mineralogical and environmental characterisation, with particular attention to particle-size distribution, shrinkage behaviour, organic content, contamination status and soluble salts. Potential pyrite-related risks were identified through the geological and chemical assessment, but their full evaluation through total sulphur analysis or long-term oxidation testing remained outside the primary scope.

The experimental scope focused on dry processing, mix composition, compaction moisture, particle-size-distribution adjustment and static compaction. Mechanical performance was assessed primarily through compressive strength tests on cylindrical specimens, supported by density and shrinkage observations. Water resistance, abrasion, erosion, wetting-drying durability and long-term dimensional stability were acknowledged as application-relevant criteria but remained outside the primary experimental scope. The resulting material and process knowledge was then translated into an outlook on future fields of application for CEBs developed from local excavation soil, using adaptable low-rise industrial buildings as an exemplary context. However, the thesis did not aim to fully validate a complete building system or a full-scale block.

Further stages of validation and implementation remained outside the scope of this thesis, including full regulatory approval, structural certification, full-scale production trials, market implementation planning and city-wide impact accounting. The thesis also did not aim to solve the governance challenges of excavated-soil reuse. Instead, it aimed to provide a technically grounded material and testing pathway that makes the transformation from excavation-derived soil to reproducible compressed-earth specimens tangible for future architectural applications

1.7 Research output

The research presents a literature review synthesising current knowledge on excavated-soil reuse, earthen material processing, compressed earth block production and performance. Building on this foundation, the thesis documents the experimental translation of a locally available soil into reproducible compressed-earth specimens through material characterisation, mix development, sample production and testing. The output is a material and process-based understanding of how excavation-derived soil can be assessed, adjusted and compacted for CEB production. It identifies the key material properties, composition parameters and production conditions that govern compressive-strength performance and translates these findings into an architectural outlook for future application.

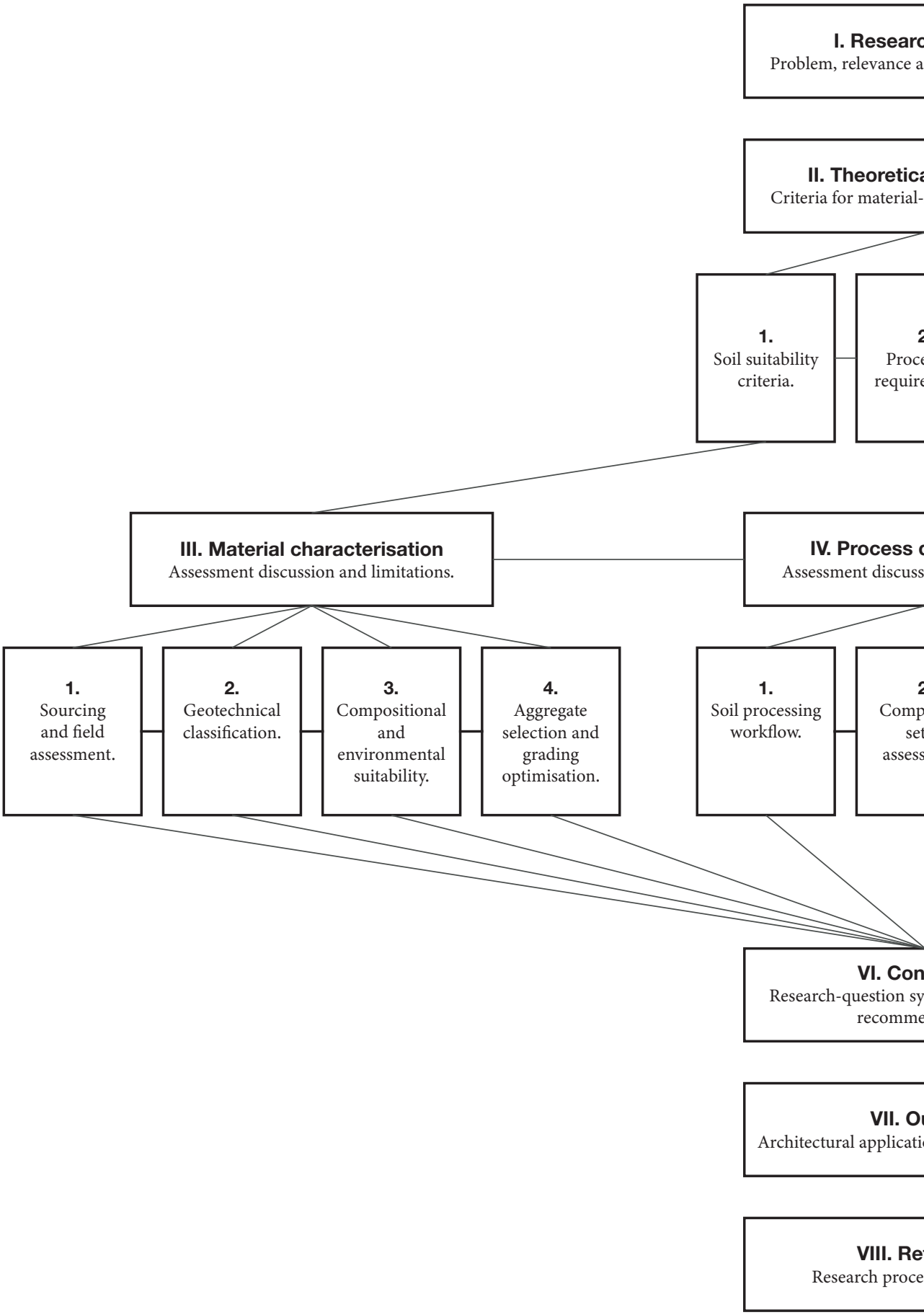
I. Researc
Problem, relevance a
II. Theoretica
Criteria for material-
1.
Soil suitability criteria.
2
Proce
require
III. Material characterisation
Assessment discussion and limitations.
IV. Process c
Assessment discuss
1.
Sourcing and field assessment.
2.
Geotechnical classification.
3.
Compositional and environmental suitability.
4.
Aggregate selection and grading optimisation.
1.
Soil processing workflow.
2
Comp
set
assess
VI. Con
Research-question sy
recomme
VII. Ou
Architectural applicati
VIII. Re
Research proce

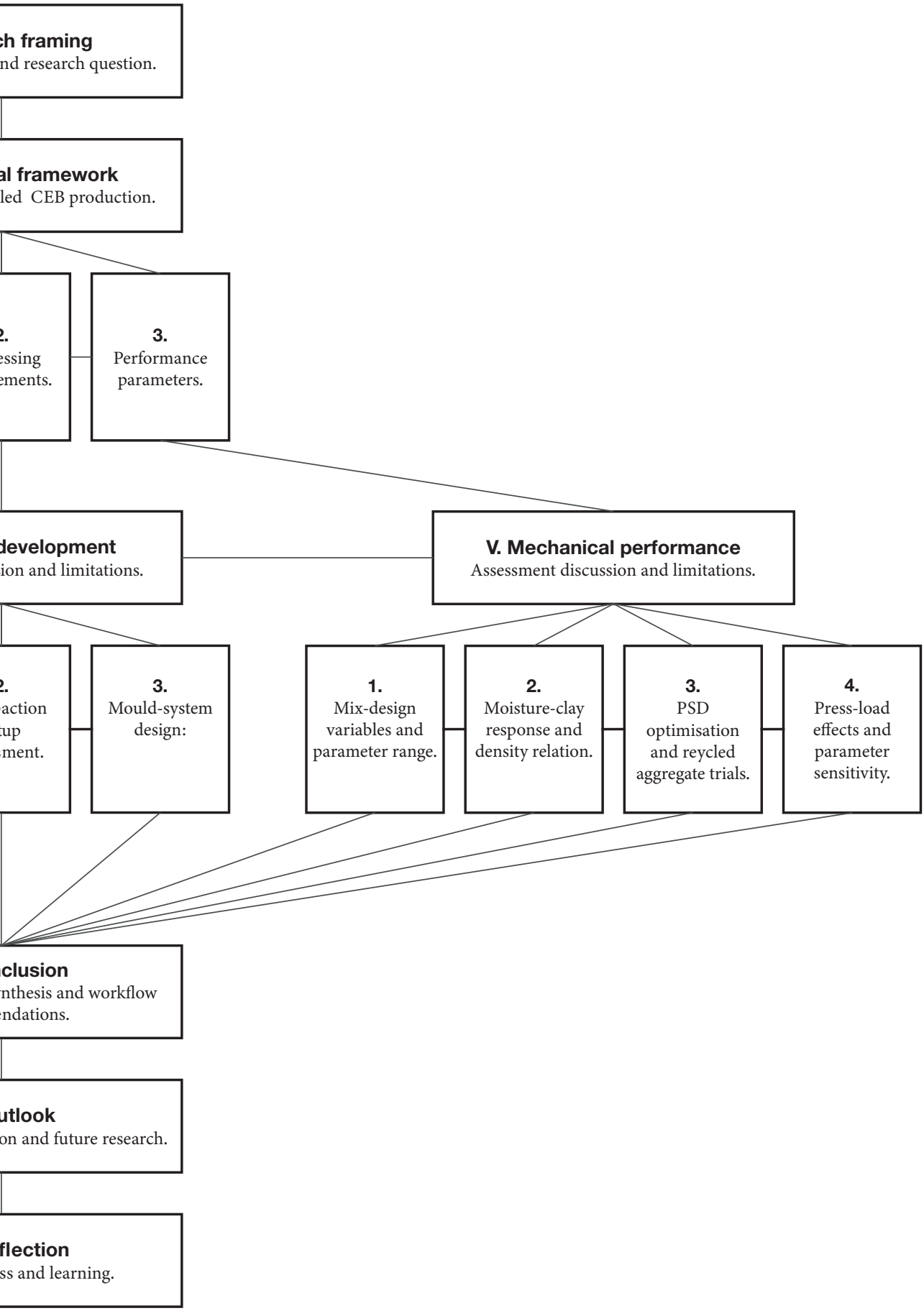

Figure 03: Research structure

2. Approach

2.1 Methods

2.1.1 Literature review

The literature review establishes the theoretical foundation for the experimental framework and the later discussion of architectural application. It examines soil composition, clay-mineral binding mechanisms, field and laboratory assessment, material processing, stabilization techniques, compaction methods, drying processes and performance evaluation criteria. It therefore defined the criteria and variables used in the experimental series. Required research papers and books were accessed through the following online databases: WorldCat, DeGruyter, Nautus, Springer Nature, Google Scholar, DIN Media and Scopus as well as through the reference lists of the reviewed literature.

2.1.2 Material sourcing

The investigated material was sourced from a soil bank in Pijnacker, which temporarily stores excavation material from construction activities in the Rotterdam-Delft region. The material was selected as a locally available excavation-derived soil stream with regional relevance for the research context. Sampling was documented in relation to source, stockpile condition, visible heterogeneity and moisture state.

2.1.3 Material characterization

The material characterisation combined preliminary field screening with targeted laboratory analyses. The visual-manual soil description and classification were carried out in accordance with EN ISO 14688, including assessment of soil type, grain characteristics, consistency, plasticity, organic indications, carbonate reaction and the dominant fine fraction. These tests provided an initial indication of workability, cohesion, shrinkage tendency and whether the material may function as a clay-rich binder fraction for compressed earth blocks. Laboratory analyses were then used to quantify and verify the material properties relevant to CEB suitability. Particle-size distribution was determined through wet sieving and hydrometer analysis. X-ray diffraction was used to identify the main crystalline phases and support the geological interpretation of the material. Environmental suitability was assessed through AP04 data, while ion chromatography was used to evaluate water-soluble salts.

2.1.4 Material processing

The characterised raw material was processed into defined compressed-earth mixtures. The clay-rich fraction was dried, pre-crushed and pulverised to obtain a controllable fine binder material. Selected granular fractions were prepared separately and combined with the binder according to the defined mix compositions. Mixing was carried out by dry blending the binder and granular fractions before adding water to reach the target compaction moisture. After mixing, the material was stored airtight to allow moisture equalisation before specimen production. The main mix-related variables were clay content, particle-size distribution and compaction moisture.

2.1.5 Mould design and fabrication

A dedicated compaction mould was designed and fabricated to produce cylindrical compressed-earth specimens under defined static loading conditions. The mould geometry was determined by the required specimen dimensions, the maximum grain size of the mixtures, the available press height and the target compaction pressures. Wall thickness was dimensioned using Barlow's equation to ensure sufficient resistance against radial pressure during compaction. The mould was manufactured by lathe machining to achieve dimensional accuracy, plane-parallel contact surfaces and repeatable specimen geometry. As mould friction and demoulding behaviour can affect specimen integrity and compressive-strength results, the mould setup was treated as part of the experimental method rather than as a neutral accessory.

2.1.6 Specimen fabrication

Specimens were produced by static compaction in the manufactured mould. The investigated production variables included applied compaction pressure and, where relevant, pressing procedure and compaction conditions. For each specimen, the relevant production data were recorded, including mix composition, water content, compaction

load, pressing procedure, demoulding behaviour and drying conditions. Additional observations on workability, clumping, moisture distribution, mould friction, specimen damage and shrinkage were documented to support the interpretation of the mechanical results.

2.1.7 Mechanical testing and evaluation

Mechanical performance was assessed through compressive-strength testing of cylindrical specimens. Compressive strength was selected as the main mechanical indicator because it is directly relevant to masonry applications and allows comparison between different material compositions and production parameters. The specimens were tested under plane-parallel loading conditions. The measured compressive-strength values were evaluated together with dry density, residual moisture content, shrinkage behaviour and observed failure pattern. The evaluation compared the relative influence of material behaviour, composition and production parameters on compressive strength. Particular attention was given to clay content, particle-size distribution, compaction moisture and applied compaction pressure. The results were used to identify material-specific trends and processing windows for the investigated soil, rather than to establish universal design rules for CEB production.

2.1.8 Evaluation strategy and constraints

Scientific rigour was addressed through consistent documentation, controlled comparison between test series and transparent interpretation of experimental constraints. The series were structured so that selected parameters could be compared individually where possible, without treating the results as a fully predictive statistical model. Due to natural material variability, manual production steps and limited specimen numbers in some configurations, the results were interpreted as material-specific trends and processing windows rather than universal design rules. Where repeated specimens were available, average values and variation were used to support comparison.

2.2 AI use statement

AI tools were used in this study for literature organisation, reference-management support, language refinement, and the production of visualisations and renderings. Their use was limited to supportive tasks, including improving readability, structure and APA 7 formatting, as well as communicating concepts and workflows visually. AI was not used as a source of evidence, for data generation or for introducing unverified academic content. All AI-supported outputs were critically reviewed, edited and validated by the author.

2.3 Theoretical framework

2.3.1 Soil composition

To enable the use of excavated soils in construction, it is necessary to clearly understand the relevant terminology and the fundamental composition of the material. Within the literature, soil is commonly defined as layers of generally loose mineral and/or organic material that are influenced by physical, chemical, and biological processes occurring at or near the Earth's surface. These layers typically contain liquids, gases, and living organisms and provide the basis for plant growth (van Es, 2017). Soil formation is driven by weathering and sediment deposition. It is also influenced by time, climate, vegetation, parent material, topography, and human activities (Reddy, 2022).

A simplified standard pedological profile, as outlined by Schroeder, (2016) distinguishes an upper topsoil (A) rich in organic matter, followed by an underlying horizon (B) with increased clay and salt accumulation. Beneath this is the parent material (C), made up of significantly weathered bedrock. Material for earthen construction is commonly sourced from the subsoil (B) or underlying mineral horizons, where organic content is much lower.

To identify soil components relevant for construction, it is necessary to understand soil as a ternary system. The gaseous phase consists of air and water vapour. The liquid phase is soil water, which can be differentiated into sorption, solvation, and free water. The solid phase divides into organic and inorganic components. The organic fraction is generally not considered relevant for construction, while the inorganic fraction, made up of mineral particles, forms the basis for building with soil. Within this component, ultra-fine grains such as clay are defined in engineering as particles with diameters smaller than 0.002 mm. The coarser grain fraction includes silt, with particle sizes between 0.002 and 0.06 mm, sand ranging from 0.06 to 2 mm, and gravel and rock fractions, which have particle sizes greater than 2 mm (Minke, 2025; Schroeder, 2016). According to Reddy (2022), the physical behaviour of soil is governed by the properties of its grains, particularly their size, shape, and overall composition. On the other hand, chemical characteristics are primarily determined by the mineral composition of its particles and the nature of the originating parent rock. The type and proportion of clay minerals are especially influential. That is because in earthen construction, coarser grains mainly act as inert aggregate, whereas the fine clay fraction largely governs cohesion and workability. This functional mix is often also commonly referred to as loam (Minke, 2025; Röhlen & Ziegert, 2020).

2.3.2 Clay as a binding agent

Clay materials form through the weathering of feldspar and other silicate minerals. Their chemical composition depends on the parent rock and the intensity and progression of weathering. In nature, these minerals occur in many forms with typical particle sizes from about 0.1 to 4 micrometres. Depending on the type, these units have either two or three sheets. These structural varieties lead to different material behaviours, which are critical for their use as construction materials. The bonding behaviour of clay minerals is governed by localized charge imbalances on the surfaces. Unlike many conventional binders in construction, clay bonding relies mainly on physical interaction forces rather than chemical reactions. Compared to three-layer clay minerals, two-layer variants have weaker binding capacity because they show lower surface charge differences. When these minerals dominate the clay fraction, this can result in lower mechanical strength. Three-layer clay minerals are further distinguished by whether they exhibit swelling behaviour. This depends on the ability of the interlayer spacing to expand when water is absorbed.

Among the most frequently occurring clay minerals in soils are for example, kaolinite, which belongs to the two-layer mineral group, and montmorillonite, a three-layer clay mineral. Less commonly encountered is illite, which also belongs to the three-layer group but does not exhibit major swelling properties. Because of the diversity of clay minerals, soils and earth materials cannot be evaluated solely based on their total clay content. Instead, the specific composition must be considered. Clay minerals present in soils can be

identified using X-ray diffraction (XRD) analysis. To investigate morphological and microstructural differences, scanning electron microscopy (SEM) and transmission electron microscopy (TEM) are commonly employed. However, these analytical methods are resource-intensive and require careful sample preparation as well as specialized mineralogical expertise (Minke, 2025; Reddy, 2022; Röhlen & Ziegert, 2020; Schroeder, 2016).

Reddy (2022) notes, that the Atterberg limit parameters discussed in chapter 2.3.4 specifically the liquid limit, plasticity index, and shrinkage limit can also be used to broadly classify the types of clay minerals present in a soil.

2.3.3 In-situ soil assessment

Beyond the type of clay minerals and their intrinsic properties, a range of additional factors influence the suitability of soil for processing into a construction material (Röhlen & Ziegert, 2020). These aspects can be roughly assessed through simple field tests and later examined by applying more advanced laboratory measurements. To ensure reliable results, multiple field tests should be combined and carried out on a representative selection of samples. In practice, soils are typically grouped into three categories according to their clay content: rich soils with high clay proportions, lean to semi-rich soils, and overly lean soils. The final category is generally unsuitable for construction applications and can only be used as a blending or additive material. As stated by Röhlen & Ziegert (2020), soil properties can be modified through blending or admixture. However, an economically viable use of local deposits requires that their suitability is assessed within a defined range from the outset. A wide range of tests exists, and their application often relies in part on professional experience. The following provides a selection of tests that are consistently recommended across the literature.

(1) Visual inspection

As an initial assessment, excavated material should be free from humus and root residues, as these organic components are generally unsuitable for construction purposes. In addition, a basic mass or volume assessment can help determine whether sufficient material is available for use. Visual characteristics such as soil colour can provide preliminary indications of clay mineral composition. For instance, greyish soils may suggest the presence of expansive clay minerals such as montmorillonite. The physical appearance of the soil also offers important clues. Presence of large cohesive clods typically indicates a rich soul with high clay content and implies increased effort during processing. On the other hand, dry soils that appear to be pulverized and contain fine or coarse grains are generally more suitable for earth construction. Where clear stratification is visible within the excavated material, the different layers should be thoroughly mixed, and representative samples should be taken from the combined material for further testing.

(2) Smell test

Earth suitable for construction is typically odourless. The presence of noticeable smells can therefore be used as an indicator of excessive organic content in the material.

(3) Spherical sample

For this purpose, spherical samples with a diameter of approximately 4 cm should be formed by hand-rolling. It is essential that the material is used in an earth-moist condition rather than in a dry state, as only samples with comparable consistency can be meaningfully evaluated against one another. The ability to form a coherent sphere increases with higher clay content and material cohesiveness. When such a sphere is dropped from a height of around 80cm (although some sources refer to heights of up to 150 cm or shoulder height), the resulting behaviour provides an indicative assessment. Rich soils tend to flatten without disintegrating, lean to semi-rich soils typically crack or tear while remaining largely intact, whereas overly lean soils break apart or pulverize upon impact. In addition, a cutting test can be performed on the formed sphere with earth moist. When the sample is cut with a knife, rich soils are typically characterized by a smooth and slightly glossy cut surface. In contrast, lean to semi-rich soils tend to produce a rougher surface, where resistance is felt during cutting and individual grain traces become visible. Following this, the spherical samples can be tested again after drying, providing an initial indication of the expected strength of the

material. When dropped, again dry spheres made from rich soils often remain largely intact, whereas those composed of lean soils tend to fracture or disintegrate. In the dry state, a further assessment can be carried out by rubbing the material between the fingers, which offers insight into its abrasion resistance and overall cohesion.

(4) Friction test
This procedure primarily allows for an assessment of the material's cohesive forces. The sample should be mixed with water to a viscous, plastic consistency. In this state, sand and fine sand fractions can be felt distinctly between the fingertips, whereas clay-rich soils tend to exhibit a smooth, soap-like texture. At the same time, the fingers can be slowly pulled apart to observe the tensile resistance of the material.

(5) Wash test
After the rubbing test, the hands are rinsed with water. Soils with higher silt or sand content are typically removed quickly and easily, whereas clay-rich soils require more effort to wash off.

(6) Sedimentation test:
This test can be used for a general assessment of grain-size distribution. It allows an initial evaluation of whether the sample is predominantly fine-grained or coarse-grained, and whether the distribution appears continuous. For this purpose, a sample of approximately 100 g is mixed with water in a transparent jar, allowing the particles to settle according to their size. Prolonged turbidity of the water indicates a higher proportion of fine particles and is typically associated with clay-rich soils. It is important to note, that the thickness of the individual sediment layers does not directly represent the proportional composition of the respective fractions (Minke, 2025; Reddy, 2022; Röhlen & Ziegert, 2020; Schroeder, 2016).

2.3.4 Laboratory soil assessment

Following these preliminary field assessments and the laboratory identification of clay minerals, it is essential to conduct further tests to evaluate the suitability of soil. These tests are necessary to ensure controlled and reproducible pressing conditions in the subsequent production stages of the earth blocks.

(1) Particle size distribution
The analysis of grain-size distribution is a widely applied method in soil mechanics. It involves determining the mass distribution of particle size fractions through a combined sieve and sedimentation analyses. This is important because poorly graded soils can lead to difficulties during the compaction process. The analysis therefore supports the determination of both the type and quantity of aggregates required to adjust the mixture toward optimal sand and clay proportions. It must be emphasized, however, that this test does not in itself constitute a suitability assessment for construction earth. As discussed in the previous section, particles smaller than 0.002 mm are commonly classified as clay sized. Yet minerals such as quartz and carbonates can also occur within this size range while exhibiting significantly lower binding capacity, which may result in an overestimation of cohesive strength. Conversely, certain clay minerals exceed these nominal size thresholds, meaning that their binding contribution may be underestimated when grain size alone is considered.

(2) Organic matter
Organic constituents increase the water absorption capacity of earth materials and, therefore, their plasticity. This also leads to a reduced dry compressive strength. One method for assessing organic content is the loss-on-ignition test, in which organic substances are removed by heating and the resulting mass loss is measured. Röhlen & Ziegert (2020) however, consider this approach to be of limited reliability, as the measured mass loss also includes released pore water and transformations of clay minerals, making it difficult to distinguish the contribution of organic matter alone. Instead, it is noted that even very small humus contents can be detected through a sensory assessment: after several days of soaking, during which the earth material is stored in a wet state within a sealed container, organic matter can be identified by a characteristic odour.

(3) Natural lime content
This test is carried out to determine whether the soil contains fine limestone particles, primarily calcium carbonate. This is relevant because it influences key material properties such as cohesion, plasticity, and

water absorption. The procedure involves applying diluted hydrochloric acid (approximately 10 %) to the soil sample. Effervescence occurs as a reaction to the carbonate content. The resulting intensity and duration of the reaction provide an indication of the amount and grain size of limestone present. A stronger reaction indicates a higher content of finely distributed limestone, whereas a reaction that persists over a longer period suggests the presence of coarser carbonate particles (Röhlen & Ziegert, 2020; Schroeder, 2016).

(4) Salinity

Röhlen & Ziegert (2020) also note, that salt contents in earth materials exceeding certain threshold values can lead to damage in the finished building component. To quantify potentially harmful salts, analytical methods such as ion chromatography or spectrophotometry are commonly employed. Acceptable limit values depend on the application context. For exposed components, these limits are lower, as salts can attract moisture hygroscopically and thereby increase the moisture content within the material.

(5) Moisture content

According to Schroeder (2016), the moisture content of a soil sample is expressed as the ratio of the mass of pore water to the mass of the dry soil, given by:

$$W = M_w / M_d$$

Here, M_w denotes the mass of water contained within the pores, and M_d represents the mass of the oven-dried sample. The water mass is determined by measuring the difference between the sample's weight before drying and its weight after drying at 105 °C.

(6) Atterberg's limits

The strength and deformation behaviour of soil are strongly influenced by its moisture content. On this basis, four distinct consistency states can be defined: liquid, plastic, semi-solid, and solid. These states represent standardized moisture conditions that describe the soil independently of its natural in-situ water content.

(a) Liquid limit (LL):

Boundary between liquid and plastic state. It describes the minimum water content for the soil to still be liquid. This provides an indication of the soil's capacity to bind water. Higher liquid limit values are generally associated with a greater proportion of active clay minerals and, consequently, increased cohesive potential.

(b) Plastic limit (PL):

Boundary between plastic and semi-solid state. It represents the minimum water content at which soil begins to crumble and is conventionally determined by rolling the material into a thread with a diameter of approximately 3 mm.

(c) Shrinkage limit (SL):

Boundary between semi solid and solid state. It defines the maximum water content at which further drying does not result in a reduction of volume. Further, it represents the lowest water content at which the soil remains fully saturated and is used to assess its shrinkage and swelling potential.

(d) Plasticity index (PI)

The difference between liquid and plastic limit of a soil:

$$PI = LL - PL$$

According to Schroeder (2016), soils with a lower PI respond more readily to the addition of water and are therefore generally easier to process and work with.

(e) Consistency number (C)

$$C = (LL\text{-}W)/(LL\text{-}PL) = (LL\text{-}W)/P$$

Here, W denotes any existing water content of the soil. However, Röhlen & Ziegert (2020) critically assess these test methods, as all particles larger than 0.4 mm must be removed prior to testing. This separation alters the deformation and flow behaviour of the material, meaning that the test is primarily considered suitable for soils with a high clay content and very fine grain structure. By contrast, Minke (2025) notes that the test results can be adjusted to account for the removal of coarser particles, provided that this fraction

constitutes less than 25 % of the total dry mass of the soil mixture. Reddy (2022) mentions, that the Atterberg limits combined with the information of particle size distribution provide a practical basis for the identification and classification of soils (Minke, 2025; Reddy, 2022; Röhlen & Ziegert, 2020; Schroeder, 2016).

(7) Shrinkage

For this purpose, test specimens are produced using the intended processing consistency. After a defined drying period, changes in length or volume are measured. This procedure is useful for estimating suitable mix designs for the intended application. In addition, it can provide an indication of the type and quantity of aggregates required for further adjustment (Röhlen & Ziegert, 2020).

(8) Swelling

This behaviour can be assessed using the free swell test, which is applied to quantify the expansion potential of soil samples. For this test, a volume of 10 cm^3 of soil is sieved through a 0.4 mm mesh and subsequently placed in a graduated cylinder filled with distilled water. After swelling has ceased, the difference between the initial and final volumes is recorded and expressed as a percentage, yielding the free swell value (Schroeder, 2016).

(9) Binding force

This testing method is used to assess whether an earth material is suitable as a construction material regarding its binding capacity. The procedure aims to capture the combined contribution of the clay mineral fraction and the surrounding soil matrix to the overall mechanical behaviour. Although the experimental setup is comparatively complex, it is considered capable of providing a meaningful characterization of material properties. By incrementally applying load to the specimen, the failure stress is determined. Identified limitations of this method include uncertainties in predicting shrinkage behaviour and compressive strength (Röhlen & Ziegert, 2020).

(10) Compression strength

The compressive strength measured on the specimen can provide an initial indication of whether the required strength levels are likely to be achieved in the final construction material. Once the basic suitability of the available earth material has been established through preliminary field tests and laboratory analyses, the mixture must be prepared for processing, as soils are rarely directly usable in their natural state for construction (Reddy, 2022).

2.3.5 Processing

Main objective of the material preparation is to obtain an earth mixture that is as homogeneous as possible and free from disruptive constituents, thereby ensuring suitability for further processing. Alongside traditional techniques such as seasonal weathering, contemporary practice predominantly relies on industrial mechanical processing methods to achieve consistent material quality. However, one of the easiest but more time-consuming methods is still to place the lumps in water so they become plastic (Minke, 2025; Schroeder, 2016).

(1) Pulverising

Breaking down soil clods is a critical step in preparation, as it enables the material to be reduced to a powdery or finely granulated state suitable for subsequent mixing with aggregates and/or stabilizing agents. This process can be carried out using a range of tools, including rollers and mechanical or hammer mills. In addition, electrically powered and motor-driven crushers are commonly used to achieve consistent particle breakdown at larger processing scales. Typically, this processing step is applied to soils in dry state (Minke, 2025; Reddy, 2022).

(2) Sieving

The removal of oversized particles and unsuitable inclusions, such as rocks, is a necessary step in material preparation. According to Reddy (2022), the typical mesh size used generally ranges between 4 and 5 mm. Schroeder (2016) points out, that depending on intended application and sieve operation the mesh size can range between 2 mm and 7 mm. Sieving can be carried out using fixed screens or rotary sieves, while mechanically vibrated sieves are often employed to improve efficiency (Reddy, 2022; Schroeder, 2016).

(3) Soil combining

In most cases, natural soils are blended with other soils or with finer aggregates to achieve the desired material composition. In addition, stabilizing

agents, such as lime, are frequently incorporated. Mixing is most effectively carried out in a dry state using a motorized rotating drum, which ensures a uniform distribution of all constituents (Reddy, 2022).

(4) Saturating
To achieve high-density compressed earth blocks, the soil mixture must be brought to a partially saturated state. According to Reddy (2022) a uniform distribution of moisture is essential for this process. Mechanical mixers are commonly used, with water introduced by spraying into the rotating drum at controlled intervals.

(5) Pan milling
This industrial preparation technique integrates the previously described steps into a single processing operation. In specific cases such as very hard or dry earth materials, or mixtures containing a high proportion of coarse stones, additional preparatory measures may nevertheless be required. During processing, earth-moist material is forced through a coarse screen by means of a millstone mechanism, ensuring an even distribution of clay, sand, water, and any added aggregates. The process yields a homogeneous mixture with a plastic consistency that is well suited for subsequent forming and compaction (Röhlen & Ziegert, 2020).

2.3.6 Stabilisation

There is a wide range of options that exists for adjusting mix designs in the production of compressed earth blocks through the addition of supplementary materials. These additions allow the properties of the soil to be tailored to specific application requirements. In technical terms, this process is commonly referred to as stabilization (Reddy, 2022; Schroeder, 2016). The simplest form of this process is mechanical stabilization, in which soils of different grain and clay fractions are blended. This step is generally necessary to reduce shrinkage cracking and to facilitate the compaction process. Such adjustments directly influence key consistency parameters, including the liquid limit and the plasticity index (Reddy, 2022). For a systematic classification of stabilization strategies, two principal categories can be distinguished: aggregates and additives. Aggregates primarily influence the material through physical mechanisms. For instance, thermal insulation properties can be improved by incorporating lightweight aggregates. Examples include perlite or expanded shale. Additives, by contrast, act primarily through chemical mechanisms, modifying the structure of clay minerals to enhance properties such as compressive strength or water resistance. Common examples include the addition of Portland cement, fly ash, or lime.

The use of such additives, however, requires critical consideration. Beyond potential health risks during handling and processing, synthetic binders can pose significant challenges when the material is intended to be reintegrated into natural material cycles, thereby limiting recyclability and circular use (Schroeder, 2016). If modification of the soil through additives is nevertheless pursued, it is important to acknowledge that, according to Minke (2025), certain properties such as compressive strength can be improved, other characteristics may be adversely affected. In particular, the addition of binders can increase shrinkage during the drying process, introducing new material-related challenges.

2.3.7 Compaction

Once the desired soil mixture has been prepared, several aspects must be considered during block pressing. In the case of static compaction using a manual press, the mixture is first weighed to achieve a controlled and consistent density. The measured amount is then placed into the mould of the press. The lever is pressed to its end position, whereby the compaction force is predefined by the press configuration and variations in applied pressure are excluded. When the lever is raised again, the mould is released and the compressed block can be removed. After demoulding, the blocks should be stored in a stable and closely spaced arrangement to prevent overly rapid drying. One limitation of manual pressing is that, as noted by Minke (2025), the soil mixture must always maintain a highly consistent moisture content and composition to ensure uniform block quality. For higher production outputs and more controllable processing conditions, particularly in the context

of industrial scaling, semi-automatic pressing systems or fully automated presses can therefore be employed as alternative production methods (Reddy, 2022). Building on the preceding, the production of compressed earth blocks can be summarized as a sequence of key steps:

(a) Identification and assessment of suitable soil through on-site investigations and laboratory testing.

(b) Excavation and transport.

(c) Definition of the required material properties for the mixture and determination of stabilization strategy.

(d) Processing and preparation of the soil mixture to achieve desired consistency and homogeneity.

(e) Compaction of mix into blocks.

(f) Drying under controlled conditions.

As already implied by the term compressed earth block, the compaction of the soil mixture is a critical step in achieving the required mechanical strength. The underlying principle is straightforward: increased density leads to improved structural stability. While dynamic compaction methods are sometimes applied in earth construction, CEB production typically relies on static compaction. According to Minke (2025), however, static compaction is less effective than compaction combined with vibration. He notes that freshly excavated earth typically exhibits a bulk density in the range of approximately 1,000-1,500 kg/m³, whereas compaction can increase this density to values between 1,700 and 2,200 kg/m³, sometimes even higher. According to Reddy (2022) soil may be understood as a three-phase material consisting of air, water, and solids. The relationships between density, void ratio, and water content are therefore decisive for the compaction process. During pressing, entrapped air is expelled from the soil matrix, while clay particles absorb water and become more plastic, which in turn facilitates compaction by reducing internal friction. The achievable density depends both on the applied compaction energy and on the moisture content of the soil. From this relationship, two key parameters from soil mechanics can be derived:

(1) OMC (Optimum Moisture Content)
The optimum moisture content refers to the water content at which a soil reaches its maximum achievable density under a given compaction energy. At this moisture level, particle rearrangement is most efficient.

(2) MDD (Maximum Dry Density)
The maximum dry density is the highest dry bulk density a soil can attain when compacted at its optimum moisture content. In the literature, this value is often referred to as the Proctor density or standard dry density.

The Proctor test represents one of the standard testing methods in engineering for determining these parameters and their interrelation. The results are typically presented in the form of a Proctor curve, which illustrates the relationship between moisture content and dry density. This curve enables the identification of the optimum moisture content of the soil for the compaction process. The test is conducted as follows: according to Schroeder (2016), a minimum of four test specimens with differing moisture contents is required. These specimens are compacted in uniform layers within a steel cylinder. Compaction is achieved by means of a freely falling hammer, applying a defined amount of energy to each layer. He further reports that, when comparing laboratory results with densities achieved in real construction projects, rammed earth structures reached approximately 95-98 % of the densities measured under laboratory conditions.

In addition to the Proctor test, which is based on dynamic compaction, Reddy (2022) identifies a static compaction test as a more suitable alternative for compressed earth block production. He reports that, under identical energy input and moisture conditions, higher densities can be achieved using this method. This improvement is attributed to the more uniform stress distribution during static loading, which reduces typical sources of error such as lateral displacement of the specimen within the compaction cylinder. In addition to the different testing approaches for determining the optimum moisture content, an important further insight must be considered. Minke (2025) emphasizes,

that the moisture content identified as optimal in laboratory testing does not necessarily correspond to the maximum achievable compressive strength in practical production. Instead, he highlights workability and binding capacity as the decisive parameters for successful processing. Accordingly, the optimum moisture content should be understood as a lower threshold rather than a fixed target value. He further indicates that moisture contents approximately 10 % above the OMC often lead to improved practical results in compressed earth block production. In this context, Schroeder (2016) likewise notes that operating on the "wet side of the Proctor curve" can lead to improved strength development. However, this approach is also associated with increased shrinkage deformation during drying.

(3) Compaction pressure

Standard manual presses typically achieve compaction pressures of up to approximately 2 MPa, while more recent manual models can reach around 3 MPa. Light motorized presses generally operate in the range of 4-6 MPa, whereas fully mechanical presses commonly apply pressures between 5 and 20 MPa (Reddy, 2022; Schroeder, 2016). In general, higher compaction pressures are associated with improved material performance. This relationship is further supported by studies conducted in France, which demonstrated that strength development is not only pressure-dependent but also strongly influenced by the type of clay mineral present. These studies showed that increasing the static compaction pressure from 2 to 8 MPa resulted in compressive strength increases of approximately 50 % or up to 100 %, depending on the specific mineralogical composition.

A further study by Bruno et al. (2015) investigated the influence of even higher compaction pressures in block production. In this work, pressures of 25 and 50 MPa, and up to 100 MPa, were examined. The findings indicate that increased compaction pressure can lead to the production of high strength blocks comparable to earth blocks stabilized with cement. However, the relationship between pressure and strength was shown to be non-linear, with lower compaction efficiency at higher pressure levels. The study also identifies compaction duration as a key parameter, emphasizing that sufficient time must be allowed for pore water to dissipate during pressing. This underscores that such parameters must always be considered and tested in relation to the intended application rather than being applied as universal values.

2.3.8 Drying

In contrast to cement- or lime-stabilized earth blocks, unstabilised compressed earth blocks do not require curing in the conventional sense through the addition of water. Their hardening occurs purely through physical drying in ambient air. Nevertheless, despite the absence of curing, several handling and storage measures are essential to ensure consistent quality. Immediately after pressing, unstabilised blocks exhibit relatively low handling strength compared to stabilized units, which gain early strength through rapid chemical reactions. As a result, freshly pressed blocks must be transported carefully without direct handling to prevent deformation. Simple handling devices, can support this process. In addition, the blocks must be protected from precipitation immediately after production and throughout the entire drying period. While drying is necessary for strength development, it must occur gradually: exposure to direct sunlight or strong wind should be avoided, as rapid surface evaporation can induce shrinkage cracking (Minke, 2025; Reddy, 2022; Schroeder, 2016).

2.3.9 Performance assessment

The prototype bricks are tested using a set of assessment methods derived from the literature and selected in relation to the intended application. As no harmonised European or Dutch material-specific standards for earthen construction currently exist, some of the applied tests are based on German DIN standards.

(1) Dry Density

A primary and decisive indicator for evaluating CEBs is the achieved dry density, as it directly reflects the material's porosity. For CEBs, target dry densities typically range between approximately 1700 kg/m^3 and 2200 kg/m^3. The dry density p_d is determined as the ratio of the oven-dry mass m_d to the specimen volume V where m_d is measured once

the mass change is less than 0,2 % within 24 hours, indicating a fully dried state (Bauwesen, 2024; Schroeder, 2016).

(2) Dry compressive strength

In earthen construction, mechanical performance assessment has traditionally concentrated on compressive strength, which is generally regarded as sufficient since the test directly reflects the material response along the primary load-bearing direction (Schroeder, 2016). However, Minke, (2025) highlights, that compressive strength measurements are highly sensitive to specimen geometry. Low height-to-width ratios can lead to overestimated strength values, as friction between the specimen and the loading plates introduces artificial confinement effects. The strength testing is carried out under strictly plane-parallel loading conditions using a hydraulic press. Where necessary, specimen surfaces are ground or levelled with a thin mortar layer to ensure uniform load transfer. The applied load is increased continuously until failure occurs. Compressive strength is calculated as the applied force divided by the loaded area (N/mm^2), yielding values in MPa. According to Minke (2025) and Schroeder (2016), unstabilised compressed earth blocks typically achieve compressive strengths between 2 and 4 MPa, with values of up to approximately 5 MPa reported under conditions of very good compaction. Of particular interest is whether, as suggested by Bruno et al. (2015) substantially higher compaction pressures and extended pressing durations throughout production could enable strength levels of up to 10 MPa to be reached.

(3) Wet compressive strength

In contrast to stabilized earth blocks, which can sustain loads even under wet conditions, unstabilised earthen products lose their entire load-bearing capacity when saturated with water. According to Reddy (2022), strength decreases exponentially with increasing moisture content and approaches zero at full saturation. Consequently, wet strength testing becomes only meaningful when stabilizing additives, such as lime, are introduced to establish a durable, water-resistant chemical bond within the material.

(4) Dip Test

Rather than assessing compressive strength under water, the performance of unstabilised blocks should be evaluated in terms of their response to water exposure, particularly erosion resistance and dimensional stability. These properties are critical for durability during the construction phase and under conditions such as driving rain. As described by Minke (2025), a specimen is immersed to a depth of approximately 5 cm in water. If it disintegrates within 45 minutes, it is considered unsuitable for earthen construction. According to DIN testing procedures, earthen blocks are immersed in water to a depth of 10 cm for a duration of 10 minutes. The resulting mass loss is measured and used as an indicator of erosion resistance. Acceptable limit values are defined depending on the specific field of application (Bauwesen, 2024).

(5) Spray Erosion Test

In this test, water is sprayed onto the block under pressure to measure the depth of material erosion.

(6) Bending tensile strength

Testing flexural tensile strength can be advantageous for assessing handling performance during transport and edge stability. Blocks with low flexural strength are prone to chipping or breaking at the corners when moved on site. The test is typically conducted using a three-point bending setup. For earthen blocks, flexural tensile strength is commonly reported to be approximately 10-20 % of the compressive strength (Minke, 2025; Schroeder, 2016).

(7) Scratch Test

The surface of the block is scratched using a wire brush or a hard object. According to Minke (2025) well-performing blocks should exhibit minimal material loss under this test, indicating sufficient surface hardness.

(8) Sorption Test

To assess moisture uptake from the air, a simple gravimetric test can be performed. A dried specimen is first weighed and then placed in a container or chamber with high relative humidity, for example above a saturated salt solution to simulate high relative humidity. After 12, 24, or 48 hours, the specimen is weighed again. The increase in mass

indicates the amount of water vapour absorbed by the material (Minke, 2025; Schroeder, 2016).

(9) Assessment of thermal behaviour
For an initial evaluation of thermal performance, dry density can be used as a direct indicator. Thermal conductivity values (λ) can then be estimated by referencing tabulated data from the literature corresponding to the measured density range. Lightweight earth with a dry density of approximately 1200 kg/m³ exhibits a thermal conductivity of around 0.47 W/mK, whereas denser earth materials typical of CEB production, with densities near 2000 kg/m³, reach values of approximately 1.1 W/mK (Minke, 2025; Schroeder, 2016).

2.3.10 Target parameters

As an initial reference for defining target values for the subsequent test series, DIN 18945 is referenced. Although it is a German standard, it remains relevant for the Dutch context since in practice, German DIN standards are sometimes used as reference frameworks in neighbouring countries when comparable regulatory guidance is lacking. This standard represents the central product specification for industrially manufactured earthen masonry units and explicitly applies to blocks in which clay is the sole binding agent. A limitation of this normative framework is that it was not developed for mortar-free construction systems. Nevertheless, the performance requirements defined in DIN 18945 particularly regarding strength and hygrothermal behaviour served as a first orientation for establishing preliminary quality benchmarks. The following baseline assumption was established:

A low-rise industrial hall with a maximum height of 6 m, constructed as self-supporting masonry, protected from direct weather exposure but uninsulated and therefore exposed to outdoor temperature conditions.

As the wall is exposed to outdoor temperatures while being shielded from direct rainfall, it falls under usage class 2 according to DIN 18940, which allows for relative humidity levels of up to 90 %. This classification requires at least application class II. More stringent requirements are defined by AC 1b or AC 1a. To this study, AC 1b was adopted as a conservative assumption to ensure frost resistance. The assigned usage class results in an environmental humidity reduction factor of 0.55, meaning that only approximately half of the dry compressive strength of the masonry unit can be considered in design. Consequently, the blocks must achieve an average dry compressive strength of 5.0 N/mm² and a minimum individual value of 4.0 N/mm² under laboratory conditions. To meet these performance requirements, the corresponding dry density of the blocks was expected to lie within a range of approximately 1810 to 2200 kg/m³.

In addition, the masonry units must be able to withstand fluctuations in ambient humidity without surface deterioration, even though they are not exposed to direct rainfall. This requirement is addressed through an erosion resistance test, in which a maximum mass loss of ≤ 5 % after 10 minutes of immersion is permitted. According to DIN 18940, the ratio of effective buckling length to wall thickness must not exceed a value of 27 (h_{ef} / t < 27). In the present case, the effective height h_{ef} was conservatively assumed to be equal to the full wall height h, as no reduction factors were applied due to the absence of mortar in the masonry system. For a wall height of 6 m, this criterion resulted in a minimum required wall thickness of 22.22 cm.

2.3.11 Local soil sources

Rotterdam is situated within the Rhein-Maas delta, shaped by sedimentary deposits originating from the Rhine, the North Sea, and former fluvial landscapes. As a result of this depositional history, three principal material groups were identified:

(1) Clay Sources
Marine clays of the Naaldwijk Formation occur widely around Rotterdam, particularly in the Wormer and Walcheren layers, and range from clayey silt to heavy clay. They are often calcareous and rich in illite and smectite, with higher smectite contents than fluvial clays. This is relevant for swelling behaviour in earthen construction. Fluvial clays from the Echtfeld formation are also present, ranging from sandy loam to heavy clay.

(2) Sand Sources
Marine sands within the Naaldwijk Formation occur in features such as beach ridges and coastal dunes, including the Zandvoort and Schoorl members, and consist mainly of fine to medium sand. In addition, fluvial deposits from the Echtfeld and Beegden formations contain layers of sand ranging from fine to coarse grain sizes alongside clay-rich sediments.

(3) Organic matter
Rotterdam also forms part of the so-called peat district, where layers of the Nieuwkoop Formation are frequently found beneath or interbedded with clay strata. Owing to their high organic content, pure peat deposits are unsuitable for earthen construction (Ritzema & Stuyt, 2015; van der Veer, 2006).

2.3.12 Mortar-free assembly constraints

If unstabilised CEBs are to be developed as mortar-free or interlocking systems, their geometry cannot be considered independently from the material and production process. The material properties and process parameters create a set of constraints that directly inform the geometric design.

(1) Dimensional accuracy
One of the primary challenges lies in achieving sufficient dimensional accuracy. Due to volumetric shrinkage during drying, earth-based mixtures inherently exhibit larger tolerance ranges than fired or cement-based units. As reported by Minke (2025), even relatively dry mixes used for CEB production can show linear shrinkage values of approximately 0.4-2 %. In conventional masonry, dimensional deviations are typically compensated for by mortar layers. However, in mortar-free systems, geometric irregularities can accumulate across successive courses and lead to misalignment (Aboziada et al., 2025). In addition, these geometric inconsistencies between individual blocks result in non-uniform load transmission, with stresses being concentrated at discrete contact points rather than distributed across the full bearing surface. This effect can significantly reduce the axial load-bearing capacity of a wall compared to that of individual blocks. One potential mitigation strategy discussed in the literature is the reduction of moisture content combined with increased compaction pressure, as explored by Bruno et al. (2015). While explicit quantitative evidence linking higher pressure directly to reduced shrinkage remains limited, increased densification leads to closer particle packing, which may reduce susceptibility to moisture-induced structural changes.

(2) Shear resistance
Unstabilised CEBs further impose limitations on the use of conventional interlocking profiles due to their comparatively low shear and tensile strength (Schroeder, 2016). As a result, tooth-like geometries are particularly susceptible to failure and edge breakage under load. Sharp-edged profiles are also prone to chipping during handling and assembly on site, increasing the risk of damage prior to installation (Minke, 2025). While rounded edges can improve robustness and reduce edge failure, they simultaneously restrict the feasibility of more complex interlocking geometries Reddy, (2022) In addition, producing such modified shapes often requires specialized and costly metal moulds, increasing fabrication effort and limiting adaptability.

(3) Manufacturing
The production process itself introduces further constraints. Static presses commonly used are limited by the available compaction force and piston stroke. Variations in material composition or moisture content can therefore result in inconsistencies in block height and mechanical performance, which in turn complicates the assembly of mortar-free systems (Reddy, 2022; Schroeder, 2016).

(4) Capillary action
When water enters the narrow interfaces of an interlocking joint, it can be retained through capillary action (Minke, 2025). In unstabilised earth, this moisture uptake may trigger swelling, which can disrupt the internal structure or compromise the stability of the interlocking mechanism (Reddy, 2022). In the absence of conventional mortar joints, interlocking interfaces may therefore be more susceptible to wind-driven rain unless supplementary sealing measures or protective design strategies are implemented (Schroeder, 2016).

(5) Resistance to lateral loads

The absence of chemical bonding through mortar generally results in reduced resistance to lateral loads, such as wind or seismic actions, compared to conventional masonry. In mortar-free systems, stability under transverse forces relies solely on friction and the geometric interlocking effect between individual blocks. Systems that do not provide full geometric restraint in all directions often require temporary external bracing during construction, as no mortar-induced cohesion is available to stabilize the assembly. This necessity can increase construction time and add complexity to the building process (Aboziada et al., 2025; Tan et al., 2025b).

2.3.13 Literature derived assessment

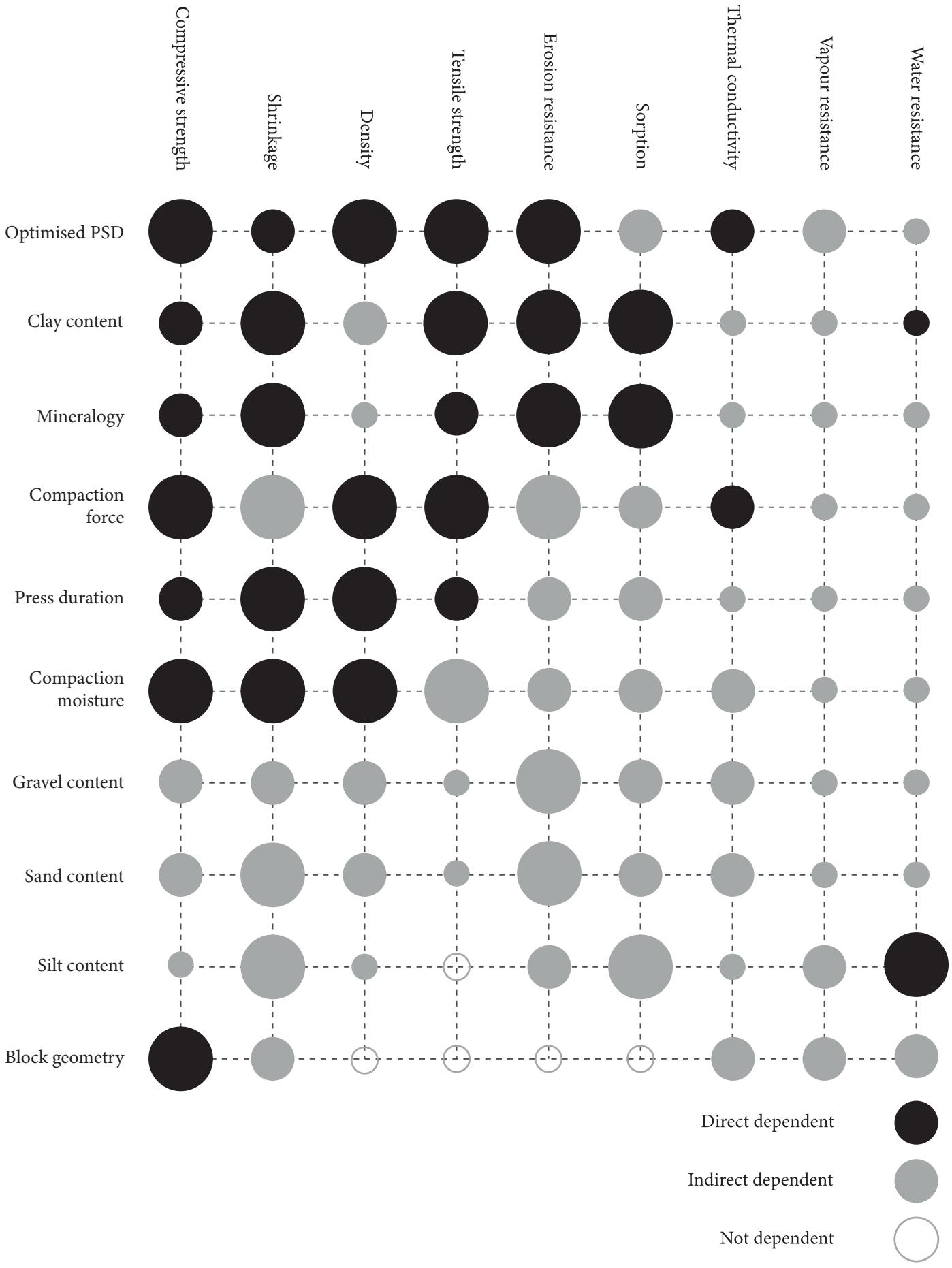

Figure 04: Parameter-performance dependency matrix by the author based on the literature review.

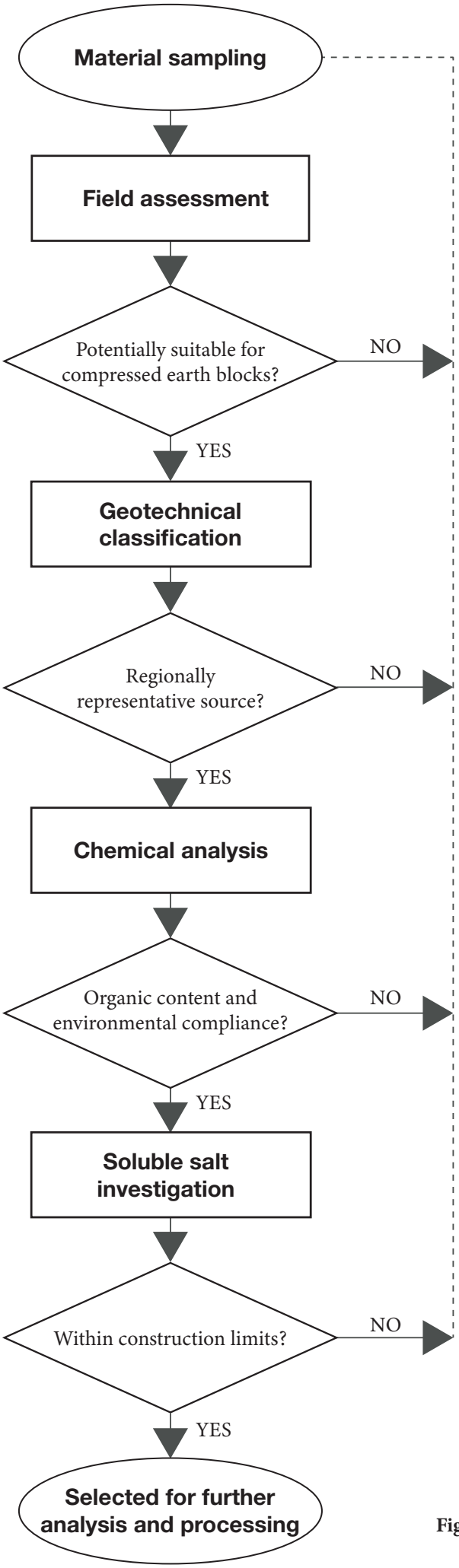

Figure 05: Workflow for soil selection and suitability assessment applied in this study, developed based on literature review.

Figure 06: Stockpiled excavation material from trench digging and pipeline installation works in Rotterdam and Delft.

3. Material characterisation

3.1 Raw binder material

3.1.1 Local clay

The selection of a suitable soil was guided by two primary criteria: local availability within the Rotterdam metropolitan region and methodological transferability, meaning the exclusion of rare geological horizons or highly specific compositions. Rather than defining a preferred composition as a starting point, the investigation focused on identifying which clay-bearing soils are realistically available within the local urban material flows.

(1) Material sourcing

As a primary material source, a soil bank located approximately 10 km from the city centre of Rotterdam, was incorporated into the study. The so called Grondbank functions as temporary storage facility for excavated soils generated by urban construction projects prior to their reuse, treatment, or disposal. The investigated material originated from infrastructure works in Rotterdam and Delft, specifically from excavation activities related to trench digging and pipeline installations. During these operations, clay-rich subsoils were extracted and subsequently transported to the soil bank for interim storage. Both excavation batches consisted of clay-bearing soils and were deposited in adjacent stockpiles (Fig. 06).

According to information provided, the excavation process involved the prior removal of the A-horizon (topsoil layer), followed by the extraction of underlying clay-bearing soils to a depth of approximately 3 m. The excavated material was stored outdoors at the soil bank. However, it was protected from direct precipitation under a roofed structure. For preliminary investigation, an initial sample of 3 kg was collected one day after excavation. Seven days later, an additional bulk sample of approximately 50 kg was retrieved from the depot. This larger batch was composed of sub-samples taken from multiple locations within the stockpile to obtain a more representative material pick. Due to the adjacent storage from Delft and Rotterdam, a strict separation of origin could not be ensured. The material may therefore represent a mixture of both sources. Approximately one month later, a further 30 kg of material was collected to secure additional quantities for testing and to assess the continuity of material supply. At the time of sampling, the depot had been newly filled, and documentation confirmed that the latest material originated from a construction site in Delft.

(2) Legal Framework and Certification

The Besluit Bodemkwaliteit constitutes the central legal framework governing the handling, reuse, and disposal of soil, dredged material, and construction materials in the Netherlands. It is carried out through the BRL guidelines (Beoordelingsrichtlijnen), which function as legally embedded technical assessment standards. They ensure material quality, full traceability, and environmental compliance throughout the handling process. According to official guidance from the Information Point Leefomgeving (IPLO) under the Environmental Management Act (Wet milieubeheer), soil that is excavated and removed from its original location is generally classified as waste. Within this regulatory context, soil banks function not merely as logistical facilities but also as legal interfaces that enable the controlled transition of excavated soil towards an end-of-waste status. In order to obtain legal non-waste classification for excavated soil, the regulations requires comprehensive chemical testing in accordance with the AP04 protocol. Certified soil banks are therefore obligated to analyse each material batch against this standard parameter package. It includes heavy metals (e.g., lead, zinc, cadmium), mineral oils, PAHs and PCBs. In addition, determination of clay and organic matter content is mandatory, as these parameters influence the applicable threshold values for contaminants. Within this framework, the preliminary analyses conducted for recovered material status can already provide a valuable initial indication of material suitability for earth construction. Fortunately, the corresponding certification was subsequently made available by the soil bank during the research process.

Figure 07: Freshly exposed spade section.

Figure 09: Soil bank depot.

Figure 08: Deposited excavation material, characterised by large cohesive clay clods.

Figure 10: Spherical clay sample after drop test.

3.2 Preliminary assessment

At the time of first inspection, the chemical certification was not yet available. Independent preliminary testing was therefore conducted to assess the material's suitability for CEB production. Even where AP04 certification is available, reliance on regulatory compliance alone is not always sufficient for performance-oriented material evaluation. Such pre-assessment steps are recommended irrespective of sourcing pathway and are even more essential when excavated soils are obtained directly from construction sites.

3.2.1 Field assessment

The stockpiled material exhibited visible heterogeneity in surface coloration, with darker zones corresponding to moisture-rich or more recently excavated material and lighter areas indicating partial air drying. No visible humus-like constituents were detected. The deposit was characterised by large clay clods (Fig. 08). When sectioned with a spade (Fig. 07), freshly exposed surfaces appeared smooth and slightly glossy. Cutting resistance was both audible and tactile, indicating the presence of granular fractions that produced minor scratch marks on the tool surface. Coarser particles were primarily observed at the outer surfaces of the clods, while the interior remained highly cohesive and plastic. No gravel fractions were identified, and granular components were limited to sand-sized particles. In its earth-moist condition, the material was readily mouldable and exhibited high plasticity. This preliminary assessment indicates a clay-rich or so called "fat" soil.

In CEB production, such characteristics suggest favourable binder properties. However, a high clay fraction may reduce workability due to clod formation during processing and typically requires substantial tempering with sand to achieve an appropriate clay proportion and particle size distribution (Minke, 2025; Reddy, 2022). In this case further testing was required to determine whether the observed formability results primarily from clay or is influenced by silt. In field assessments, silt may be misinterpreted as clay, as wet silt can exhibit apparent cohesion due to capillary forces and may feel smooth and plastic when moulded. In contrast, clay derives its binding capacity from the electrochemical properties of its minerals and their plate-like structure, which silt lacks (Minke, 2025; Schroeder, 2016). However, the observed spade section provided an initial indication of a dominant clay fraction.

3.2.2 Smell test

For application as a building material, the absence of organic matter is crucial, as it reduces the dry compressive strength and increases water absorption of the future building material (Schroeder, 2016). At the time of examination, the sample was in an earth-moist condition. Olfactory assessment revealed no putrid or musty odour, indicating the absence of significant organic decomposition processes and suggesting a low organic content. Furthermore, no characteristic sulphurous smell was detected.

3.2.3 Simple tests

For an initial assessment of the material, a series of simple tests were conducted:

(1) Spherical sample

First, the earth-moist sample was formed into a sphere with a diameter of approximately 40 mm using the palm of the hand and was subsequently dropped from table height. The specimen flattened upon impact without disintegrating (Fig. 10), indicating high cohesion and, consequently good binding capacity in the moist state. The procedure was repeated with an air-dried specimen. The sample likewise withstood the impact without fragmentation, suggesting high dry-strength.

Figure 11: Jar sedimentation test after complete settling, illustrating the separation of the soil into distinct grain-size fractions

(2) Jar Sedimentation

For this test, 100 g of the earth-moist sample were placed in a glass with 750 ml of de-mineralised water. Subsequently, the jar was shaken until all clay clods were fully dispersed. It was then left undisturbed to allow sedimentation to occur. The heavier sand particles settled first at the bottom of the container, and their very fine grain size could already be observed during this process. After 24 hours, the water remained distinctly turbid, and slight turbidity persisted even after 72 hours. This prolonged suspension indicated a high proportion of very fine particles and a potentially elevated clay content (Schroeder, 2016). The fully settled layers after the jar sedimentation test are visible in Fig. 11.

(3) Biscuit sample

Cylindrical specimens with a diameter of 40 mm and a height of 10 mm were formed using a plastic tube. After drying, the specimens exhibited a reduced diameter of 35 mm, corresponding to a shrinkage of 12.5 %. This pronounced shrinkage once more indicated a high clay content but also exceeded by far the acceptable range for CEB production, where final mixtures typically aim for shrinkage values below 2% (Reddy, 2022). Consequently, it was already clear, that substantial sand addition will be required for the final mix design. Further manual tests relevant to assessing the suitability of the excavated material for earthen construction are embedded within the geotechnical classification and determination of the dominant fraction according to EN ISO 14688.

3.2.4 Key findings

Preliminary testing provided an essential basis for assessing the excavated material. Field observations and simple manual tests indicated a clay-rich, highly plastic soil with strong binding capacity in both the moist and dry state, while the smell test suggested a low organic content. At the same time, the observed shrinkage and high apparent fine content showed that the material in its untreated state was not directly suitable for CEB manufacture as substantial tempering would be required. The next steps were therefore defined to further investigate the material under laboratory conditions, with particular focus on verifying the organic content, determining the clay and silt fractions, and confirming the contamination status. In addition, geotechnical classification was identified as a necessary step in order to relate the material to its likely geological formation and horizon, thereby providing further insight into its characteristic properties, regional availability, and representativeness.

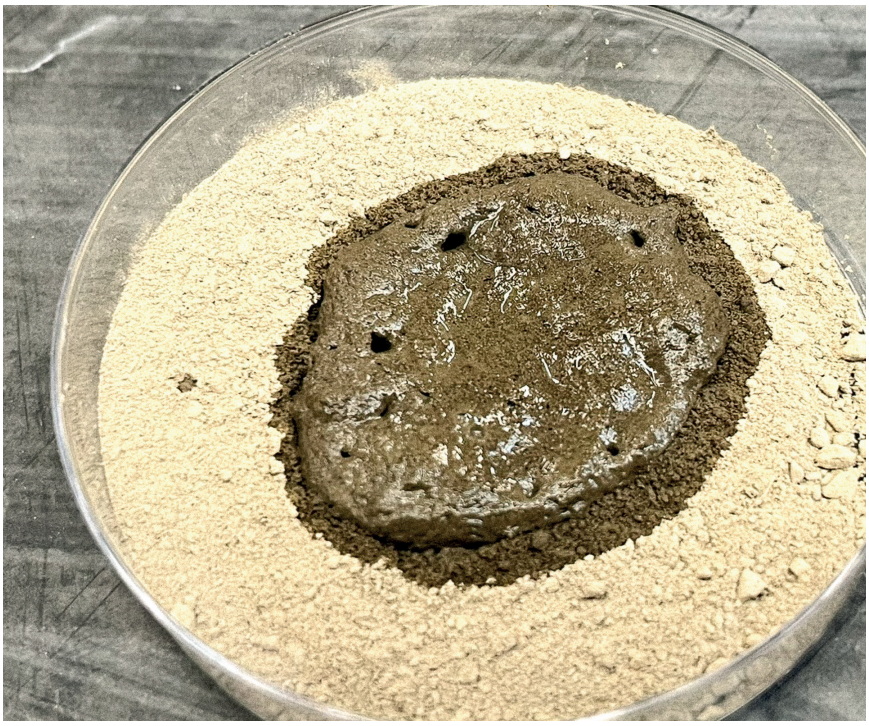

Figure 12: Natural carbonate assessment using 10% acetic acid solution, showing strong and sustained effervescence.

Figure 13: Excavated material showing occasional lighter grey streaks and isolated darker grey zones.

Figure 14: Fine granular fractions of the investigated material examined in a Petri dish against transmitted light.

3.3 Geotechnical classification

Following the initial pre-assessment, a soil classification was conducted in accordance with EN ISO 14688. This harmonised European norm provides a structured framework for soil classification based on visual-manual assessment and basic laboratory investigations.

3.3.1 Designation and description

For soil designation, the decision flowchart provided in EN ISO 14688 was applied. Based on this framework, the sample was first identified as a soil of natural origin, formed through geological processes. The material did not exhibit low density and showed no visible signs of organic constituents and was therefore classified as a mineral soil. No particles larger than 63 mm were present in the sample. In its moist condition, it displayed cohesive behaviour and was readily knead-able, indicating that it belongs to the fine-grained soil fraction.

(1) Colour

The colour of the material was determined in situ in accordance with EN ISO 14688, based on the observation of a freshly cut surface under full daylight conditions: Colour tone according to first description: blue. Colour tone according to second description: greyish. Brightness according to third description: light.

(2) Naming convention

The soil was classified clay, slightly sandy, highly silty.

(3) Estimation of grain size distribution

For particle size differentiation, the comparative criteria defined in the standards were applied: Fine sand is described as smaller than semolina. However, individual grains remain visible to the naked eye. As the observed granular fractions were very fine, a small quantity of the material was distributed in a Petri dish and examined against transmitted light (Fig. 14). This procedure allowed the identification of individual sand particles and supported the classification as weakly fine-sandy.

(4) Mineral composition

It is stated that the mineralogical composition of soils is generally not of primary relevance for conventional geotechnical engineering applications. However, as outlined in the preceding chapters, mineralogical composition can be a critical parameter when evaluating suitability for earthen construction. For this reason, X-ray diffraction (XRD) analysis was performed to determine the mineralogical composition of the material. The results are presented in Section 3.4.

(5) Consistency

The soil can be indented up to approximately 10 mm and can be moulded with light finger pressure. Based on these observations, it is classified as “soft”.

(6) Organic content

The excavated material exhibited occasional lighter grey streaks as well as isolated darker grey zones (Fig. 13). While such colour variations may suggest minor organic influences, colour alone is not sufficient to confirm the presence of organic matter. To further assess potential humus content, an extended olfactory test was conducted by soaking the material in a sealed glass container. No putrid or musty odour was detected, indicating the absence of significant organic decomposition. The AP04 laboratory analysis later quantified the organic matter content at 2.2 % and 2.4 % for the respective samples, supporting the findings of the qualitative field assessment.

(7) Natural lime content

This aspect is particularly relevant for examined region, where soils with elevated calcium carbonate contents commonly occur in and around coastal areas. Such deposits are often of marine origin. The presence of shell fragments within the sample supports this interpretation. For the qualitative assessment of carbonate content, a deviation from the standard procedure was applied: instead of 10 % hydrochloric acid as specified in the norm, a 10 % acetic acid solution (vinegar essence) was used. As acetic acid is a weaker reagent, the expected reaction intensity may be lower compared to hydrochloric acid. However, in this case, a strong and sustained effervescence was observed even with acetic acid (Fig. 12). The soil was therefore classified as highly calcareous. The dry strength of the material may additionally be attributed to calcium carbonate acting as a natural cementing agent (Schroeder, 2016).

Figure 15: Manual plasticity assessment showing cracking and crumbling of the soil thread at the rolling limit.

Figure 16: Texture assessment of the earth-moist material, indicating a cohesive, slightly sticky and rubber-like consistency.

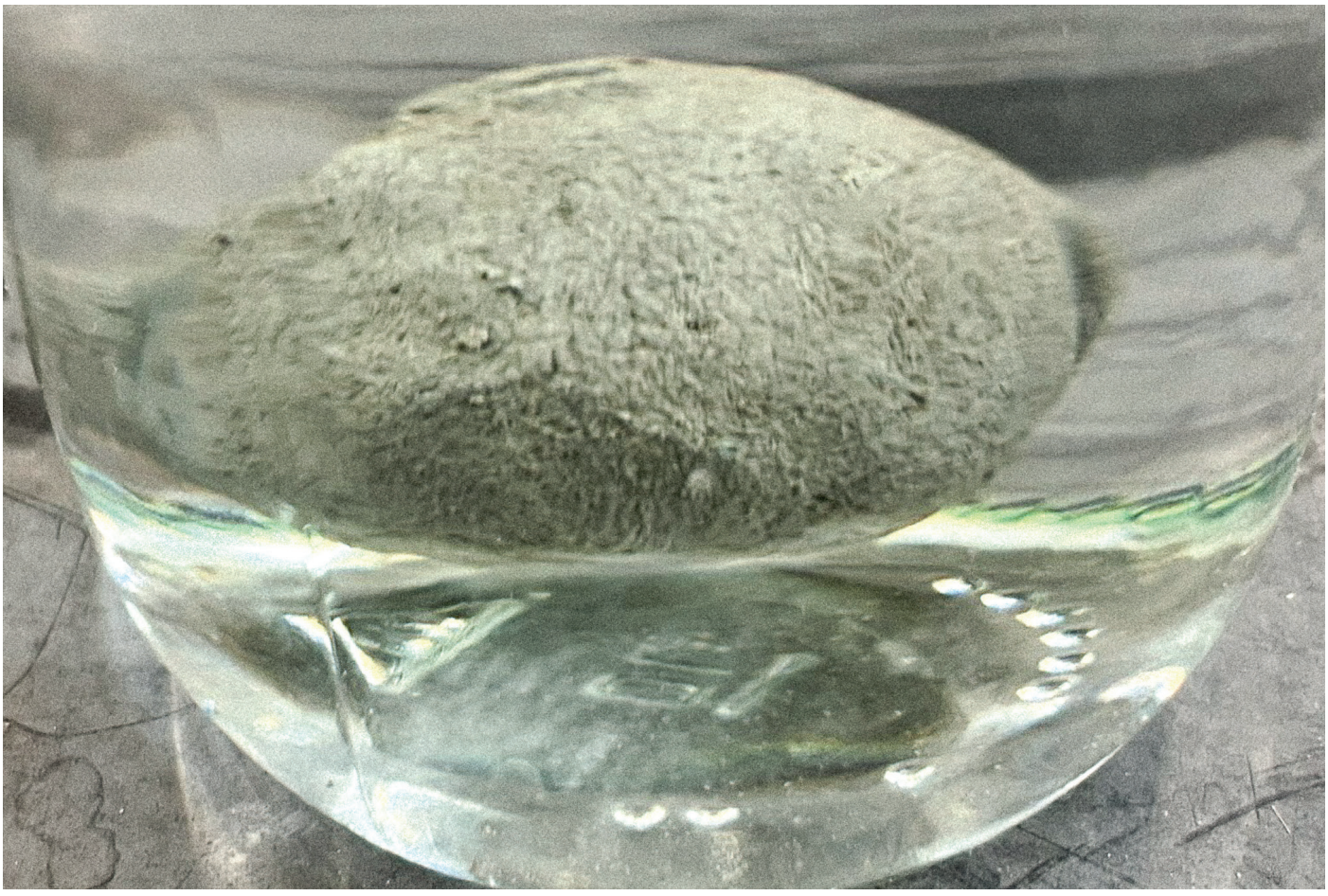

Figure 17: Immersion test of a spherical specimen in demineralised water, showing no significant disintegration after 180 min.

3.3.2 Dominant fraction

As silt and clay particles cannot be distinguished visually with the naked eye, EN ISO 14688 prescribes a series of manual tests to determine the dominant fine fraction.

(1) Dilatancy

For the assessment, the material was kneaded into a spherical shape until a soft but non-sticky consistency was achieved. If necessary, small amounts of water were added. The sphere was then flattened and subjected to horizontal shaking and repeated firm impacts against the opposite hand. The rate of water emergence at the surface was observed. No visible water release occurred during the test, which indicated a dominant clay fraction.

(2) Toughness

The sample was rolled between the palms into a thread of approximately 3 mm in diameter. It was ensured that the material was not excessively moist. Where necessary, slight air drying was allowed prior to testing. The pressure required for rolling was assessed as low. The tensile strength of the formed thread was determined to be moderate, while its mould-ability was high. These characteristics indicated clay as the dominant constituent.

(3) Plasticity

To material was repeatedly rolled and kneaded until the rolling limit was reached, indicated by cracking, crumbling, or disintegration of the thread (Fig. 15). An extended rolling time was required before this limit occurred. Accordingly, the soil was classified as having high plasticity, which further confirmed clay as the dominant fraction.

(4) Dry Strength

Several spherical specimens with a diameter of approximately 12 mm were formed and air-dried. After, the specimens could no longer be disintegrated by simple finger pressure. The dry strength was therefore classified as very high. This pronounced strength may, in addition to the clay content, be partly attributed to the elevated calcium carbonate content acting as a cementing component.

(5) Grittiness

In its earth-moist condition, no granular particles could be detected when the material was rubbed between the fingertips (Fig. 16). The mass appeared cohesive, slightly sticky, and rubber-like in texture. When rubbed with the addition of water, fine sand particles became perceptible. However, the material simultaneously developed a more soapy and smooth texture. Due to this overlapping sensory response, no unequivocal conclusion could be drawn solely from this test regarding the relative proportion of fine sand and clay. When the prepared test spheres were cut open, a smooth and slightly glossy surface was observed, consistent with earlier field observations. This surface characteristic supported the interpretation of clay as the dominant fraction.

(6) Behaviour in water

A spherical specimen with a diameter of approximately 40 mm was immersed in de-mineralised water. Even after 180 minutes, no significant signs of disintegration were observed (Fig. 17). However, when exposed to running tap water, the material could be removed relatively easily from the surface, which may indicate the presence of a notable silt fraction. Based on these contrasting observations, no unequivocal conclusion could be drawn.

(7) Behaviour in air

The sample was spread in a thin layer onto a smooth plastic surface using a spatula. Drying was classified as slow, as a substantial portion of the material remained moist even after 60 minutes. After complete drying, characteristic desiccation cracks became visible, indicating volumetric shrinkage typical of clay-rich soils.

(8) Cohesion

A spherical specimen with a diameter of approximately 25 mm was formed and compressed plastically between the fingers. The sample retained its integrity during deformation, with minor cracking occurring only at the outer edges. This behaviour indicated pronounced cohesion, consistent with a clay-dominated fine fraction.

(9) Conclusion

Following the execution of these manual tests, the dominant fine fraction was classified as clay. To obtain a quantitative assessment of its composition, a hydrometer test was subsequently conducted.

Figure 18: Wet sieving of the dispersed sample through a 0.063 mm sieve, using a spatula and distilled water to separate the sand fraction.

Figure 19: Oven-drying of the sand fraction retained on the 0.063 mm sieve

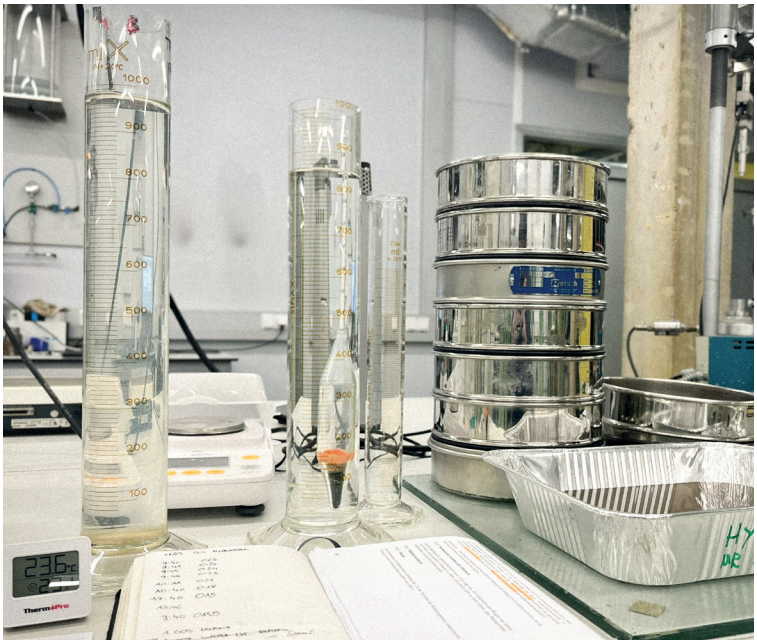

Figure 20: Hydrometer test setup with three graduated cylinders: soil suspension, reference solution and distilled water for meniscus correction.

3.3.3 Particle size distribution (PSD)

Given the fine-grained nature of the material, the particle-size distribution within the silt and clay fractions had to be determined using a hydrometer analysis. This method is based on Stokes' law, which relates the settling velocity of particles in a fluid to their diameter, the density difference between particle and fluid, and the viscosity of the fluid. The sand fraction and its PSD were determined through prior wet sieving. The test was conducted in accordance with BS 1377, Part II.

(1) Sample preparation

The sample was oven-dried at 105 °C for 24 h until constant mass was reached. For sample preparation, 50.11 g of dry soil was then immersed in 100 ml of dispersing solution for 48 h and stirred repeatedly to facilitate particle separation. Immediately before testing, the suspension was mixed for 10 min using a high-speed stirrer.

(2) Test setup

For the test, three graduated cylinders were prepared (Fig. 20). The first, a 1000 ml cylinder later containing the soil suspension. The second, a 1000 ml reference cylinder filled with 100 ml of dispersing solution and 900 ml of distilled water. A third cylinder, containing 800 ml of distilled water, used to determine the meniscus correction of the hydrometer. In addition, a thermometer was placed alongside the test setup to monitor temperature fluctuations during the measurement.

(3) Procedure

The dispersed sample was first passed through a 0.063 mm sieve to separate the sand fraction. Sieving was carried out using a spatula and a wash bottle filled with distilled water to ensure that all fine particles were washed through the sieve (Fig. 18). The material retained on the 0.063 mm sieve was transferred to an evaporating dish and oven-dried at 105°C (Fig. 19). The fraction passing the sieve was collected in the first sedimentation cylinder and filled up to the 1000 ml mark with distilled water. The cylinder was then sealed with a rubber stopper and inverted end-over-end at least 60 times over a period of 120 s. Once the cylinder was returned to the upright position, the stopwatch was started, the hydrometer was inserted, and the readings were recorded. Measurements were taken after 0.5, 1, 5, 8, 30, 60, 480, and 1440 min at the top of the meniscus. After the first two readings, the hydrometer was removed after each measurement and placed in the reference cylinder containing the dispersing solution. It was then reinserted into the suspension 30 s before each subsequent reading to avoid disturbance of sedimentation between readings. Furthermore, the meniscus correction was determined separately in the 800 ml cylinder. During the test, the ambient temperature was monitored and remained stable at 23.0 ± 0.2 °C.

(4) Data correction and calculation

All hydrometer readings, R_h' were taken at the upper rim of the meniscus. Accordingly, a density reading of 1.025 was recorded as $R_h' = 25$. The meniscus correction, C_m, was determined as 0.5. Corrected hydrometer readings, R_h, were therefore calculated as:

$$R_h = R_h' + C_m$$

Thus, a recorded reading of $R_h' = 26$ corresponds to a corrected value of $R_h = 26.5$. For calibration of the hydrometer, the volume of the bulb, V_h, was determined as 70 ml by immersing the hydrometer in distilled water and measuring the corresponding volume displacement. The bulb length, h, was 159 mm, while the distance from the bulb neck to the lowest calibration mark, N, was 15 mm. The spacing between successive calibration marks was measured as 20 mm. The distance between the 100 ml and 1000 ml scale markings of the sedimentation cylinder, L, was determined as 306 mm. The variable H denotes the distance from the neck of the bulb to the respective graduation mark and was determined separately for each major calibration mark from the initial offset N and the mark spacing. Based on these values, the effective depth, H_r, corresponding to each major corrected hydrometer reading, R_h, was calculated according to:

$$H_r = H + \frac{1}{2}\left(h - \frac{V_h}{900}L\right)$$

As an example, a corrected hydrometer reading of $R_h = 26.5$, corresponding to H = 29mm, yields an effective depth of $H_r = 96.6$mm. Using the effective

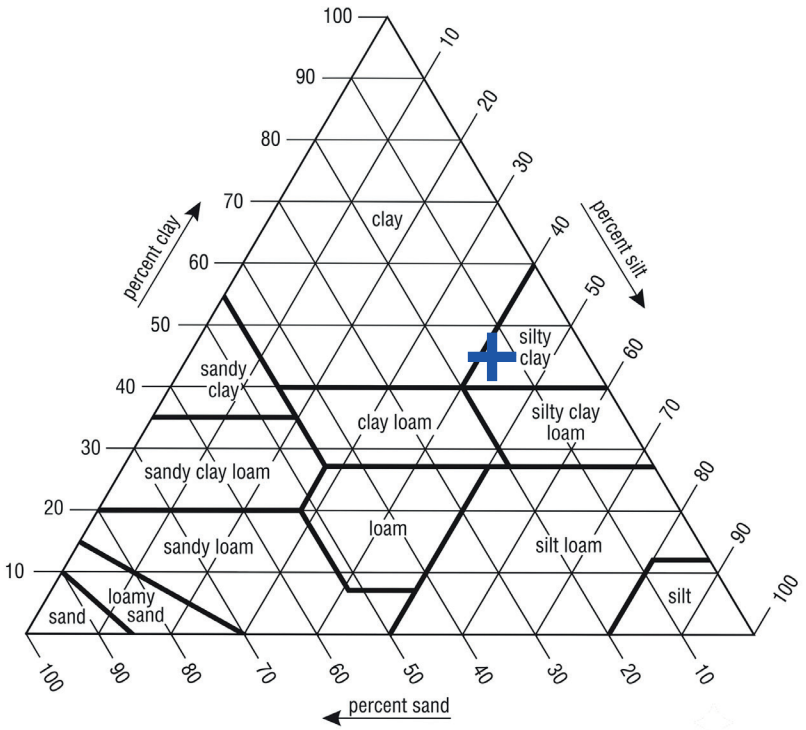

Figure 21: USDA soil texture triangle used for textural classification based on the relative proportions of sand, silt and clay.

Time [h]	Time [min]	R'_h [-]	$R'_h + R_0$ $R_0=C_m+R'_0$ [-]	Grain size [mm]	T [°C]	H_r [mm]	η [-]	Passage [%]
0	0.5	27.00	25.50	0.0573	23.0	94.60	0.93583	85.65
0	1	26.00	24.50	0.0414	23.0	98.60	0.93583	82.89
0	5	24.00	22.50	0.0192	23.0	106.60	0.93583	76.12
0	8	23.00	21.50	0.0155	23.0	110.60	0.93583	72.74
0	30	21.00	19.50	0.0083	23.0	118.60	0.93583	65.97
1	0	18.00	16.50	0.0061	23.0	130.60	0.93583	55.82
8	0	15.00	13.50	0.0023	23.0	142.60	0.93583	45.67
24	0	13.50	12.00	0.0013	23.0	148.60	0.93583	40.60

Figure 22: Overview of the hydrometer analysis, showing the recorded hydrometer readings over time together with the corresponding calculated particle diameters and mass percentages.

depth, the equivalent particle diameter, D (mm), was subsequently calculated according to:

$$D = 0.005531\sqrt{\frac{\eta H_r}{(\rho_s - 1)t}}$$

A dynamic viscosity of water of 0.9353 mPa.s was adopted for the test temperature of 23 °C. As the particle density was not determined experimentally, a standard value of 2.65 Mg/m³ was assumed for the calculations, following (Batjes & Van Oostrum, 2023). This value can be adopted as a representative average for mineral soils, although actual values may vary depending on mineralogical composition and organic matter content. Accordingly, for an effective depth of H_r = 96.6 mm and a sedimentation time of t = 1 min, the equivalent particle diameter was calculated as 0.041 mm. Subsequently, the modified hydrometer reading, R_d, was calculated as:

$$R_d = R_h' - R_0'$$

where R_0' denotes the hydrometer reading taken at the upper meniscus rim in the 1000 ml reference cylinder containing the dispersing solution. Accordingly, for a value of R_h' = 26, the modified reading was calculated as R_d = 24.0. Thereafter, the percentage by mass, K, of particles smaller than the corresponding equivalent particle diameter, D (mm), was calculated according to:

$$K = \left(\frac{100\rho_s}{m(\rho_s - 1)}\right)R_d$$

For a dry sample mass of 50.11 g, this resulted in 82.89 % of particles finer than the previously calculated equivalent diameter of 0.041 mm. An overview of the calculated particle diameters and their corresponding mass percentages is presented in Fig. 22.

(5) Results

Based on the hydrometer results, the fraction below the clay-size threshold of 0.002 mm was calculated as 44.0 %. The dry sand fraction retained during sieving amounted to 6.81 g, corresponding to 14.3 % of the total sample mass. Based on these results the silt fraction was determined as 41.7 %. In addition, the fine fraction remaining in the sedimentation cylinder was subsequently oven-dried at 105°C and weighed to verify that no material had been lost during the analysis. A very illustrative textural classification could be obtained using the USDA soil texture triangle, which is based on the relative proportions of sand, silt, and clay (Fig. 21). Accordingly, the soil could be classified as silty clay. These results did not contradict the previously conducted manual tests for determination of the dominant fine fraction in accordance with ISO 14688. In this system, soil designation is not governed primarily by particle-size distribution, but by the plastic behaviour of the fine fraction. Accordingly, the soil may be described as clay, slightly sandy, highly silty.

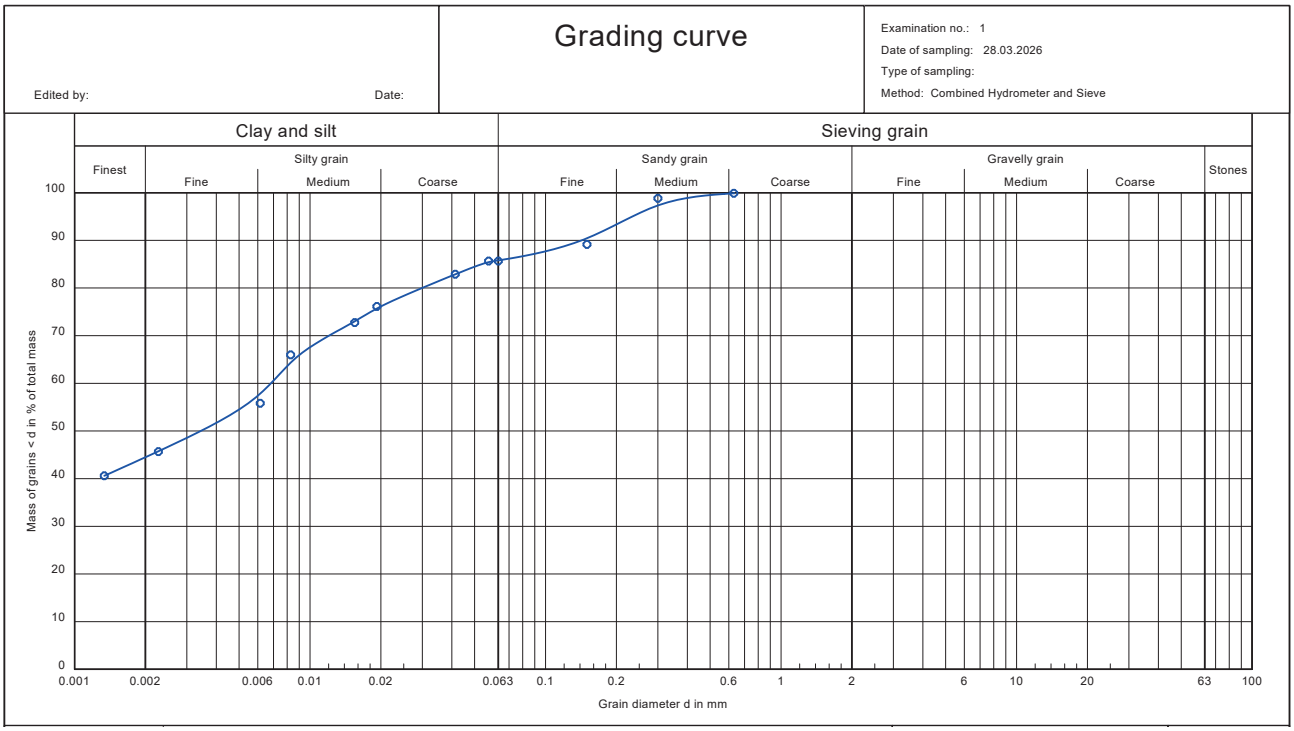

Figure 23: Combined particle-size analysis of the soil based on wet sieving and hydrometer testing.

ANALYSECERTIFICAAT

Projectcode	:	[redacted]	
Uw project omschrijving	:	[redacted]	
Opdrachtgever	:	[redacted]	
Uw Monsterreferenties			
9159342 = Mm3-Mm3a (100-300)			
9159343 = Mm3-Mm3b (100-300)			
Opgegeven bemonsteringsdatum	:	[redacted]	
Ontvangstdatum opdracht	:	[redacted]	
Startdatum	:	[redacted]	
Monstercode	:	[redacted]	
Uw Matrix	:	**AP04**	**AP04**
AP04 : Monstervoorbewerking			
aangeleverd monsterhoeveelheid	g	**13842**	**13981**
AP04 : Algemeen onderzoek - fysisch			
A droge stof	%	**68,4**	**71,9**
A organische stof	% (m/m ds)	**2,2**	**2,4**
A lutum	% (m/m ds)	**28,1**	**21,3**
AP04 : Anorganisch onderzoek - metalen			
A barium (Ba)	mg/kg ds	**55**	**46**
A cadmium (Cd)	mg/kg ds	**0,30**	**< 0,20**
A kobalt (Co)	mg/kg ds	**6,9**	**6,5**
A koper (Cu)	mg/kg ds	**15**	**8,0**
A kwik (Hg) (niet vluchtig)	mg/kg ds	**0,09**	**< 0,05**
A lood (Pb)	mg/kg ds	**30**	**12**
A molybdeen (Mo)	mg/kg ds	**< 1,5**	**< 1,5**
A nikkel (Ni)	mg/kg ds	**22**	**20**
A zink (Zn)	mg/kg ds	**66**	**43**
AP04 : Organisch onderzoek - niet aromatisch			
A minerale olie	mg/kg ds	**< 35**	**< 35**

Figure 24: Extract from the AP04 certificate provided by the soil bank, showing the organic matter and clay contents determined from samples obtained through the soil bank's internal sampling procedure.

3.3.4 Experimental outcome

Following the initial pre-assessment, classification according to EN ISO 14688 and the subsequent combined particle-size analysis (Fig. 23) confirmed the material as clay, slightly sandy, and highly silty. It is characterised by its colour, shell fragments, high carbonate content, and cohesive behaviour. Quantitative analysis further showed that the material contains approximately 44.0% clay, 41.7% silt, and only 14.3% sand. Although this composition provides favourable binding capacity, it also confirmed that the soil is unsuitable for CEB production in its untreated state. For suitability as an unstabilised brick material, the clay fraction must therefore be reduced to approximately 10-20 % (Reddy, 2022).

Any tempering strategy should therefore place particular emphasis on introducing coarser particles that improve the overall particle-size distribution. However, the simultaneously high silt content complicates this adjustment, as increasing the proportion of the clay-rich source material also raises the total fine content, which may become detrimental to the targeted grading. As an optimal particle-size distribution requires the fine fraction to remain within a limited range, the challenge was in identifying a clay content close to the lower acceptable threshold that would still ensure adequate matrix binding without excessively increasing the proportion of fines.

With the availability of the AP04 analysis, organic matter contents below 2.5 % were confirmed for both samples, supporting the general suitability of the material for earthen construction, although local variation remains possible. The clay contents reported in the AP04 analysis were somewhat lower, at 21.3 % and 28.1 % (Fig. 24), which already demonstrates the extent to which this parameter may vary between individual samples. This deviation may in part be explained by differences in sampling position, as the hydrometer analysis was carried out on a batch that likely included a more clay-rich near-surface portion of the stockpile. The classification of the material as a highly plastic, clay-rich soil nevertheless remains unchanged. To achieve a more controllable and consistent clay content for future production, it may therefore be beneficial to determine the clay fraction on homogenised powder batches after processing. On this basis, the subsequent research steps were defined to address the remaining uncertainties identified in the material assessment. These included analysis of the mineralogical composition to inform the mix design, determination of the geological origin and further evaluation of the chemical analysis to ensure the material's safe use.

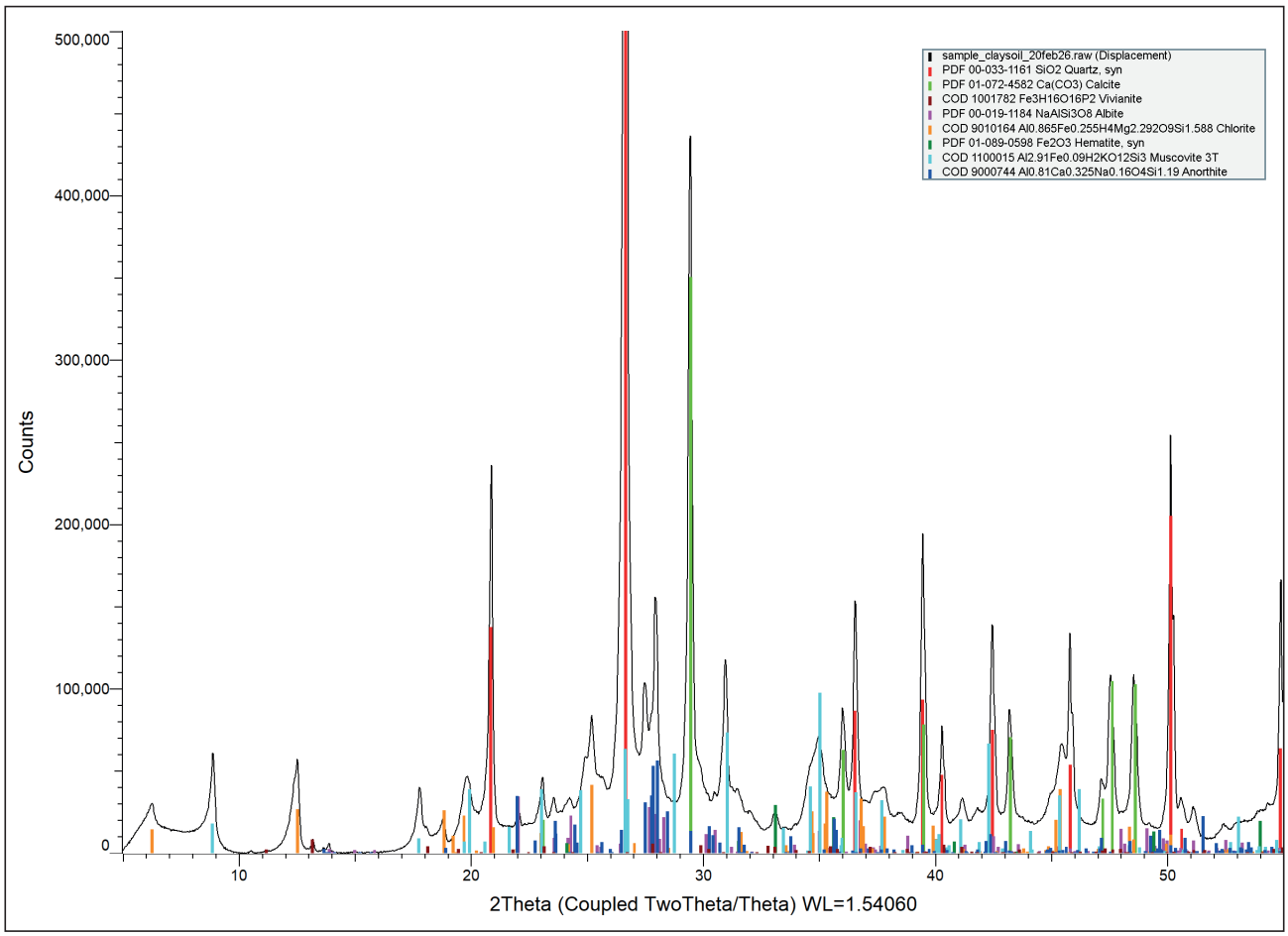

Figure 25: X-ray diffraction pattern of the investigated sample showing the identified crystalline phases.

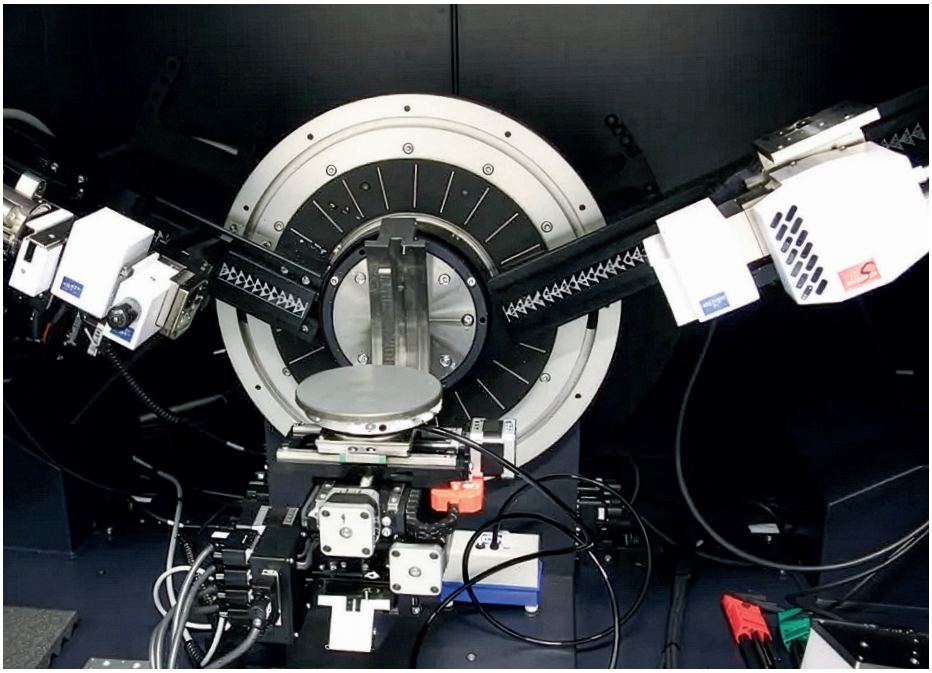

Figure 26: Bruker D8 X-ray diffractometer used for crystalline phase analysis. Reproduced from TU Delft, Kavli Nanolab Delft.

3.4 Compositional analysis

Knowledge of the mineralogical composition of the material forms the basis for defining suitable mix proportions and aggregate additions, as the type and proportion of clay minerals govern plasticity, shrinkage behaviour, and mechanical performance (Reddy, 2022).

3.4.1 Mineralogical analysis

X-ray diffraction (XRD) is an analytical method used to investigate the crystallographic structure of materials (X-ray Facility Group, TU Delft, 2023). Throughout the analysis, the sample is irradiated with an X-ray beam while a detector records the scattered radiation as a function of the diffraction angle (2θ). When the X-rays interact with the periodically arranged atoms of the crystal lattice, they are scattered in different directions. A peak in the diffraction pattern occurs only when the scattered waves interfere constructively. This condition is described by Bragg's law, which relates the diffraction angle to the spacing between atomic lattice planes. In the resulting diffractogram (Fig. 25), the measured X-ray intensity is plotted on the vertical axis against the diffraction angle on the horizontal axis. The x-axis is primarily used for qualitative phase identification, as each mineral possesses characteristic lattice spacings that produce peaks at specific diffraction angles. The y-axis represents the intensity of the scattered radiation, reflected in the height and area of the peaks. Heavier atoms with a larger number of electrons scatter X-rays more strongly than lighter elements, which can result in higher peak intensities. Consequently, peak height alone cannot be directly interpreted as a measure of mass fraction, as it is influenced by crystallinity effects and differences in scattering behaviour between minerals (Waseda et al., 2011).

(1) Sample preparation

For the analysis, a representative sample was collected, dried in an oven at 60 °C until mass constancy was reached, and subsequently ground into powder using a disc mill for approximately 5 seconds. For the XRD analysis of powder materials, a minimum sample amount of approximately 10 mg was required to prepare a specimen.

(2) Setup

Crystalline phase analysis was conducted using a Bruker D8 (Fig. 26) diffractometer. The instrument utilizes Cu Ka radiation and is equipped with a Lynxeye position-sensitive detector. Measurements were performed on the rotating sample over a range of 5° to 120° (20).

(3) Data evaluation

The collected data were analysed using Bruker DiffracSuite software. Initially, background subtraction was performed. The resulting peak pattern was then compared with reference patterns from the ICDD (PDF-5) and COD databases. Not all small peaks could be identified. These signals likely indicated minor impurities or trace constituents that fell below the reliable detection threshold of the employed reference databases. Due to the large number of different phases present in the sample, it was not possible to perform reliable quantitative analysis. Consequently, the diffractogram allows only qualitative interpretation of the mineral composition. The identified crystalline compounds are indicated in the legend of Fig. 26. The following section outlines the detected phases and their relevance for earth construction.

(a) Quartz, SiO_2

Is one of the most abundant minerals in the earth's crust and represents the sand fraction within the sample. It forms the rigid skeletal framework of the soil matrix. As an inert mineral phase, quartz does not contribute to binding but acts as a granular filler that reduces plasticity and shrinkage while improving dimensional stability (Schroeder, 2016).

(b) Calcite, $CaCO_3$

Represents the carbonate content of the soil and confirms the preliminary field observations, including the acid reaction test and the occurrence of shell fragments. In the context of CEB production, calcite can act as a natural tempering component while reducing the susceptibility of the material to disintegration in water. This behaviour was already indicated in the preliminary experiments, particularly in the immersion test of the clay sphere. It may further contribute to the formation of a carbonate matrix between particles such as silt and sand, which can impart cement-like

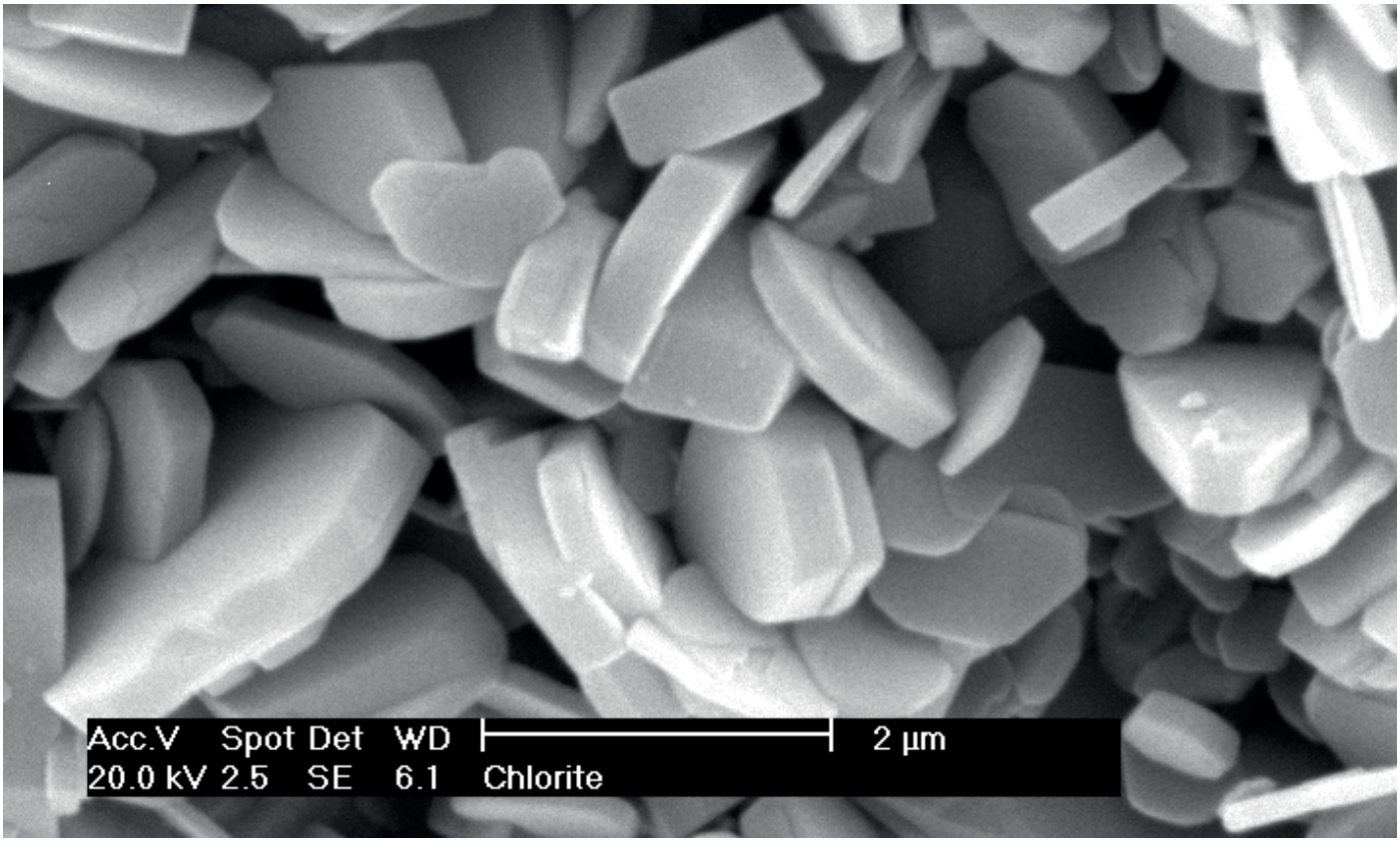

Figure 27: SEM micrograph showing the plate-like crystal morphology of chlorite, the only clay mineral initially identified by XRD in the investigated soil sample. Image reproduced from the 'Images of Clay Archive' of the Mineralogical Society of Great Britain & Ireland and The Clay Minerals Society.

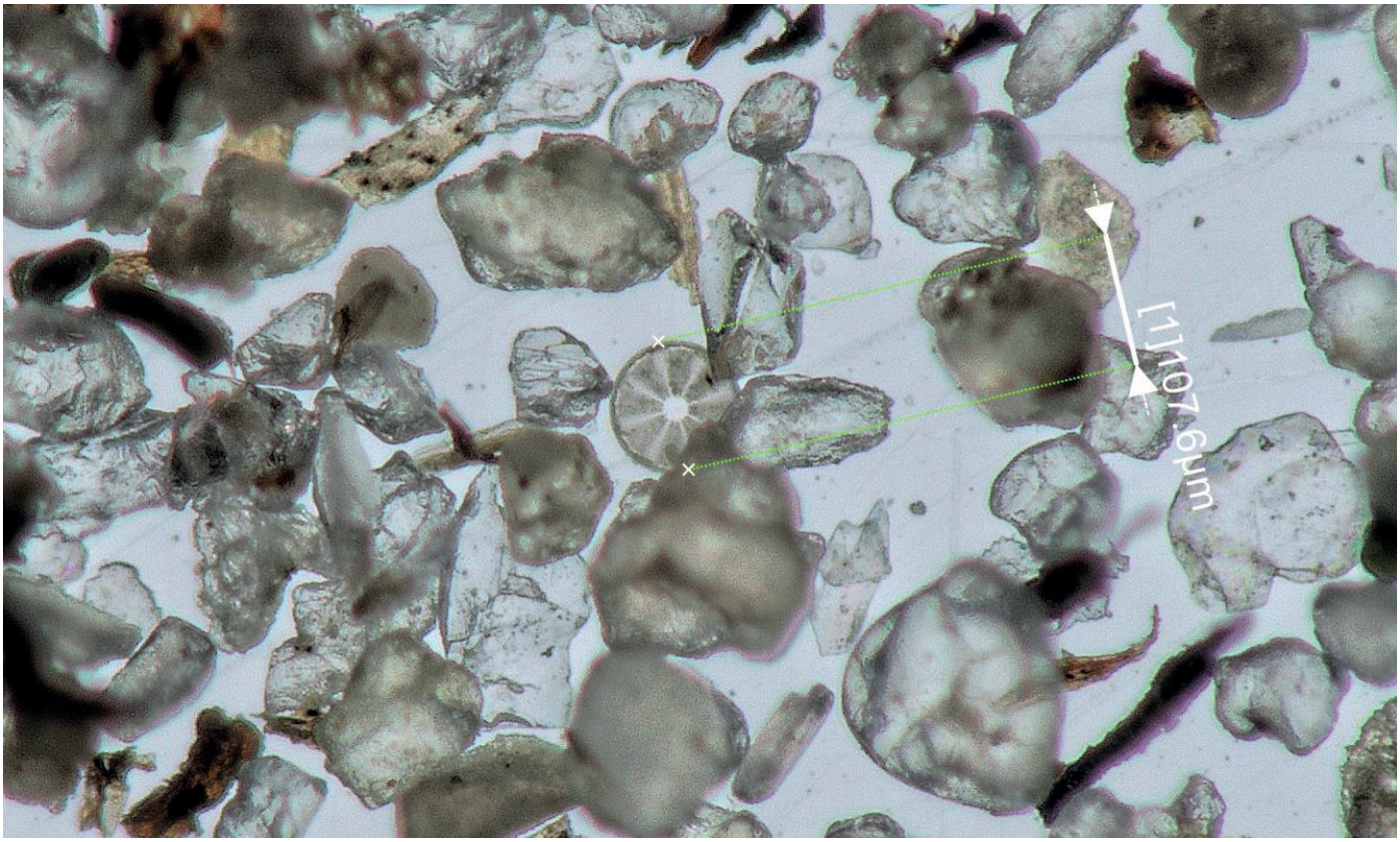

Figure 28: Diatom skeleton observed in the sand fraction of the investigated soil, providing an additional indication of marine or alluvial origins, consistent with the identified occurrence of vivianite.

properties. Furthermore, it may have contributed to the high dry compressive strength observed in the preliminary tests.

(c) Vivianite, $Fe_3H_{16}O_{16}P_2$

Is a hydrated iron phosphate mineral that typically forms under oxygen-deficient conditions. It is commonly associated with water-saturated environments which indicates marine or alluvial origins. This interpretation was further supported by the observation of diatom skeletons during microscopic examination of the sand fraction (Fig. 28). Vivianite is known to undergo rapid oxidation, resulting in a characteristic colour change from pale tones to deep blue or greenish black. (Hongu et al., 2021; McGowan & Prangnell, 2006). This behaviour was clearly observable during sample extraction. The oxidation could also provide a possible explanation for the dark streaks observed in the material, which might otherwise be interpreted as indications of high organic content. However, the subsequent chemical analysis revealed an organic matter content below 2.5 %, supporting the interpretation that these colour variations are related to mineralogical processes rather than organic contamination. As the mineral is not discussed in the detailed mineralogical analyses of standard reference works on earthen construction, it can be assumed that it does not play a significant role in the technical performance.

(d) Albite, $NaAlSi_3O_8$

Belongs mineralogically to the feldspar group and represents common primary rock-forming minerals in soils. Within the soil matrix they function as part of the granular framework together with minerals such as quartz and calcite. As they do not exhibit intrinsic binding capacity, feldspars act as tempering components in clay-based systems and contribute to the reduction of plasticity. Geologically, feldspars gradually transform into clay minerals through chemical weathering processes, during which alkali ions are leached and secondary minerals such as kaolinite may form. Clay-rich soils therefore often contain finely ground feldspar remnants originating from this weathering process (Schroeder, 2016).

(e) Chlorite, $Al_{0.865}Fe_{0.255}H_4Mg_{2.292}O_9Si_{1.588}$

Is a naturally occurring clay mineral that can be found alongside the main minerals in soil. Under scanning electron microscopy (SEM), chlorite typically exhibits a plate-like crystal morphology (Fig 27). In terms of water reactivity, chlorite is generally classified as having moderate swelling behaviour. At the same time, platelet contacts in Chlorite-rich systems tend to be more point-like rather than extensive surface contacts. Compared to clay minerals such as kaolinite, which often form larger face-to-face contact areas, this geometry results in comparatively weaker mechanical bonding within the matrix. Chlorite exhibits a moderate cation exchange capacity (3 - 40 m_{eq}/100 g). The card-house structure, however, provides an advantage for drying behaviour, as it offers lower resistance to water migrating toward the surface, allowing comparatively faster drying with reduced shrinkage deformation (Reddy, 2022; Schroeder, 2016).

(f) Hematite, Fe_2O_3

Is an iron oxide mineral commonly associated with brick-red to cinnamon-brown soil colours. As these characteristic reddish tones were not observed in the investigated material, either in the wet or dry state, hematite is likely present only in minor quantities or as a trace constituent. At such minor concentrations, it is not expected to have a significant influence on the performance of the material. However, in soils where hematite occurs in higher proportions, it can contribute to increased strength and weathering resistance by forming a stable, water-insoluble mineral framework within the soil matrix (Reddy, 2022; Schroeder, 2016).

(g) Muscovite, 3T $Al_{2.91}Fe_{0.09}H_2KO_{12}Si_3$

Is a mica mineral that commonly occurs in natural clay soils. In its primary form, muscovite belongs to the non-plastic mineral fraction, like quartz and feldspar. It does not contribute to binding but acts as a structural filler within the soil matrix. From a geological perspective, muscovite can serve as a precursor mineral that, through chemical weathering, may transform into clay minerals such as illite (Schroeder, 2016).

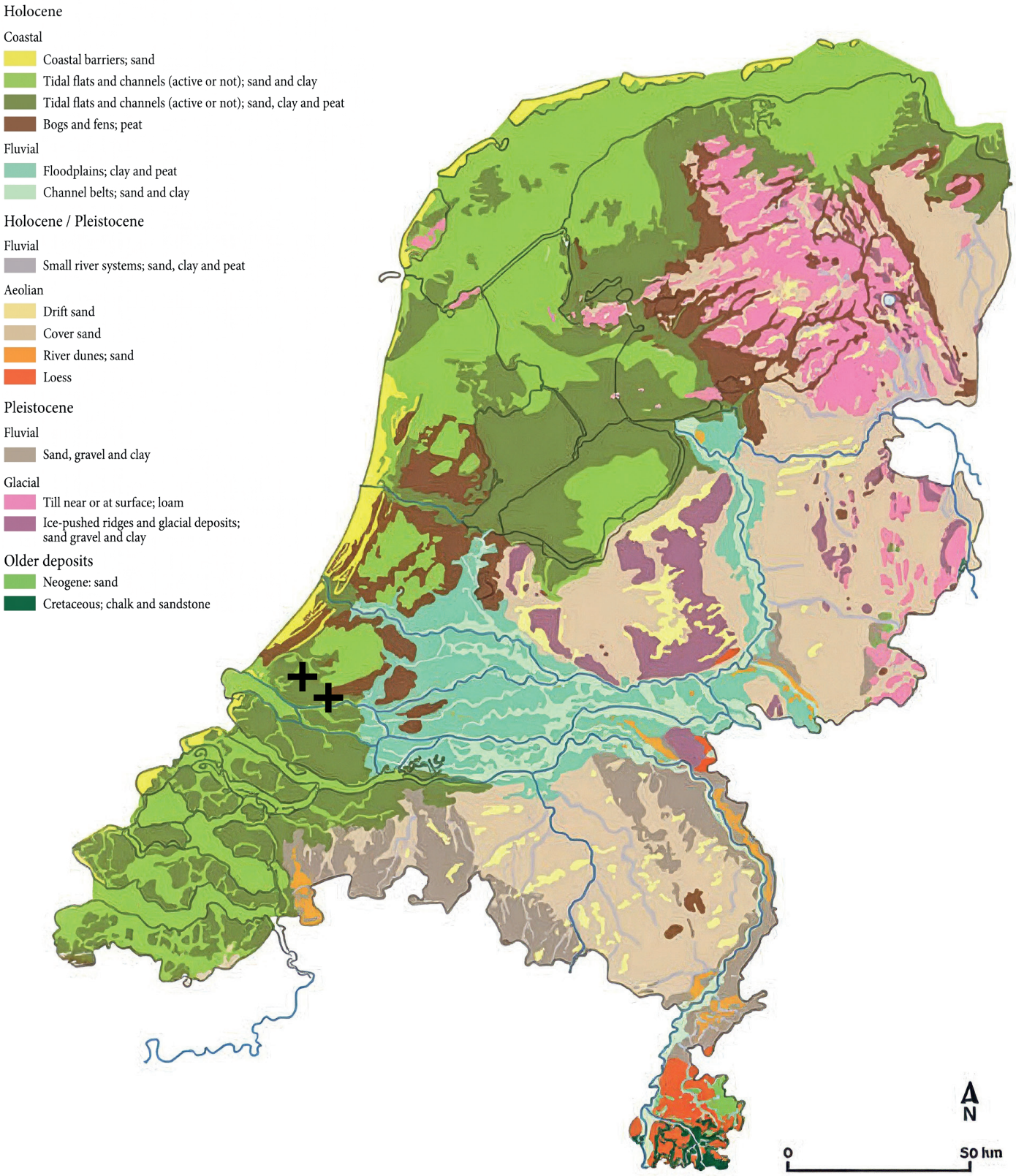

Figure 29: Surface geology of the Netherlands, with the excavation sites in the Rotterdam–Delft region indicated. Adapted from Griffioen et al. (2016, Fig. 3), licensed under CC BY 4.0.

(h) Anorthite, $Al_{0.81}Ca_{0.325}Na_{0.16}O_4Si_{1.19}$
Is a calcium-aluminium silicate. Mineralogically, anorthite belongs to the feldspar group. While Albite represents the sodium-rich end member of the feldspar series, Anorthite corresponds to the calcium-rich variant. It can therefore also be classified as non-plastic mineral without intrinsic binding capacity (Diko-Makia & Ligege, 2020; Masuda, 2020).

(4) Limitations
When comparing the XRD analysis with geological reference literature, limitations became apparent that explain why certain clay minerals and the actual mineralogical composition were not fully reflected in the results. The absence of Smectite and Illite clay minerals can most likely be attributed to methodological limitations of the applied XRD procedure. As described by (Griffioen et al., 2016), a simple standard powder analysis is not sufficient for reliable clay mineral identification. For an accurate analysis, samples typically require extensive pre-treatment to remove carbonates, organic matter, as well as iron and manganese hydroxides. Furthermore, it is stated, that only the < 2 µm fraction should be analysed. Furthermore, the analysis should be conducted using oriented preparations to significantly improve detection quality. This is necessary because the plate-like layered silicates of clay minerals remain randomly oriented in conventional powder samples. Additional treatments such as exposure to ethylene glycol vapour at approximately 80 °C and heating of the sample to 550 °C are also mentioned in the literature. Based on these methodological requirements, it could be concluded that the applied sample preparation did not allow for the reliable detection of smectite or illite signals. Without chemical cleaning, fraction separation, thermal treatment, and particle orientation, these minerals may remain effectively undetected. Nevertheless, the analysis still provided valuable insights into the geological origin of the material, allowing the probable presence of such clay minerals to be inferred based on established geological reference literature.

3.4.2 Geological origin

The excavated material originates from a depth of approximately 1 to 3 metres in the Rotterdam-Delft region. Geologically, this area lies within the coastal and alluvial plains of the western Netherlands (Fig 29). These plains are covered by a seaward-thickening wedge of Holocene sediments, which formed when the sea invaded the western and northern parts of the Netherlands. Stratigraphically, the material could most likely be assigned to marine and estuarine deposits of the coastal plain, which strongly interact with the Rhine-Meuse delta (Griffioen et al., 2016). According to the geological mapping by van der Veer (2006), the material presumably represented the coastal clayey deposits of the Naaldwijk Formation. If the excavation had been located further east, the material could also have been originated from fluvial clayey deposits of the Echteld Formation. However, given the location and the mixed origin of the material from Rotterdam and Delft, this was considered unlikely. Marine deposits of this formation are commonly described as calcareous, silty and clayey sediments inter-layered with fine sand, which was consistent with the observations from the preliminary assessment. In the coastal plains, groundwater in the upper 30 metres is typically oxygen-deficient, preventing the oxidation of iron minerals. This was reflected in the characteristic grey colouration of the material. Furthermore, the presence of black traces, consisting of organic matter and amorphous iron sulphides, strongly supported a marine to estuarine origin (Griffioen et al., 2016). Based on this information, the composition of the sample could be further interpreted beyond the previously identified mineral phases.

(1) Extended clay mineralogy
Griffioen et al., (2016) refer to the studies of Zeelmaekers (2011) and Adriaens (2014) regarding the proportional occurrence of clay minerals. According to these sources, the reported ranges (wt%) for three Holocene coastal samples were: illite 48-57 %, smectite 34-45 %, kaolinite 9-11 %, and chlorite 1 %. Although the number of samples was not statistically representative, these values provided an indication of the likely presence and approximate proportions of the clay minerals.

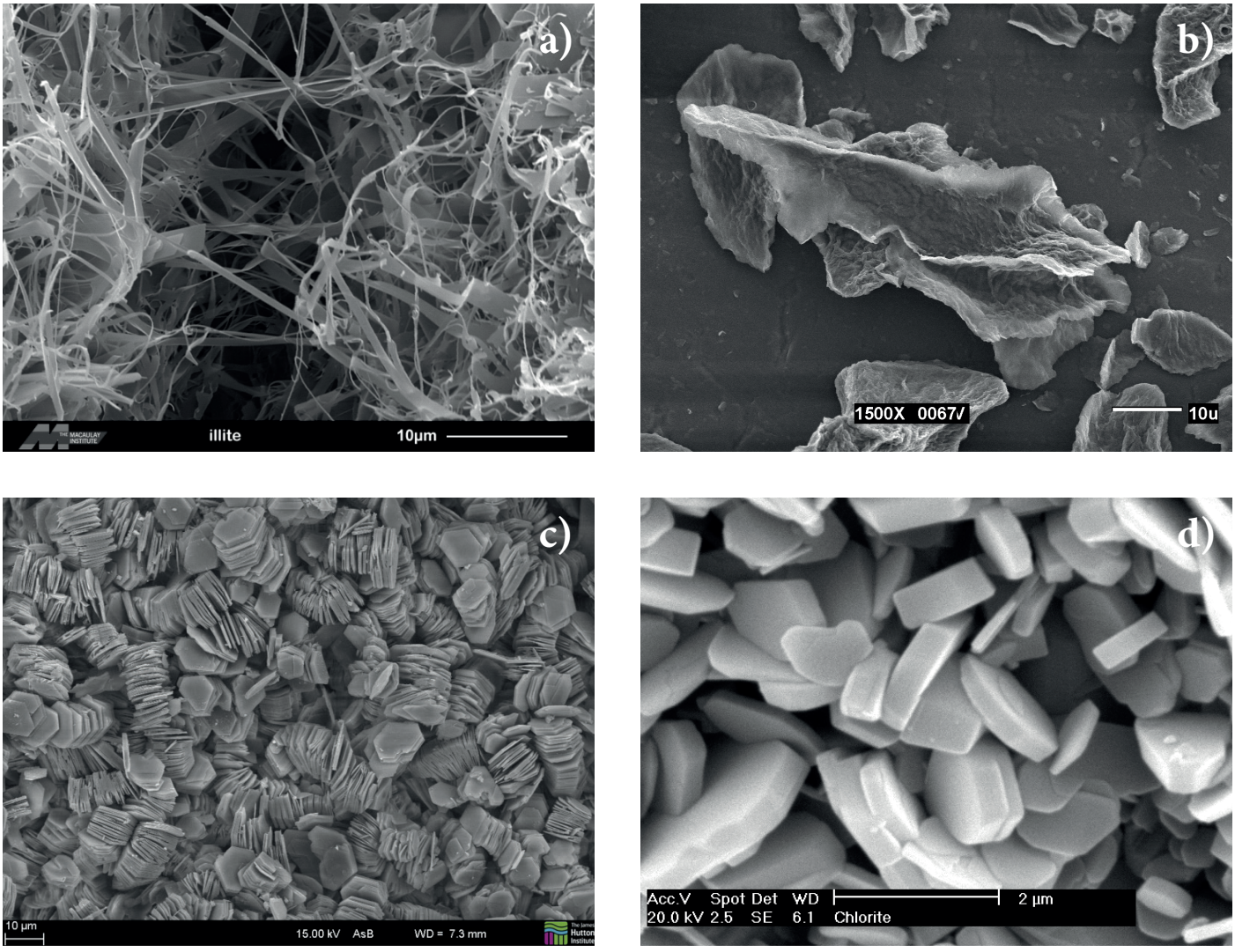

Figure 30:SEM micrographs of the clay minerals identified in the investigated soil, showing characteristic particle morphologies: (a) Illite with needle-like particles, (b) Smectite with needle- to crystal-like particles, (c) Kaolinite with plate-like particles and planar contact surfaces (d) Chlorite with plate-like particles and point contacts between individual plates. All images reproduced from the 'Images of Clay Archive' of the Mineralogical Society of Great Britain & Ireland and The Clay Minerals Society.

(a) Illite, $Al_2Si_4O_{10}(OH)_{12}$
Is a naturally occurring clay mineral that can be found alongside the main minerals in nearly all types of cohesive soils. It is a three-layer clay mineral that primarily forms through the weathering of mica. The parent mineral muscovite was already identified in the previous XRD analysis. Illite exhibits a needle-like structure (Fig. 30) and shows moderate swelling and shrinkage behaviour. Like chlorite, it has a moderate binding capacity, reflected in a cation exchange capacity of approximately 3-40 m_{eq}/100 g (Schroeder, 2016).

(b) Smectite, (Montmorillonite, $[Al_2(OH)_2](Si_2O_5)_2$)
Is also a three-layer clay mineral and can exhibit a needle-like structure similar to illite. However, it is characterised by extremely high swelling capacity and very strong binding properties. This behaviour is associated with its high cation exchange capacity of approximately 60–150 m_{eq}/100 g (Schroeder, 2016).

(c) Kaolinite, $[Al_2(OH)_4](Si_2O_5)$
Is a two-layer clay mineral with a plate-morphology and predominantly planar contact surfaces. Compared to chlorite, it shows a lower binding capacity, reflected in its cation exchange capacity of approximately 0-15 m_{eq}/100 g. Its swelling behaviour is generally regarded as moderate.

(2) Regional characteristics
(Griffioen et al., 2016) also refer to a study by (Van Gaans et al. 2007), which describes the percentiles of pyrite, reactive iron, organic matter, and carbonate contents (wt%) in several Dutch marine formations. For the Naaldwijk Formation, 231 samples from Holland were analysed. In this context, the P50 value represents the median, meaning that 50 % of the samples show equal or lower values, while the P90 value indicates that 90 % of the samples fall below this threshold. For pyrite, the P50 value is 1.8 wt%, while the P90 value reaches 3.7 wt%. Reactive iron shows a P50 value of 1.24 wt% and a P90 value of 2.66 wt%. Organic matter contents are reported with a P50 of 1.78 wt% and a P90 of 4.02 wt%. The carbonate content reaches a P50 of 13.07 wt% and a P90 of 18.98 wt%.

(a) Pyrite, FeS_2
Is an iron sulphide mineral commonly associated with marine environments. Its formation is linked to the presence of sea- or brackish water, which introduces dissolved sulphate into the sediment. Dead organic matter serves as a substrate for sulphate-reducing bacteria, which promote the formation of iron sulphides under oxygen-deficient conditions. Griffioen et al., (2016) further note that the dark dis-colorations already observed during the initial material screening are often closely associated with organic matter and frequently consist of amorphous iron sulphides or manganese oxides, which represent precursor phases to pyrite.

The presence of pyrite is a critical issue in regards of the soil use as a construction material. Once pyrite-bearing clay is exposed to oxygen, reactions are initiated that can lead to the formation of sulphuric acid. If the carbonate content of the soil is insufficient to neutralise this acidity, the pH may drop substantially. Under such acidic conditions, clay minerals become unstable and may undergo hydrolytic decomposition. For earthen construction, this can result in a significant loss of plasticity, binding capacity, and structural integrity. In the present case, however, the high carbonate content of the sample is expected to buffer this process to an extent, so that the immediate risk for CEB production was considered lower. At the same time, this buffering effect gave rise to a secondary concern. The sulphuric acid formed during pyrite oxidation can react with calcium carbonate to form gypsum. As this process is associated with evaporation and local over-saturation, gypsum may crystallise preferentially in drying cracks and pore spaces. In earthen materials, this can lead to white efflorescence and, in more severe cases, to volumetric changes and cracking. A further consequence of pyrite oxidation is the release of iron, which may subsequently oxidise and cause uncontrolled dis-coloration in rust-brown, ochre, or, in extreme cases, pale yellow tones. Interestingly, geological observations from the Netherlands describe marine soils that, despite a high pyrite content, did not oxidise in air or did so only with considerable delay. Griffioen et al., (2016) refer to geological studies, such as Harmsen (1954), which

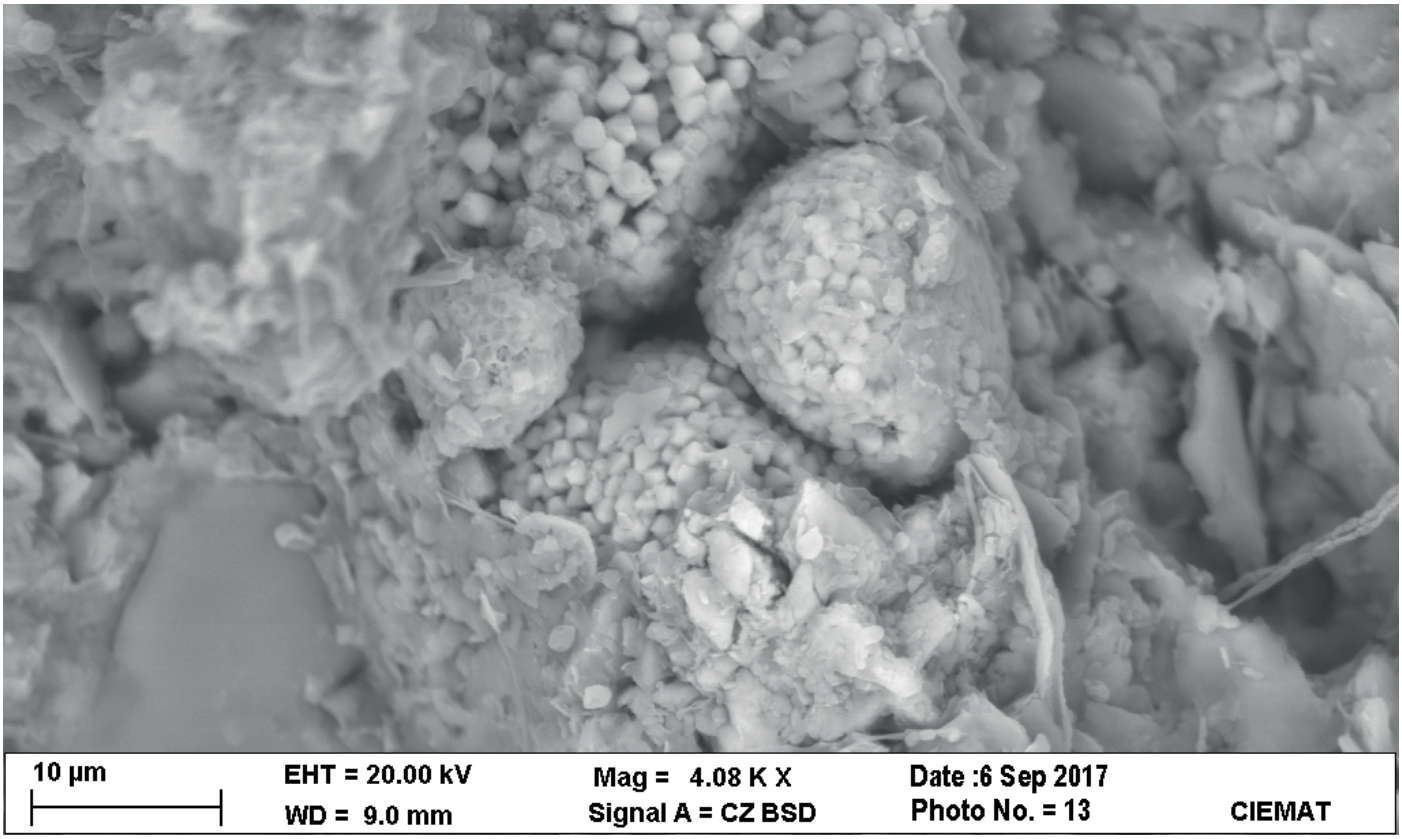

Figure 31: SEM micrograph of pyrite showing characteristic framboidal morphology. Image reproduced from the 'Images of Clay Archive' of the Mineralogical Society of Great Britain & Ireland and The Clay Minerals Society.

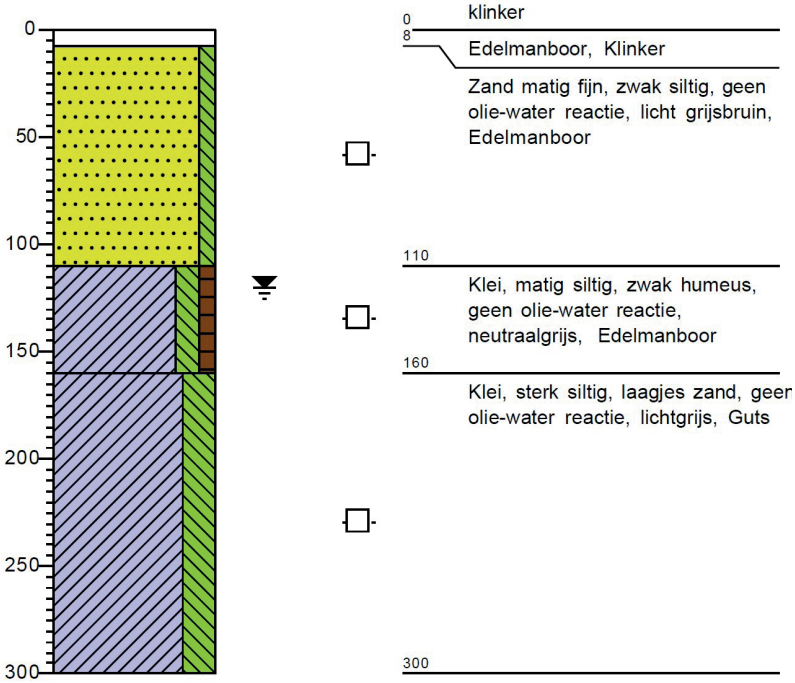

Figure 32: Borehole section indicating the approximate sampling depth of the investigated material, providing context for the possible leaching of marine pore salts.

showed that some old and well-aerated polder soils still contained significant amounts of pyrite that would otherwise have been expected to oxidise long ago. This apparent interruption of the reaction has been attributed to the formation of insoluble iron (III) phosphates, which inhibit further reactivity. A further observation, highly relevant to CEB production, is that geological research indicates that pyrite oxidation occurs primarily along larger cracks, channels, and root passages. This raised the question of how great the oxidation risk would be in a highly compacted earth block without shrinkage cracks. For conventional earthen construction, however, the presence of pyrite (Fig 31) and, by extension, sulphate salts is generally regarded as a direct exclusion criterion. Strict limit values apply, such as a maximum sulphate content of 0.10 wt% for earth blocks and mortars according to DIN 18945.

(b) Reactive iron

Unlike pyrite, it does not generate sulphuric acid during oxidation. For example, the oxidation of siderite results primarily in the formation of iron oxides and dissolved CO2. Therefore, neither significantly consumes the carbonate buffer, nor destabilises the clay mineral structure, nor promotes the formation of expansive gypsum (Griffioen et al., 2016). In the context of earthen construction, the associated risk was therefore considered to be primarily aesthetic, due to the development of discolouration.

(c) Organic content

According to ISO 14688, soils with an organic content of 2-6 % of the dry mass are classified as slightly organic. In addition, the clay-rich base material intended for CEB production was expected to be further tempered with aggregates, which reduced the relative proportion of organic matter even further. On this basis, the soil was considered uncritical for use in earthen construction. Nevertheless, local peaks in organic content may occur at layer boundaries, as marine clays are often closely inter-bedded with organic horizons (Griffioen et al., 2016). Such zones may, however, be identified visually during excavation and separated on site to recover more pure clay material for construction.

(d) Free salts

In the geological reference study consulted, Griffioen et al. (2016) did not quantify the exact concentrations of readily soluble marine salts, such as sodium chloride, present as free salts in the pore water. Nevertheless, given that this horizon was formed in a marine to estuarine coastal environment, whose original seawater likely had a high salinity, it could reasonably be assumed that the clay-rich deposits of the formation contain appreciable amounts of readily soluble salts derived from entrapped marine pore water. The present salt content of the earth material depends strongly on whether the deposit has remained geologically undisturbed or has already been partly leached by later rainfall infiltration or groundwater flow. Van Baaren et al. (2017) further explained that the pronounced local variation is primarily a consequence of the very low permeability of clay. Following the construction of dykes and the reclamation of land, the continuous inundation by seawater ceased, while infiltration by rainwater gradually began to freshen the system from above. Despite this process, parts of these sediments have remained saline or brackish to the present day due to the hydrological inertia of clay.

For CEB production, this may represent a significant concern, as strict limit values also apply to such salts in earthen construction. According to DIN 18945, the total content of construction-damaging salts must not exceed 0.12 wt.%. This is because moisture can transport dissolved salts through the earth block, where they crystallise at the surface. Such crystallisation may lead to efflorescence and, in more severe cases, impair the structural integrity of the material (Schroeder, 2016). However, no visible salt efflorescence was observed during the initial preliminary tests. This suggests either that the material has already been substantially leached by rainwater, or that it has not yet been exposed to a sufficient number of wetting and drying cycles for salt crystallisation to become visible.

Parameter	Measured value (max) [mg/kg]	Corrected value (standard soil)' [mg/kg]	Limit value (Class AW) [mg/kg]	Assessment
Barium (Ba)	55	Not applicable	(1)	Compliant
Cadmium (Cd)	0.30	0.37	0.60	Compliant
Cobalt (Co)	6.9	6.3	15	Compliant
Copper (Cu)	15	16.3	40	Compliant
Mercury (Hg)	0.09	0.09	0.15	Compliant
Lead (Pb)	30	31.7	50	Compliant
Nickel (Ni)	22	20.2	35	Compliant
Zinc (Zn)	66	67.2	140	Compliant
Mineral oil	< 35	< 159	190	Compliant
Total PAHs (10)	0.35	0.35	1.5	Compliant
Total PCBs (7)	0.005	< detection limit	0.020	Compliant

Figure 33: Comparison of the measured and standard-soil-corrected concentrations of the analysed constituents with the threshold values of the Dutch Soil Quality Regulation (2022, Annex B, Table 1) for the soil quality class, agriculture/nature.

3.4.3 Environmental analysis

The chemical evaluation of the excavated material was based on the AP04 analysis provided by the soil bank. As a reference framework, the Dutch Soil Quality Regulation 2022 was applied, specifically Annex B, Table 1, which defines the quality requirements for the highest soil quality class, 'agriculture/nature'. To assess compliance with these threshold values, the soil-specific background parameters first had to be considered to correct the laboratory results in accordance with Annex G. For Sample 01, the organic matter content was reported as 2.2% and the clay content as 28.1%, whereas Sample 02 showed an organic matter content of 2.4% and a clay content of 21.3%. The measured concentrations were subsequently converted using the prescribed soil correction formula:

$$G_c = G_m * \frac{(A + B*25 + C*10)}{(A + B*\%clay + C*\%organic)}$$

Here, G_c denotes the corrected value and G_m the measured value. Taking zinc as an example, the following boundary parameters were adopted from Table 2: A substance-specific base constant of A = 50, a substance-specific constant for the clay correction of B = 3, and a substance-specific constant for the correction of organic matter of C = 1.5. This resulted in a standard-soil-corrected concentration for Sample 01 of 67.15 mg/kg, which was well below the limit value of 140 mg/kg. The same calculation was carried out for all constituents of the analysis, as summarised in Fig. 33.

The assessment showed that the examined contaminant parameters were present at very low concentrations, allowing the soil to be assigned to the highest quality class. It should be noted, however, that the AP04 analysis was based on material with a lower clay content than the batch characterised in this study. Since the measured values remained sufficiently below the relevant limit values, this difference was not considered critical for the material evaluation within the scope of this research. From an environmental perspective, the material was therefore considered uncontaminated and suitable for reuse.

3.4.4 Synthesis

The XRD analysis formed the basis for understanding the mineral framework of the soil. It provided direct insight on both the structural composition of the horizon and its depositional history. Quartz, feldspars, and muscovite constituted the non-plastic mineral skeleton, while calcite verified the high carbonate content previously indicated by shell fragments and the acid reaction test. Minerals such as vivianite further pointed to formation under water-saturated, oxygen-deficient conditions and thus supported interpretation of a marine to estuarine origin. At the same time, chlorite was the only clay mineral directly detected, indicating that the applied standard powder preparation did not capture the full clay mineral assemblage reliably. Even so, the identified phases provided a sufficient basis for subsequent geological classification, which allowed the material's origin, associated characteristics, and regional representativeness to be assessed. This led to the conclusion that the material most likely originates from clayey deposits of the Naaldwijk Formation, making it broadly representative of a characteristic excavated soil type within the Rotterdam-Delft region. This regional attribution also enabled the identification of associated constituents and potential risks, including pyrite, reactive iron, organic matter, carbonate content, and soluble salts. The subsequent environmental analysis confirmed low organic matter and contaminant concentrations. As a next step, analysis of the water-soluble salt content was identified as essential, since it represented an inherent risk for earthen construction and may also indicate prior oxidation processes. In parallel, it was noted, that the pyrite risk should be reassessed once the final mix proportions are established.

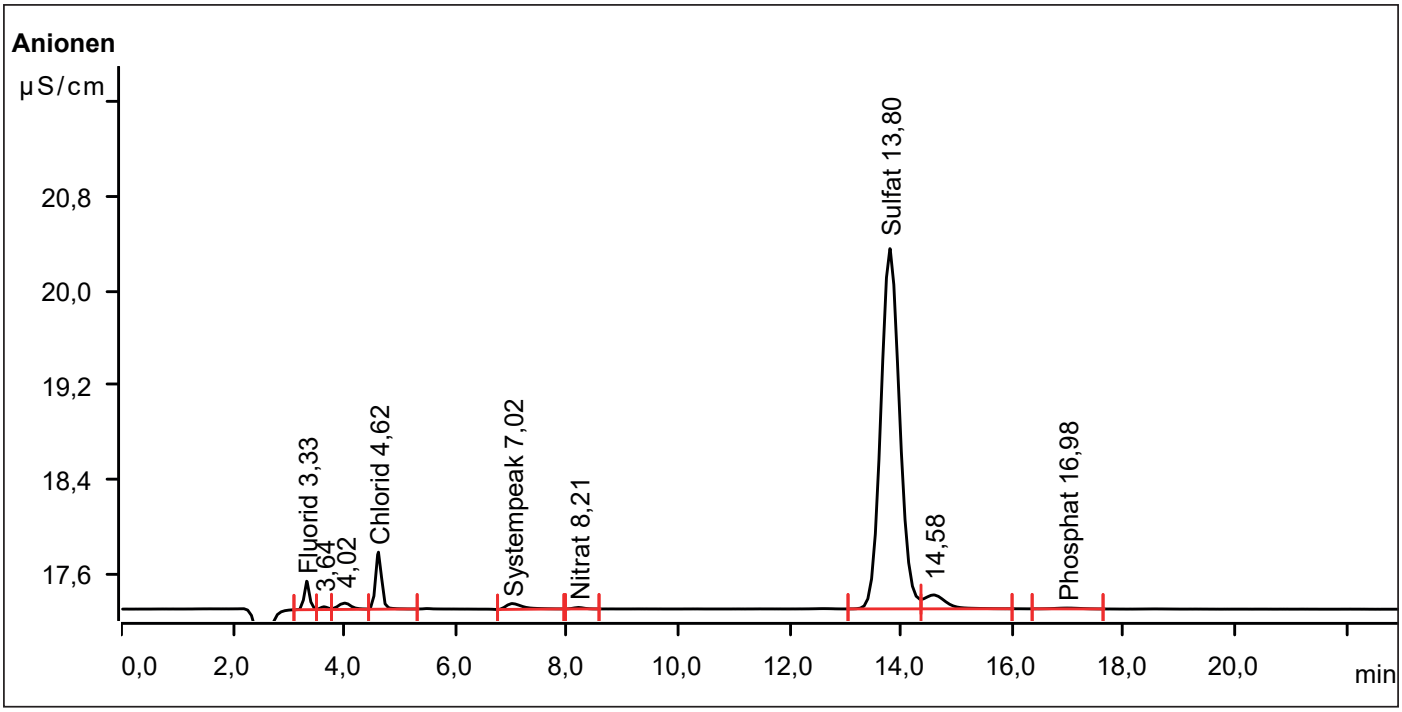

Figure 34: Ion chromatogram of the water-soluble salt extract, showing electrical conductivity as a function of retention time.

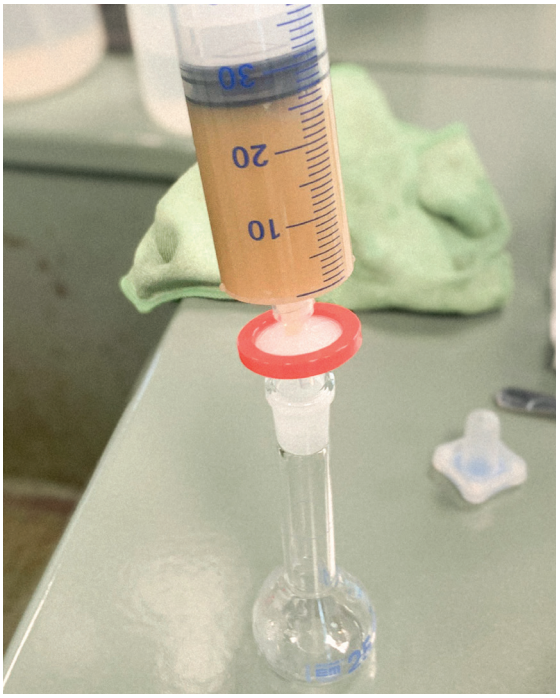

Figure 35: Preparation of the extract by syringe filtration through a 0.45 µm filter prior to analysis.

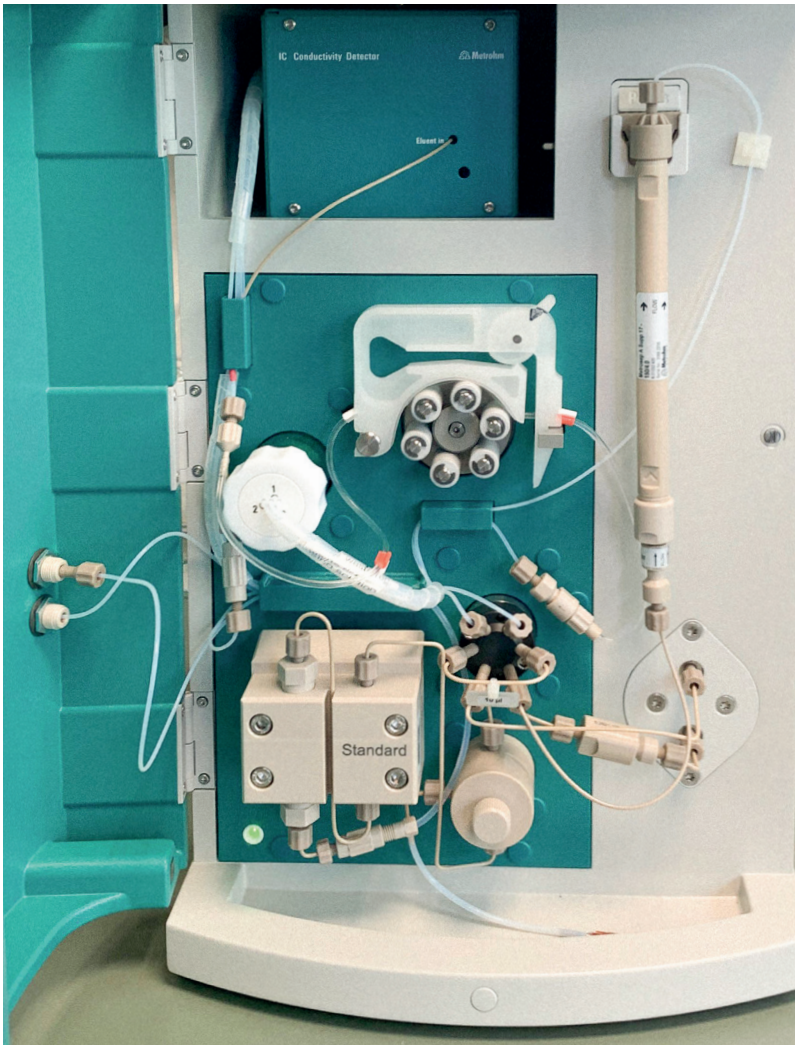

Figure 36: Internal components of the ion chromatography system used for anion determination, including the injection unit, separation column, suppressor and conductivity detector.

3.5 Water-soluble salts

The water-soluble salt content was analysed with reference to EN 16455. Ion chromatography was used for quantification since it is both accepted by the standard and widely established for the separate determination of anions and cations. While EN 16455 provides for a full profile of both anions and cations, the present study was limited to the anion's, mainly chloride, sulphate, and nitrate for reasons of time and practical relevance. This was considered sufficient for an initial assessment of salt-related deterioration risk in the investigated soil.

3.5.1 Ion chromatography

(1) Sample preparation

The clay was first ground to a particle size below 0.106 mm using a disc mill. The resulting powder was then dried to constant mass. From this material, 4 g were weighed and mixed with 200 ml of deionized water. The suspension was stirred for 24 h at room temperature to transfer the soluble salts into the liquid phase. This was followed by a settling period of 2 h to allow the solid particles to separate from the solution. The supernatant was then filtered through a 0.45 µm filter (Fig. 35).

(2) Test procedure

After calibration of the chromatography system, the filtered extract was introduced into the injection loop with a syringe. Therefore, the liquid sample was injected into a continuous eluent flow passing through a separation column, where negatively charged ions are temporarily retained by the stationary polymer resin. Due to differences in charge and ionic size, the anions interact with the resin to different extents and therefore move through the column at different rates, allowing them to be separated. Before reaching the detector, the separated ions pass through a suppressor, which chemically reduces the background conductivity of the eluent. Finally, a conductivity detector records the anions as they eluted from the column. The ion type is identified by its retention time, while the signal intensity is used to quantify the concentration of each anion. The main internal components of the ion chromatograph are shown in Fig.36.

(3) Results

The results were automatically plotted as a chromatogram, with retention time on the x-axis and electrical conductivity on the y-axis (Fig. 34). The concentrations calculated by the instrument software were 0.636 mg/l for chloride, 0.093 mg/l for nitrate, 13.836 mg/l for sulphate, and 0.135 mg/l for phosphate. Since the values were initially obtained as concentrations in the extract, they had to be converted using the dry sample mass and extraction volume. For the assessment of harming salts, the results are expressed as mass percentages. Based on the applied boundary conditions, this conversion corresponds to 0.05 mg of salt per gram of sample for each 1 mg/l measured in the extract. The mass fractions were then calculated for the individual ions resulting in 0.00318 mass-% for chloride, 0.000465 mass-% for nitrate, 0.06918 mass-% for sulphate, and 0.00675 mass-% for phosphate.

(4) Evaluation

The assessment of salt-related deterioration risk was based on the threshold values specified in DIN 18945, Section 6.5. For application classes Ia, Ib, and II, the standard defines maximum mass fractions of 0.02% for nitrate, 0.10% for sulphate, and 0.08% for chloride. All measured values remained below these limits. In addition, the total salt content must not exceed 0.12% by mass. This requirement was also fulfilled, with a calculated total mass fraction of 0.084%.

3.5.2 Implications

It could therefore be concluded that the investigated clay did not contain concentrations of water-soluble salts that would have excluded its use as a construction material. This suggested that, despite its original marine environment, the material no longer retained critical salt concentrations in its pore water. It is likely that these salts were leached over time by rainfall infiltration or groundwater flow. A reliable assessment of the pyrite-related risk, however, was not possible on the basis of this method alone. Since unoxidised pyrite is water-insoluble, the test solution only captures sulphate that has already formed through previous oxidation processes. The measured sulphate content therefore indicated, that no concentration exceeding the

Figure 37: Microscopic view of the crushed sand selected for the mix design, captured using a 100 mm lens.

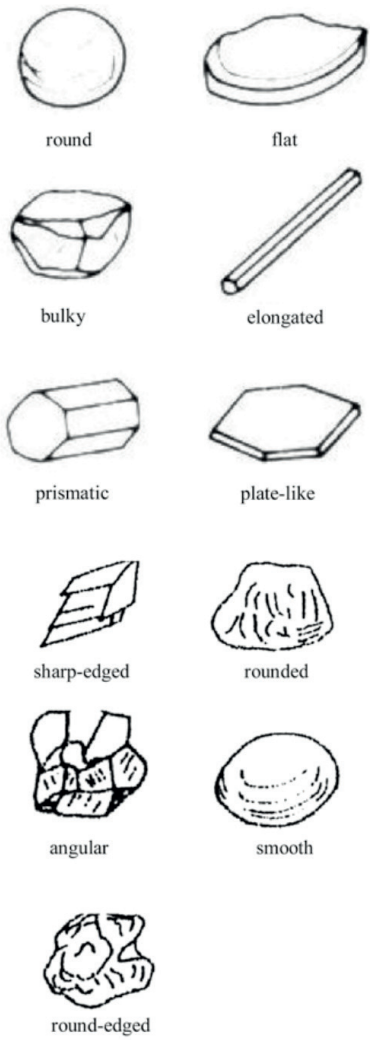

Figure 38: Grain shape and angularity classification. Reproduced from Schroeder (2016).

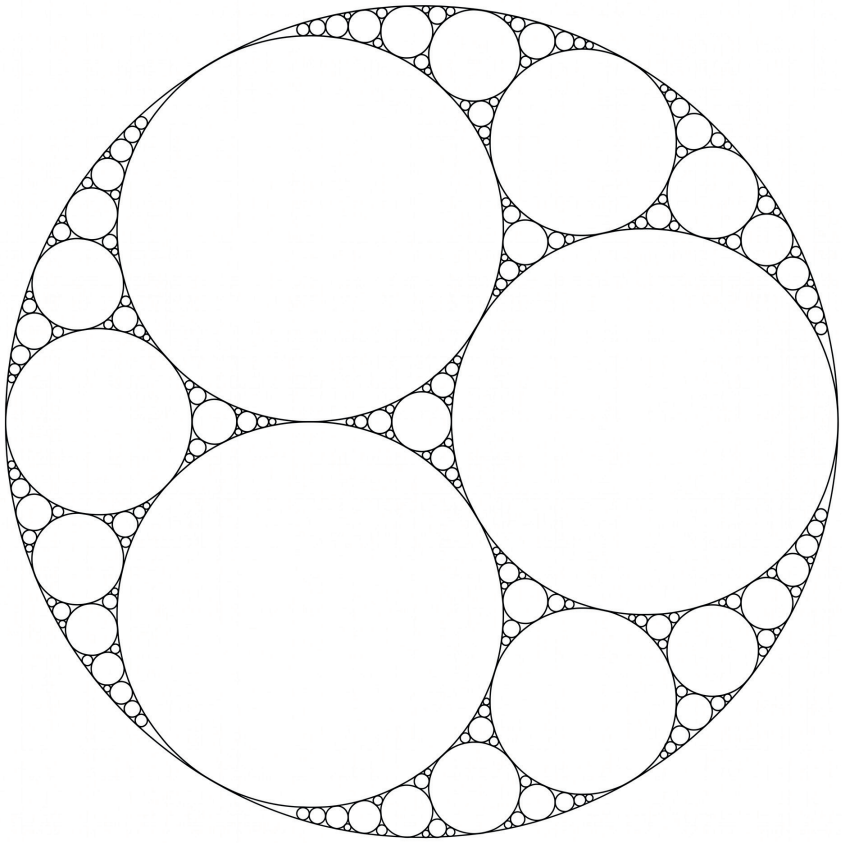

Figure 39: Idealised two-dimensional Apollonian packing illustrating the filling of voids between larger particles by progressively smaller spheres. Adapted from Borkovec et al. (1994).

DIN 18945 limits has developed so far, but it did not exclude the possibility of future sulphate and gypsum formation from reactive pyrite. However, these additional analyses were considered beyond the scope of this thesis. Since no direct restriction due to water-soluble salts was identified, the next steps were defined as aggregate selection, material processing, and the development of suitable mix formulations. The pyrite risk remained a point for future reassessment once the final mix proportions were defined, taking into account aggregate dilution and the expected moisture exposure of the component.

3.6 Aggregates

As already found by the preceding chapters, the composition of the raw material implied a high proportion of aggregate additions. The selection and composition therefore became a key parameter in the mix design. Traditionally, so called 'fat' soils are tempered with sand. Like in concrete mix design, a well-graded mineral skeleton forms the basis for producing strong and durable CEBs. The addition of sand not only reduces the relative clay content of the overall mix, thereby limiting drying shrinkage and the risk of cracking, but also improves the erosion resistance of the material. An optimized granular skeleton minimizes pore volume and enables mechanical loads to be transferred through a stable matrix of direct grain-to-grain contact (Reddy, 2022; Schroeder, 2016).

3.6.1 Conventional sand

(1) Maximum Grain Size

In contrast to monolithic rammed earth, compressed earth blocks require a considerably finer granular skeleton. While maximum grain sizes of 20 mm, or even up to 60 mm, can be used in thick rammed earth walls without difficulty, the literature commonly adopts a maximum grain size of 4 mm as the basis for calculating an optimal grading curve. In pressed earth blocks, excessively coarse particles may lead to edge spalling and can interfere with uniform and dense compaction in the press (Reddy, 2022; Schroeder, 2016). For the mix design, however, a maximum grain size of 6 mm was selected, as the intended application was not only in conventional small-format bricks, but also in larger blocks or interlocking units.

(2) Particle Morphology

As described by (Reddy, 2022; Schroeder, 2016), particle morphology, including grain shape and angularity, is determined by the depositional and weathering history of the sand. Sands transported by water, such as river sands, or by glacial processes tend to become smooth and rounded through continuous abrasion. By contrast, sands produced by crushing rock or formed in situ through weathering generally retain sharper edges. These angular particles are particularly important for the skeleton of compressed earth blocks (Fig. 38). Schroeder (2016), notes that sharp-edged sands provide higher interlocking resistance and are therefore generally preferable. For this reason, crushed sand from the concrete laboratory was selected for the mix design (Fig. 37).

(3) Optimal Grain Size Distribution

In concrete technology, the classical Fuller curve is commonly used to determine an optimal particle-size distribution:

$$P_i = 100 \left(\frac{d_i}{D}\right)^n$$

Where P_i is the percentage passing a given sieve size, d_i the mesh size, D the maximum grain diameter, and n the grading coefficient. According to Schroeder (2016), the classical grading coefficient of n = 0.5, which is based on idealised sphere packing (Fig. 39), cannot be applied directly to earth materials, as the particle shape of natural soils is not spherical. Minke (2025) further notes, that the classical Fuller equation would result in a clay content of only approximately 2-3 %, which would be far too low to provide sufficient binding capacity. Houben & Guillaud (1994) therefore proposed a coefficient of n = 0.35 for sand and gravel mixtures and n = 0.25 for clay-rich soils. The starting point for selecting a suitable exponent for the present test series was therefore a fine fraction that would still allow a clay content of at least 10%, corresponding to the lower limit commonly reported in the literature. On this basis, an exponent of n = 0.3 was selected, resulting in a fine fraction of 25.12 %, which, for the investigated soil, corresponded to a clay content

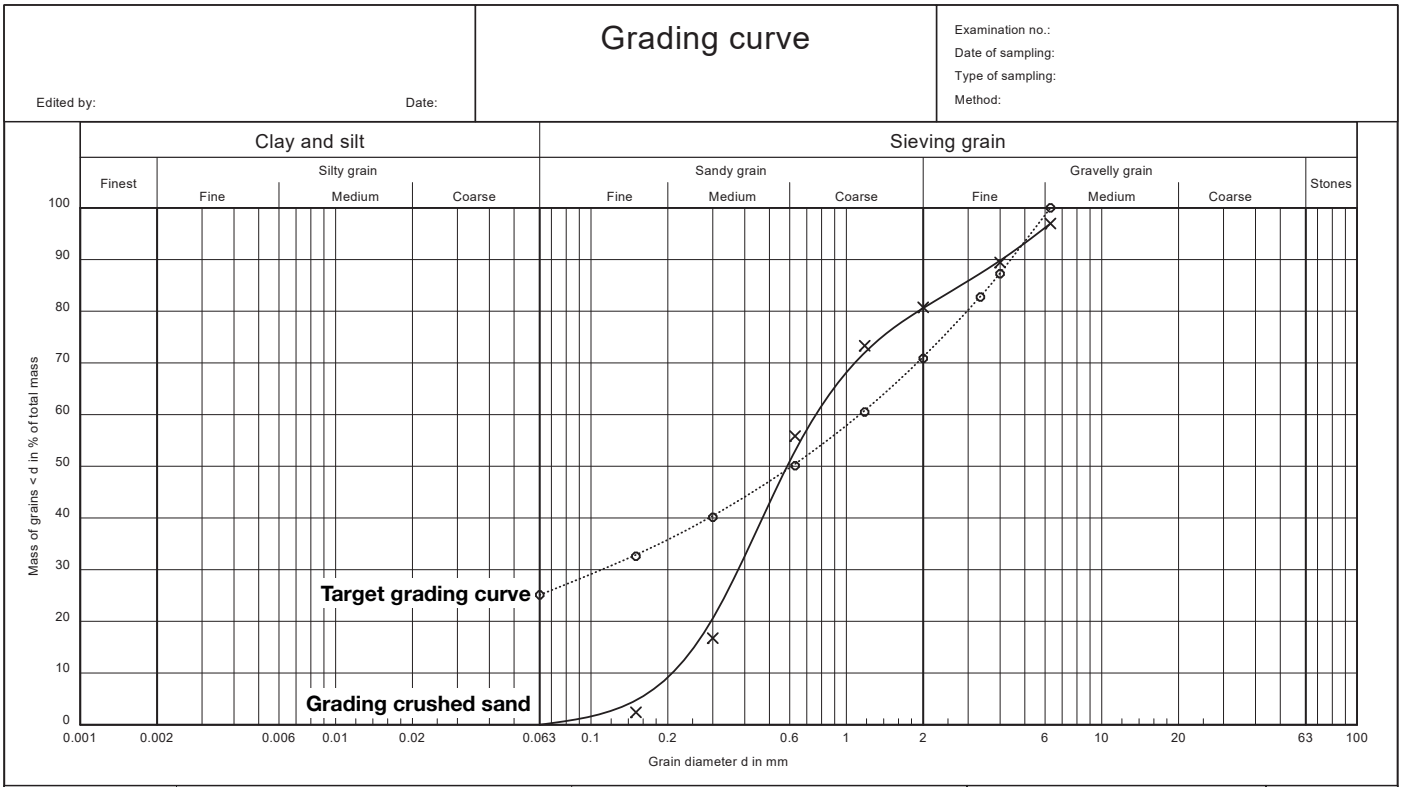

Figure 40: Comparison between the actual particle-size distribution of the dry-sieved sand and the target grading curve, indicating an excess of fine sand and an insufficient proportion of coarser particles.

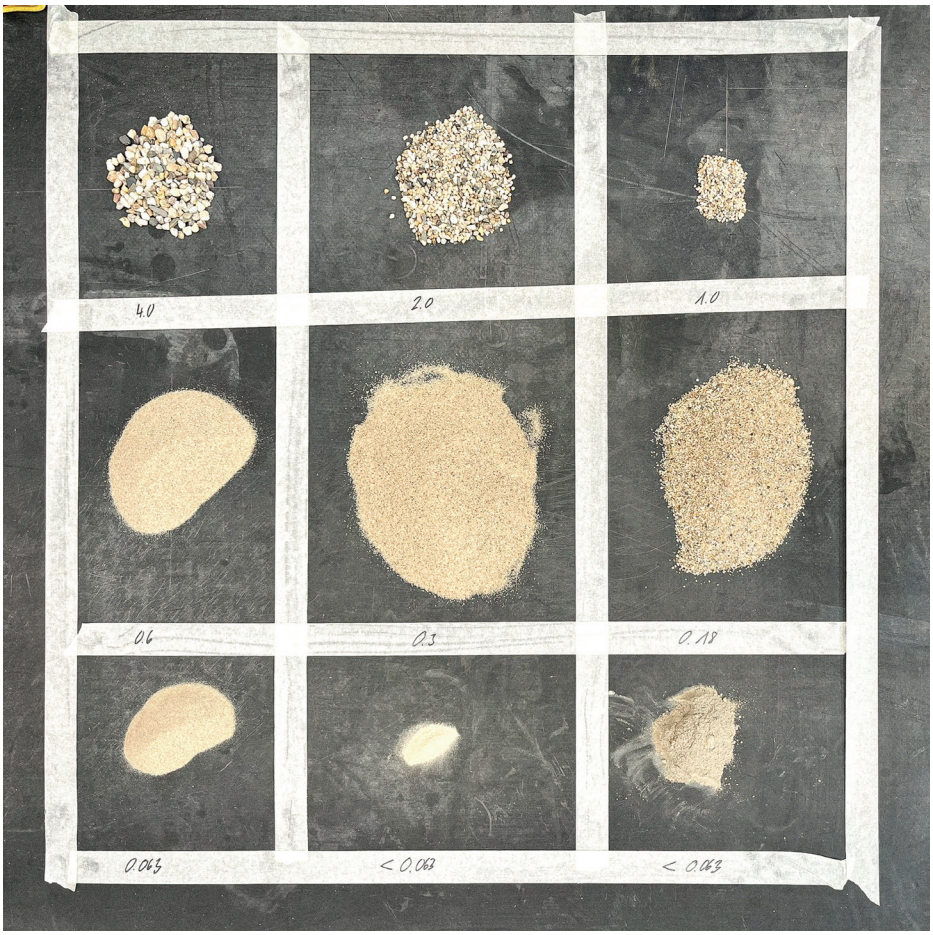

Figure 41: Overview of the individual sieve fractions obtained from 1 kg of laboratory sand, together with the corresponding clay content considered in the mix design.

of approximately 11 %. This ensured that, even in the case of a slight measurement error throughout the sedimentation analysis, the final mix would still remain above the 10 % threshold. The resulting expression used for the grading calculation was therefore:

$$P_i = 100 \left(\frac{d_i}{6.0} \right)^{0.3}$$

(4) Sieve Analysis

To determine the particle-size distribution of the sand and to subsequently adjust it to the target grading curve, a representative 1000 g sample was dry-sieved. As a 6.0 mm sieve was not initially available, the analysis was carried out using sieve sizes of 6.3, 4.0, 3.35, 2.0, 1.18, 0.630, 0.300, 0.150, and 0.063 mm. Subsequently, the retained mass on each sieve fraction was recorded resulting in the grading curve shown in (Fig. 40). It revealed an excess of fine sand, particularly in the 0.300 mm range, and an insufficient proportion of coarser particles.

(5) Grading Adjustment

Based on these findings, the sand had to be adjusted to match the target grading curve. At the same time, the procedure was intended to remain transferable to later production practice. For this reason, simply removing surplus grain fractions was not considered an appropriate approach. Instead, a spreadsheet was developed in which the available sieve sizes, maximum grain size, grading coefficient, representative screening mass, and total sand mass to be regraded were defined as adjustable input parameters. The calculation was based on the retained mass of each sieve fraction. After entering the measured retained masses, the spreadsheet automatically determined the deviation from the target grading curve and calculated a target mass for each fraction. The portion showing the greatest surplus in absolute mass was normalised to zero, meaning that no addition was assigned to this sieve fraction, while all other shares were supplemented accordingly. In this way, the tool generated the required mass addition for each sieve size as well as the resulting total mass of the regraded sand. The laboratory sand was then re-sieved into its individual fractions (Fig. 41) and recombined according to the calculated target masses. This proved to be the most practical solution for the experiment. For later production, however, the same principle could also be implemented by combining several sands with different grading characteristics, for example three or four stockpiled sand types, rather than by re-sieving a single source material.

3.6.2 Alternative aggregates

Even when compressed earth blocks are discussed as a more environmentally preferable alternative to classic bricks, the resource implications of sand must also be considered critically. This was particularly relevant within the study, where the locally available excavated soil itself was associated with comparatively low environmental impact, yet required tempering with at least 60 % sand. However, it is a critical resource, especially in relation to concrete production. Because desert sand is generally too fine, too smooth, and too rounded, the construction industry has traditionally relied on river and marine sands. The environmental consequences include river erosion, habitat loss, groundwater impacts, and of particular relevance in the Dutch context, increased coastal vulnerability (Attri et al., 2022; Dan Gavriletea, 2017). As discussed in the previous paragraph, CEB production generally favours sharper, non-marine sands, such as crushed quarry sand, to achieve a more stable granular skeleton. However, these materials are not available without environmental burdens either. In many regions, the concrete industry is shifting away from natural river, marine, and offshore sands towards crushed alternatives, as natural sources become scarcer, more expensive, or more strongly regulated. This does not resolve the sand problem, but rather displaces its impacts towards quarrying, land use, dust and noise emissions, and the additional energy required for crushing and sieving (Mishra et al., 2023).

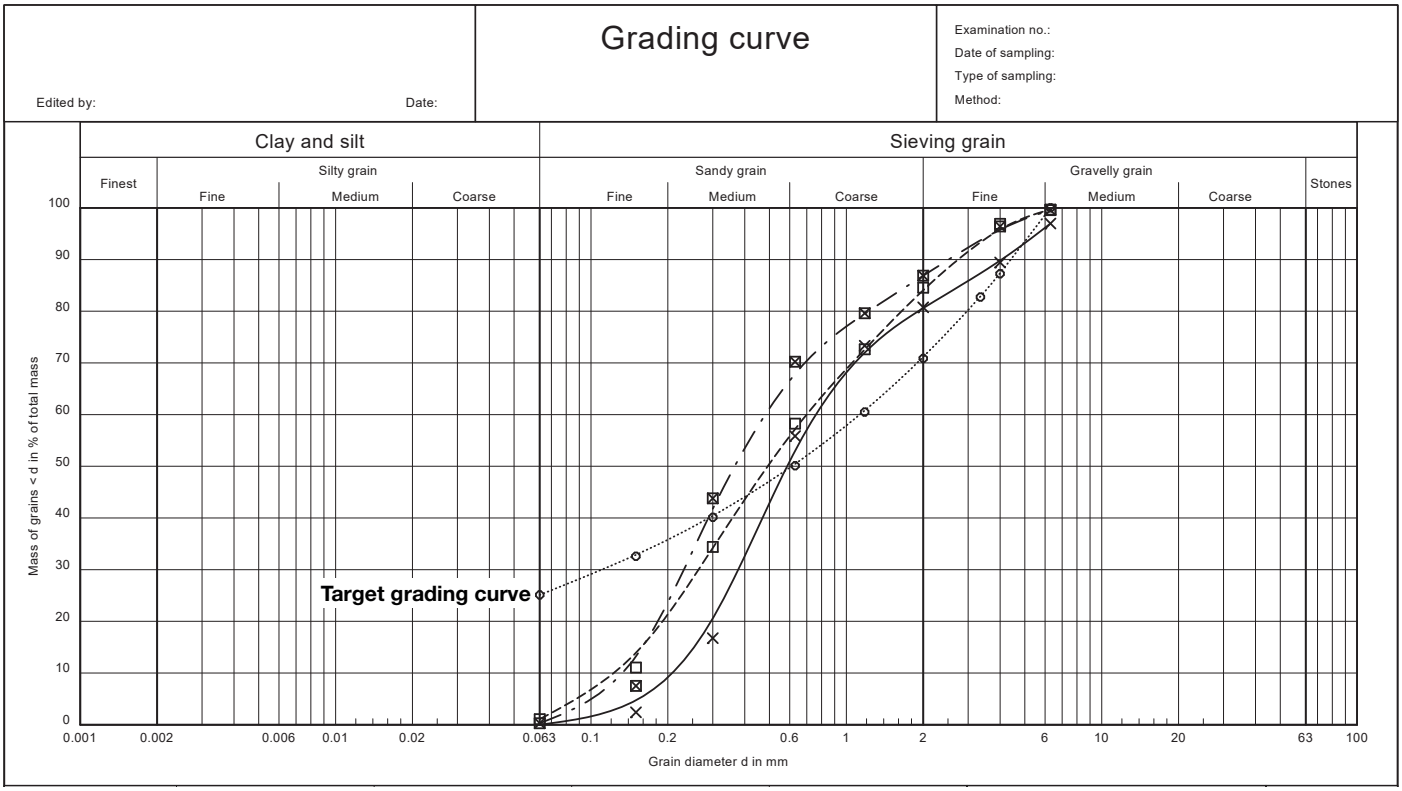

Figure 42: Particle-size distributions of the alternative aggregates determined by dry sieving of 1000 g samples.

Figure 43: Unwashed concrete sand 0-4 mm.

Figure 44: Washed concrete sand 0-4 mm.

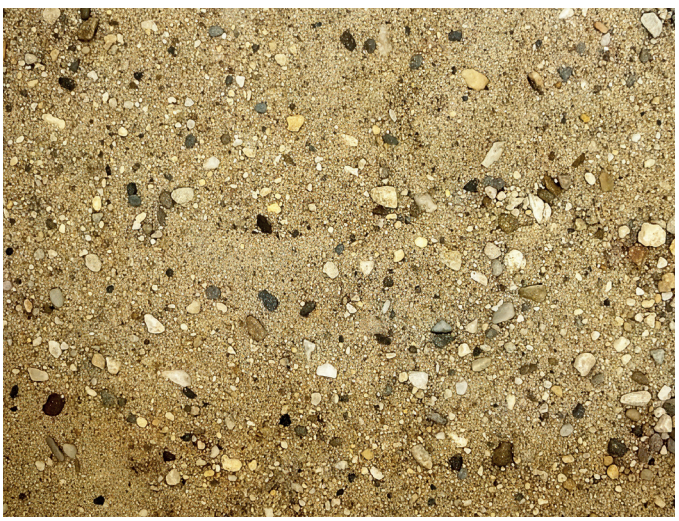

Figure 45: Crushed sand.

Figure 46: Mineral ash.

(1) Renewi

As with the selection of the locally available excavation soil, the choice of alternative aggregates was likewise shaped by regional availability, since long transport distances or imported material streams may quickly offset the environmental benefits. In the Benelux region, Renewi represents a major actor in the recovery and processing of secondary resources. Within the mineral waste sector, the company processes c&d waste streams into certified secondary raw materials, with the aim of substituting primary construction materials with lower-impact alternatives. For the present investigation, recycled aggregate products were sourced from two regionally available Renewi facilities: The concrete recycling facility in Westpoort, Amsterdam, located 70.2 km by road, and the mineral ash facility in Moerdijk, located 45 km from Rotterdam city centre.

(2) Unwashed concrete sand

A recycled aggregate used as a secondary raw material to substitute primary sand in earthworks, road construction, and hydraulic engineering with particles ranging from fine fractions up to a maximum size of 4 mm (Fig. 43). It is produced by mechanically crushing source-separated concrete demolition waste. A key material characteristic is that no subsequent washing step is applied. As a result, the fine fraction generated during crushing remains in the material. This fraction may contain microscopically small cement particles that were not fully hydrated during the original concrete production and were exposed during mechanical fragmentation. These particles can impart latent hydraulic properties to the material, which may lead to secondary hardening under moisture and compaction.

(3) Washed concrete sand

By contrast, the washed concrete sand (Fig. 44) undergoes an additional wet-mechanical cleaning step. This removes the finest particles and reactive cement residues from the aggregate, suppressing the hydraulic behaviour and resulting in a more defined and chemically stable secondary sand. Owing to these controlled properties, it is used primarily as a higher-grade aggregate for new concrete production.

(4) Mineral ash

The secondary construction material is derived from mineral bottom ash, the residual fraction remaining after the thermal treatment of municipal solid waste in incineration plants (Fig. 46). During processing, the bottom ash is dried and sieved, and metallic constituents such as iron, aluminium, and copper are removed. The remaining granulate is then subjected to wet washing. This treatment stabilizes the leaching behaviour of the material to a level that complies with environmental requirements for unrestricted construction use. It is subsequently used as an alternative secondary raw material for conventional foundation layers in earthworks, road construction, and hydraulic engineering.

(5) Mineral filler

In contrast to bottom ash, this filler is derived primarily from contaminated soil and asphalt granulate. The resulting powder fraction is characterized by a particle size that lies predominantly below 63 µm. In the concrete and cement industry, the material is primarily used to substitute conventional mineral fillers.

(6) Grading

To determine the particle-size distribution of the alternative aggregates, 1000 g samples of each material were again dry sieved. As in the sieve analysis of the crushed sand, a maximum particle size of 6.3 mm was adopted. Figure 42 shows the resulting grading curves of the materials, except for the mineral filler, which was excluded from this comparison because it consists solely of fine particles. The results show that all recycled aggregates exhibited the same general tendency as the laboratory sand, namely an excess of fine fractions and an insufficient proportion of coarser grains.

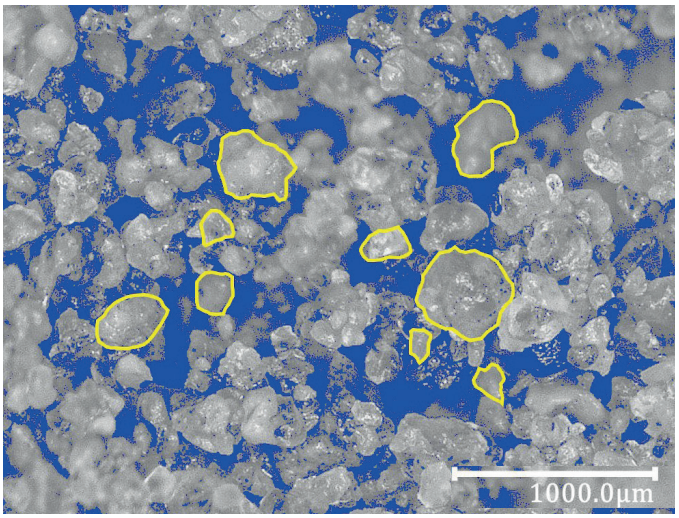

Figure 47: Grain morphology of unwashed concrete sand.

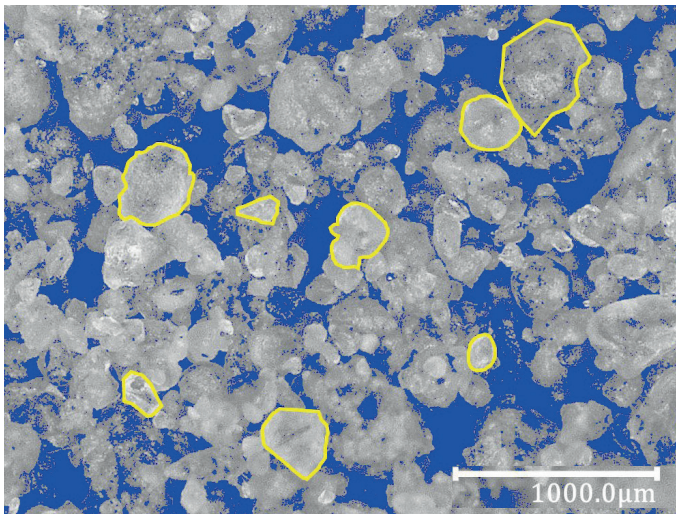

Figure 48: Grain morphology of washed concrete sand.

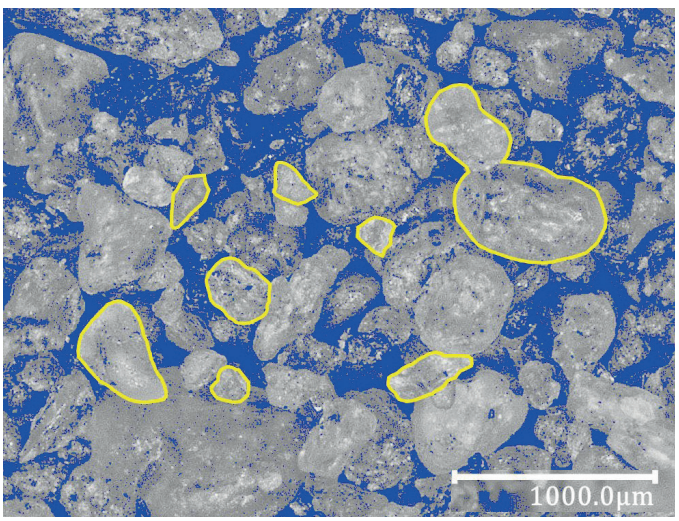

Figure 49: Grain morphology of crushed sand.

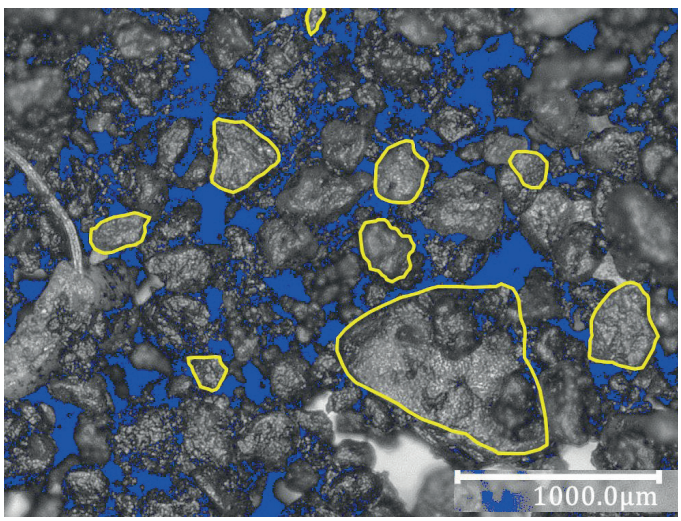

Figure 50: Grain morphology of mineral ash.

(7) Particle Morphology

The particles, excluding the mineral filler, were examined qualitatively under the microscope to compare their grain morphology (Fig. 47). After conversion to grey scale, the background was tinted blue to reduce depth effects caused by the bulk arrangement of the particles. For illustrative purposes, the edges of selected grains were additionally traced in yellow. The crushed laboratory sand exhibited a mixed morphology of rounded and bulky particles with predominantly rounded edges. A similar morphology was observed for the mineral ash. However, as the material was still slightly moist during imaging, the images also revealed distinctly darker mineral residues, likely originating from the thermal treatment process, which appeared to promote visible adhesion between individual grains. In addition, isolated mineral constituents were identified that could not be clearly assigned to a regular grain shape. By contrast, both the washed and unwashed concrete sand contained a visibly higher proportion of sharp-edged particles, suggesting greater potential for interlocking resistance. No comparable intermediate residues or adhering non-granular mineral phases were observed between the grains of the crushed concrete.

3.6.3 Resulting strategy

The need for substantial tempering made the aggregate fraction a decisive part of the mix-design process. However, this could not be reduced to the simple addition of sand, as maximum grain size, particle morphology, and PSD all had to be defined in relation to the intended application. A maximum grain size of 6.0 mm was selected with a view to the later transfer from laboratory specimens to larger block formats. The particle morphology assessment further supported the selection of crushed sand, as its sharper grains are generally associated with higher interlocking potential. Further, the target particle-size distribution was calculated with reference to the Fuller curve but adapted for earth construction by reducing the exponent to n = 0.3. This allowed the granular skeleton to be improved while maintaining a sufficient clay fraction for binding. The subsequent sieve analysis showed that the available laboratory sand contained excess fine sand and insufficient coarser particles. To translate the theoretical grading curve into a practical workflow, a spreadsheet-based adjustment tool was developed. This allowed the sand to be regraded through dry sieving and recombination, using targeted additions of missing grain fractions rather than removing surplus material.

At the same time, the high aggregate demand of the clay-rich soil made the choice of sand environmentally relevant. Regionally available recycled aggregates were therefore investigated as potential alternatives. Based on their grading and particle morphology, unwashed concrete sand and mineral ash were identified as possible contributors to the granular skeleton. The sieve analyses showed that the recycled aggregates followed a similar tendency to the laboratory sand. In conclusion, standard crushed sand was selected as the reference aggregate for the controlled test series, as it reduced the number of unknown variables and provided a stable basis for investigating the main mix and compaction parameters. Recycled aggregates were retained for a later exploratory comparison, in which the transferability of the reference workflow could be assessed. The next methodological steps were therefore defined as material processing, suitable mix formulation, and the development of an appropriate compaction setup.

Figure 51: Mechanical pre-crushing of the dried material using a tamper.

Figure 52: Disc mill used to process the material into a fine powder.

Figure 53: Clump formation during manual mixing trials.

Figure 54: Stepwise water addition using a syringe.

Figure 55: Adhesion of the material to the drill-mounted mixer.

Figure 56: Homogenisation of the material using a conventional kitchen hand mixer.

4. Material processing

4.1 Preliminary mix design

4.1.1 Processing binder

For processing the highly plastic soil, two alternative approaches were considered. The first was wet processing by soaking the material in water to disperse the fine particles and subsequently enable the addition of aggregates and coarser fractions. This approach offers the advantage that it can be carried out independently of solar drying or energy-intensive oven drying. In addition, the large clay clods are broken down by the water, so that no extensive mechanical pre-processing is required. Nevertheless, dry processing was selected to allow precise control of the moisture content of subsequent mixes. Portions of the moist soil were first spread on baking trays and dried in an oven at 60°C for 6 h to avoid any alteration of the clay minerals. As sufficient oven capacity was not always available, it also proved effective to form the material into spheres of approximately 30-40 mm diameter and air-dry them for 7 days at indoor laboratory or workshop temperatures of 15-19°C. Both the oven-dried material and the air-dried spherical samples were then wrapped in a kitchen towel and mechanically pre-crushed using a hammer or tamper (Fig. 51). The material was subsequently milled in a disc mill for 5 s per cycle to obtain a fine powder, which could then be mixed directly with the aggregates as a fine binder (Fig. 52).

4.1.2 Mix setup

The initial challenge was that the mixing tools recommended in the literature, such as compulsory mixers (Minke, 2025) or screw mixers as used by (Reddy, 2022) were not suitable for the very small batch sizes required for preliminary testing. Even the Hobart mixers available in the laboratory, which are normally used for concrete preparation, proved unsuitable for batches smaller than 2 kg, as the material was merely pressed against the bowl wall without being mixed effectively. Initial trials were therefore carried out in a plastic bucket using two spatulas. Although this method allowed the material to be mixed by pressing and rubbing it between the spatulas, it proved highly time-consuming and physically demanding. In addition, large clumps formed during mixing, making it difficult to achieve a homogeneous distribution of moisture (Fig. 53). A further attempt was made using a metal drill bit typically employed for mixing cement or paint. However, this did not produce satisfactory results, as the material once again adhered to the bucket wall and mixing rod without being homogenised properly (Fig. 55). The most effective solution was ultimately found to be the use of a standard stainless-steel kitchen bowl in combination with a dough hand mixer operated at the lowest speed (Fig. 56).

4.1.3 Water dosing

Because the fine powder, with its high silt and clay content, tended to form lumps immediately upon contact with water, the direct addition of moisture adversely affected the homogeneity of the mix. For this reason, both a pressurised spray system and a standard household spray bottle were initially tested to introduce moisture gradually. In both cases, however, a certain distance from the mixing bowl was required to avoid localised clumping, which also resulted in water loss outside the bowl and thus reduced control over the exact moisture content of the mix. In addition, water tended to run down the bowl wall and cause localised agglomeration at the outer edges of the material. The most effective solution was therefore found to be the use of a syringe (Fig. 54), by which moisture was added drop-wise in several stages, followed by repeated mixing between each addition step. The sequence of component addition also proved relevant. The best results were achieved when the clay powder was first dry-mixed with sand before any moisture was introduced.

Figure 57: 3D printed preliminary mould.

Figure 58: Pressed pancake sample.

Soil share [%]	Corresponding clay content* [%] unknown at time of experiment	Outer shrinkage [%]	Notch-to-notch shrinkage [%]
90	39,60%	8,00%	6,25%
75	33,00%	4,00%	3,75%
60	26,40%	2,50%	1,25%
45	19,80%	2,00%	0,00%
30	13,20%	1,50%	0,00%
15	6,60%	1,00%	0,00%

Figure 59: Initial trial compositions and corresponding shrinkage values from the preliminary composition tests.

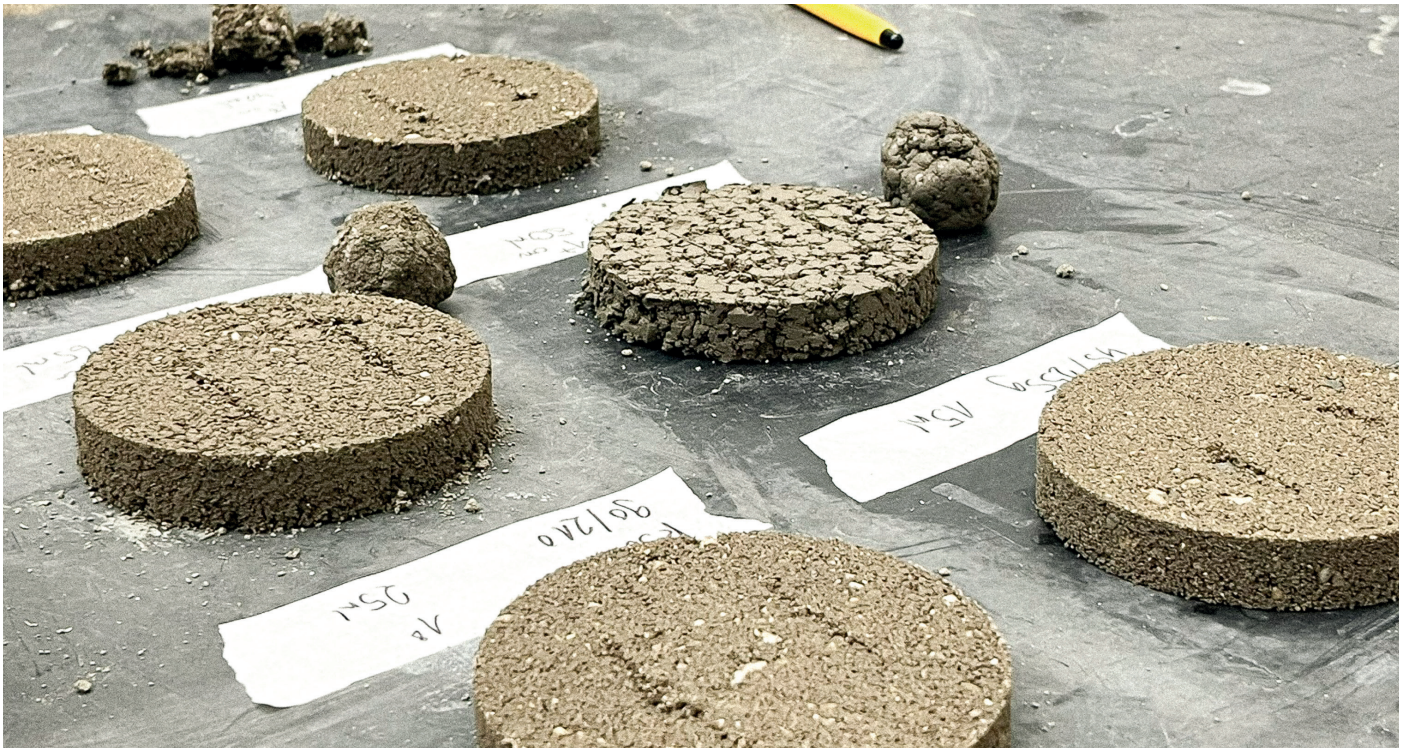

Figure 60: Pancake specimens with central grooves incised for shrinkage measurement.

4.1.4 Pancake tests

These preliminary tests were carried out before the exact composition of the soil had been determined. They were therefore not intended to provide scientifically comparable performance data, but rather to obtain an initial indication of swelling and shrinkage behaviour, to assess workability and mixing homogeneity, and to identify practical processing constraints at an early stage. In addition, they helped to estimate the maximum grain sizes that could still be accommodated within the tested material system. For this purpose, a simple cylindrical mould with a diameter of 100 mm was designed and produced by 3D printing (Fig. 57). Six mixes with a total mass of 300 g each and varying proportions of soil and sand were then prepared and compacted manually. As mixes with a higher clay content also required higher water addition, care was taken to adjust each mixture to an earth-moist consistency. This was checked by means of a drop test, in which a sphere dropped from a constant height was required to break into four to six larger coherent fragments. Although this method does not ensure strict scientific comparability, it allows a rapid and practical assessment of material behaviour during early-stage testing. After compaction, two grooves spaced 40 mm apart were incised in the centre of each specimen in order to measure subsequent shrinkage (Fig. 60). The respective composition together with the corresponding shrinkage values were summarised in (Fig. 59).

4.1.5 Processing implications

Dry processing was selected as the key methodological step because it allowed precise control of compaction moisture. At the same time, this required a reliable preparation work flow, including drying, pre-crushing, and short disc-mill grinding, to transform the plastic raw soil into a mixable powder. For small laboratory batches, conventional mixing equipment was not effective. Manual mixing was possible but inefficient, while drill-based mixing did not achieve sufficient homogenisation. The most practical method was therefore a stainless-steel bowl combined with a dough hand mixer at low speed. Moisture addition also proved critical: Direct water addition and spraying caused local clumping or water loss, whereas staged drop-wise dosing with a syringe allowed better control. The best sequence was to dry-mix the clay powder with sand before gradually adding water. Preliminary pancake tests did not provide comparable performance data, but they were useful for identifying early processing constraints, workability, shrinkage behaviour, and suitable consistency before moving into more controlled compression tests. With this in mind, the next step was the development of a compaction setup.

4.2 Compaction setup

4.2.1 Dynamic compaction

Because a suitable brick or industrial press with an appropriate mould was not available, and both would have required substantially larger material quantities, a simple formwork for manual compaction was built first. This made it possible to examine how an initial soil mix behaved under increased compaction force, whether sufficient binding could be achieved, and which dry density could be attained. As the mould was already subjected to considerable dynamic loads during manual compaction and was not intended to deform plastically, a steel tube with an internal diameter of 90 mm and a wall thickness of 5 mm and the height of 180mm was selected. The tube was cut into two halves along its length and secured using several standard threaded steel clamps. The tamper was designed from a heating pipe fitted with an end flange. A corresponding insert with a diameter of 89 mm, allowing air to escape during compaction, was laser-cut from plywood and protected against moisture using duct tape (Fig. 61).

For this type of mould, it is advisable to incorporate an additional element that holds the form-work down against the ground during tamping, as otherwise material may escape from the underside. In the present case, hand clamps were attached to the mould and used as footholds to stabilise the assembly during compaction. Based on the shrinkage values and the good workability observed in the preceding pancake tests, a mix containing 30% soil was selected for the dynamic compaction test. The mix therefore consisted of 360 g of soil, 840 g of sand, and 100 ml of added water. As in the

Figure 61: Experimental setup for dynamic compaction, showing the tamper and the split steel tube secured by threaded steel clamps.

Figure 62: Freshly demoulded specimen after compaction.

previous tests, the mixture was adjusted to an earth-moist consistency and checked by means of the drop test, in which the sphere was required to break into four to six coherent fragments. The mix was then placed into the tube in layers of approximately 25-30 mm and compacted with the tamper until a hollow sound became audible through resonance with the steel form-work. This was taken as an indication that the maximum degree of compaction for the respective layer had been reached. The surface was roughened with a cutter, and the procedure was repeated until the full mass had been compacted. After compaction, the specimen could be de-moulded immediately and weighed (Fig. 62). The density directly after de-moulding was 2250 kg/m³. The specimen was then air-dried for 72 h and subsequently oven-dried at 60 °C for 6 h until constant mass was reached. The resulting dry density was 2067 kg/m³, corresponding to the bulk density class of a solid fired clay brick at approximately 2.0-2.2 kg/dm³.

This confirmed that, even without full optimisation of the mix design, the material exhibited high compaction potential and could therefore be regarded as a promising raw material for CEB production, provided that the clay fraction ensured sufficient binding strength. This result had, however, to be considered against the background of the applied compaction method. While dynamic compaction is comparable to the principle of the classical Proctor test and suitable for assessing the general compactability, it cannot be transferred directly to the conditions required for CEB production. According to Minke (2025), compaction by beating, ramming, or vibration can be more effective, as it allows the clay discs to arrange themselves in a denser and more parallel structure, thereby promoting stronger electrochemical bonding within the material. As a next step, it was therefore necessary to design a dedicated static compaction setup.

4.2.2 Static compaction

(1) Formwork Dimensioning

Against the background of the findings reported by (Bruno et al., 2015) which showed that press pressures of 25, 50, and even 100 MPa could possibly allow block strengths comparable to those of cement-stabilized units, the required wall thickness became the governing starting point and principal constraint for the formwork design. To obtain an initial estimate of the required tube wall thickness under these high press pressures, Barlow's formula, commonly used for the design of pressure vessels and pipes, was applied. It relates the internal pressure that a cylindrical element can withstand to its dimensions and the allowable stress of the material:

$$P = \frac{2St}{D}$$

Where P is the internal pressure, S the allowable stress, t the wall thickness, and D the outside diameter. Further, the required press force was governed by the relationship $\sigma = F/A$, which introduced an additional constraint for the mould design. The production of such high-pressure samples required an internal diameter that was large enough to accommodate the relevant particle-size distribution, yet small enough to keep the required wall thickness within a feasible range and the target pressure achievable by the available testing machine. Since $D_{outside} = D_{inside} + 2t$, the required wall thickness as a function of the internal diameter was calculated with the following expression:

$$t = \frac{PD_i}{2\sigma - 2P}$$

After the formwork used for dynamic compaction had an internal diameter of 90 mm, this dimension was first checked for its feasibility in static compaction. The design was carried out under the assumption of ideal pressure transfer. The lateral earth pressure coefficient was neglected, such that the radial wall pressure was assumed to be equal to the applied press pressure. Owing to this conservative overestimation of the actual radial loads, a reduced material safety factor of 1.25 applied to the yield strength of the cylinder

Figure 63: Filled mould prior to compaction.

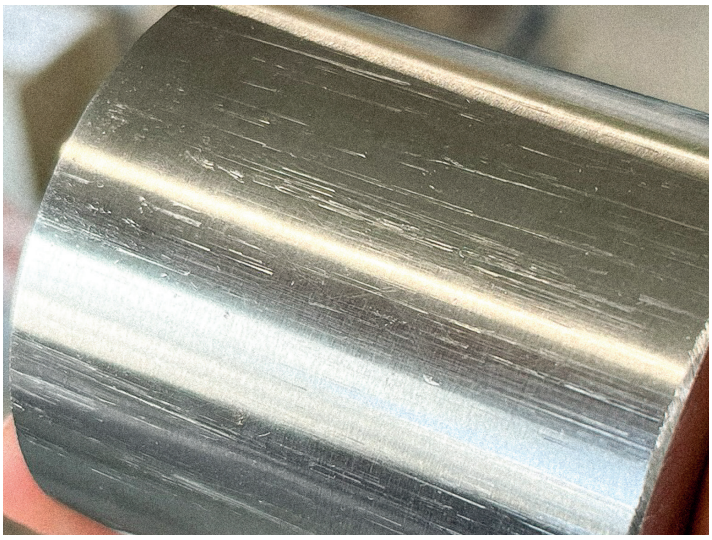

Figure 65: Scratch marks on the stainless-steel plunger after only two ejection attempts.

Figure 67: Demoulding setup with a hollow steel section positioned beneath the mould for specimen ejection.

Figure 64: Stainless-steel plunger inserted 40 mm into the mixture, ensuring guided alignment within the mould before compaction.

Figure 66: Compacted specimen after ejection from the mould.

material was considered sufficient. According to Mayr (2015), however, Barlow's formula can only be applied reliably to thin-walled rings, for which the stress distribution across the ring section is assumed to be nearly constant. He further states that, from a ratio of t/r = 0.2 onwards, the equations for thick-walled rings should be used instead. To obtain an initial assessment, calculations were therefore carried out for structural steels S235 and S355, as well as for 42CrMo4 steel with a yield strength of 550 N/mm², while also checking whether the resulting geometries still fell within the thin-walled range. The results clearly showed the structural implications of high press pressures. For S235 steel, a wall thickness of 16.3 mm was already required at 50 MPa, while 100 MPa would have theoretically required 51.14 mm. For S355 steel, the wall thickness at 100 MPa still amounted to 24.45 mm. In both cases, the geometry falls directly into the thick-walled range at 100 MPa. Only for 42CrMo4 steel, a wall thickness of 13.2 mm remains sufficient within the thin-walled range at 100 MPa. These results demonstrated not only the challenges of formwork design at laboratory scale, but also the implications for potential production machinery, which would need to be designed for substantially larger pressing areas. As many moulds available in the laboratory were not designed for such high pressures, or were made of brittle materials such as cast iron, it was initially not possible to fabricate a sufficiently thick-walled and at the same time openable formwork within a reasonable time frame and budget. A thick-walled tube was, however, directly available in the laboratory, with an internal diameter of 61.5 mm, a height of 150 mm, and a wall thickness of 22.5 mm. A plunger with a height of 180 mm and a diameter of 60 mm was also available. As this plunger contained a central hole of 20 mm diameter, an additional stainless-steel insert with a diameter of 60 mm and a height of 60 mm was cut to size for the pressing process.

(2) Initial compaction tests

To test the static compaction process, the same mix design with 30% soil as used in the dynamic compaction tests was adopted, with adjusted quantities to suit the smaller internal diameter of 60 mm. In total, 133 g of soil, 311 g of sand, and 37 ml of water were prepared. The mixture was filled into the mould to its upper edge without intermediate layering (Fig. 63). To allow the escape of water during pressing, a paper insert, cut from a standard coffee filter, was placed below the setup. The stainless-steel plunger was then pressed manually 40 mm into the mixture so that it was already guided by the mould and could not tilt or shift eccentrically (Fig. 64). After the plunger had been positioned, the mix was compacted under a total load of 50 kN at a compaction rate of 0.1 kN/s, corresponding to a compaction pressure of 17.68 MPa.

(3) Limitations

During the process, several difficulties associated with the closed mould setup became apparent. While high-pressure compaction itself could be carried out without major problems, substantial difficulties arose during demoulding without damaging the specimen. In the first trial, it was not possible to push the specimen through the mould using a vice, let alone by manual force alone. Removal was only achieved by heavy tapping with a hammer. However, this method not only risks renewed delamination of the compacted layers through vibration, but also led to edge damage and, in many cases, caused the specimen to fracture before it could be fully removed. In an attempt to improve this, silicone spray was applied to the inner surface of the mould before the mixture was filled in. This proved only of limited benefit, most likely because the earth-moist mix absorbed a large proportion of the release agent immediately upon contact with the mould wall. The only viable demoulding method was to place a hollow steel section beneath the mould inside the press and to reapply load at 0.1 kN/s to eject the specimen (Fig. 67). While this made demoulding possible, it also demonstrated the high frictional forces acting along the inner mould surface. After only two ejection attempts, both the mould interior and the stainless-steel plunger exhibited clear scratch marks (Fig. 65), which would impair the production of subsequent specimens. In addition, an ejecting force equivalent to approximately 600 kg was required to remove a specimen with a diameter of only 60 mm (Fig. 66). Further, the combined pressing and demoulding process took just over 25 minutes, limiting extensive test series.

Figure 68: Shell-like detachment of outer layers from the specimen edges after failure.

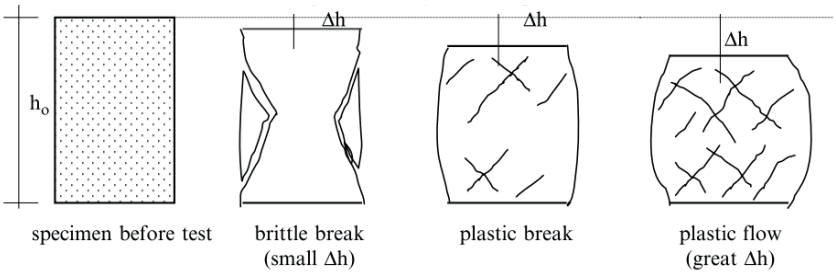

Figure 69: Failure patterns of cylindrical specimens during dry compressive strength testing of rammed earth. Reproduced from Schroeder (2016).

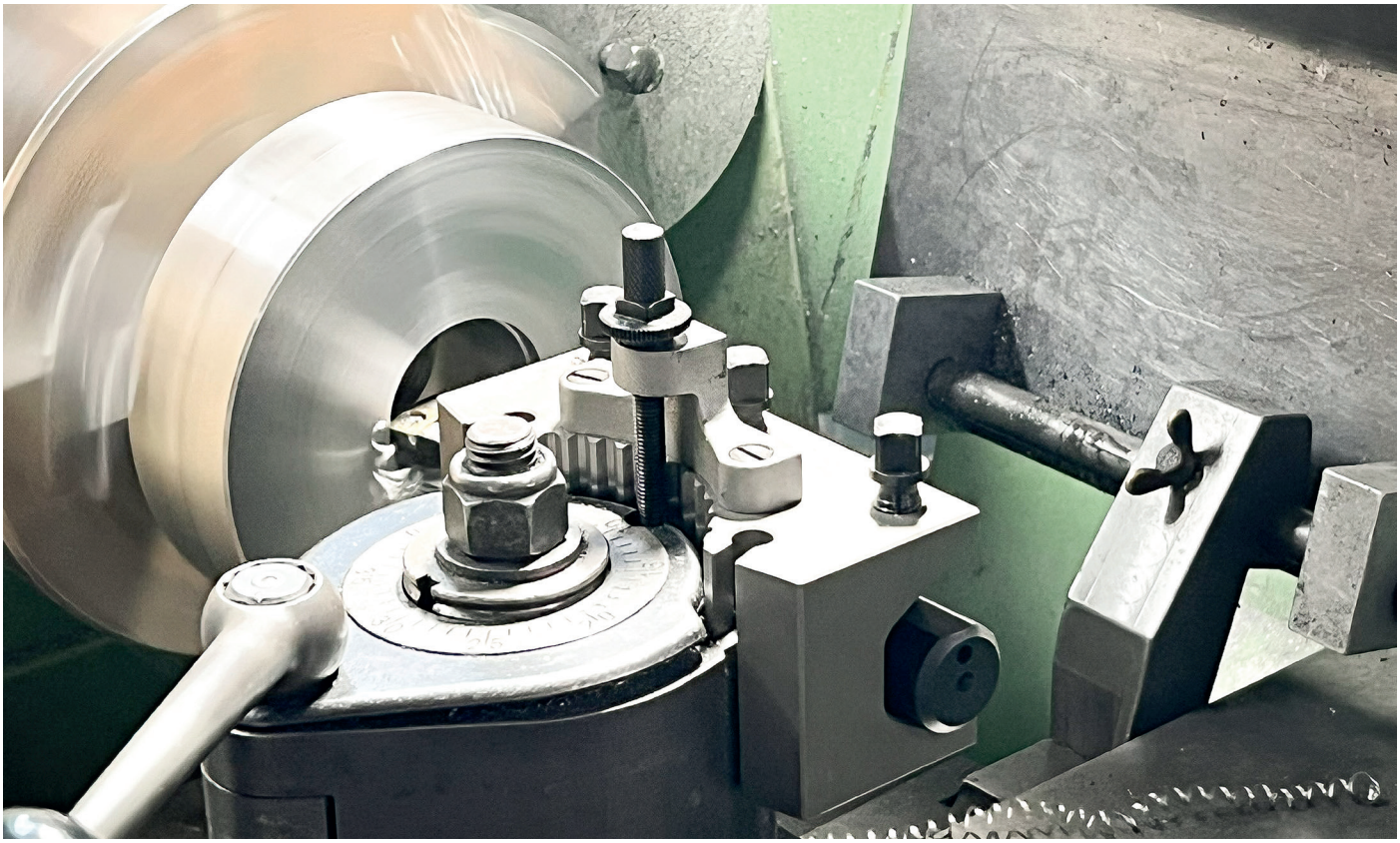

Figure 70: Lathe machining of the solid steel blank.

4.2.3 Performance assessment

Two successfully demoulded specimens, each with a diameter of 60 mm and a height of approximately 75 mm, were subsequently tested in compression. The observed failure pattern showed that thin outer layers detached from the specimen edges in a shell-like manner (Fig. 68). This suggested, that the outer zones had already delaminated from the main body during ejection from the closed mould, which likely contributed to premature failure. At the same time, fracture within the interior followed a curved path towards the centre, indicating a homogeneous aggregate distribution. Against this background, the specimens reached form-factor corrected compressive strengths of 4.14 MPa and 4.42 MPa, respectively. Despite the shortcomings of the mould setup, these results showed that even under non-optimised static compaction and with a mix design that had not yet been refined, compressive strengths could already be achieved that, if reproducible at scale, would be sufficient for load-bearing masonry. While this provided a first positive indication of the suitability of the excavated soil as a building material, the setup did not allow the production of a larger test series, primarily due to the time required and the difficulties associated with demoulding. As a result, it would not have been possible to isolate and investigate individual variables in a systematic manner. It therefore became clear that further time and resources had to be invested in the design and fabrication of an openable mould setup.

4.2.4 Openable mould design

(1) Basic concept

The first concept was to fabricate the formwork from two cylindrical components: An inner, thin-walled ring designed to be openable, and an outer, thick-walled ring intended to withstand the high pressures. Initially, both rings were intended to be manufactured with a slight taper relative to one another to facilitate removal of the inner ring. However, this could not be realised due to fabrication constraints and cost limitations. It was therefore decided to produce both rings with parallel surfaces and to apply machine grease between them to reduce friction.

(2) Mould components and materials

The internal diameter of the openable tube was determined primarily by the question of whether a precisely fitting plunger could also be obtained from solid stock material. This proved difficult when working with standardised pipe diameters and round bars, as no components were available that combined, for example, an internal tube diameter of 60 mm with a plunger of matching measurements. Although custom fabrication would in principle have been possible within the laboratory context, it proved too time- and cost-intensive. From the metal stock available, however, a thin-walled S235 tube with an internal diameter of 51 mm and a wall thickness of 3 mm could be sourced. In addition, a solid aluminium round bar with a diameter of 50 mm was available for use as a corresponding plunger. The resulting clearance of 1 mm in total, corresponding to approximately 0.5 mm at the perimeter, was regarded as potentially advantageous, as it was assumed that it could facilitate the escape of entrapped air and excess water during pressing. For the thick-walled outer component, two solid C45 steel cylinders, each with a diameter of 160 mm and a height of 50 mm, were acquired at low cost from former German railway material stock.

(3) Manufacturing

First, the solid material was turned on a lathe to an outer diameter of 150 mm, so that its dimensions would be compatible with the smaller laboratory press, which was likewise capable of providing the required press load and more frequently available for use. The centre of both steel cylinders was then drilled out and machined to an internal diameter of 57.5 mm (Fig. 70), allowing the thin-walled tube to be inserted with a precise fit. To facilitate assembly, the upper steel cylinder of the mould was machined with a slight internal taper of 1.5° over the first 20 mm, while all other edges were chamfered. This was intended to ensure that the tube could be inserted between the two cylinders without jamming. The original idea was to divide the thin-walled tube into two halves. In practice, however, the handling and insertion of two separate parts proved problematic, as it repeatedly led to jamming. The tube was therefore cut open on one side only, while the opposite side was merely saw-cut to a

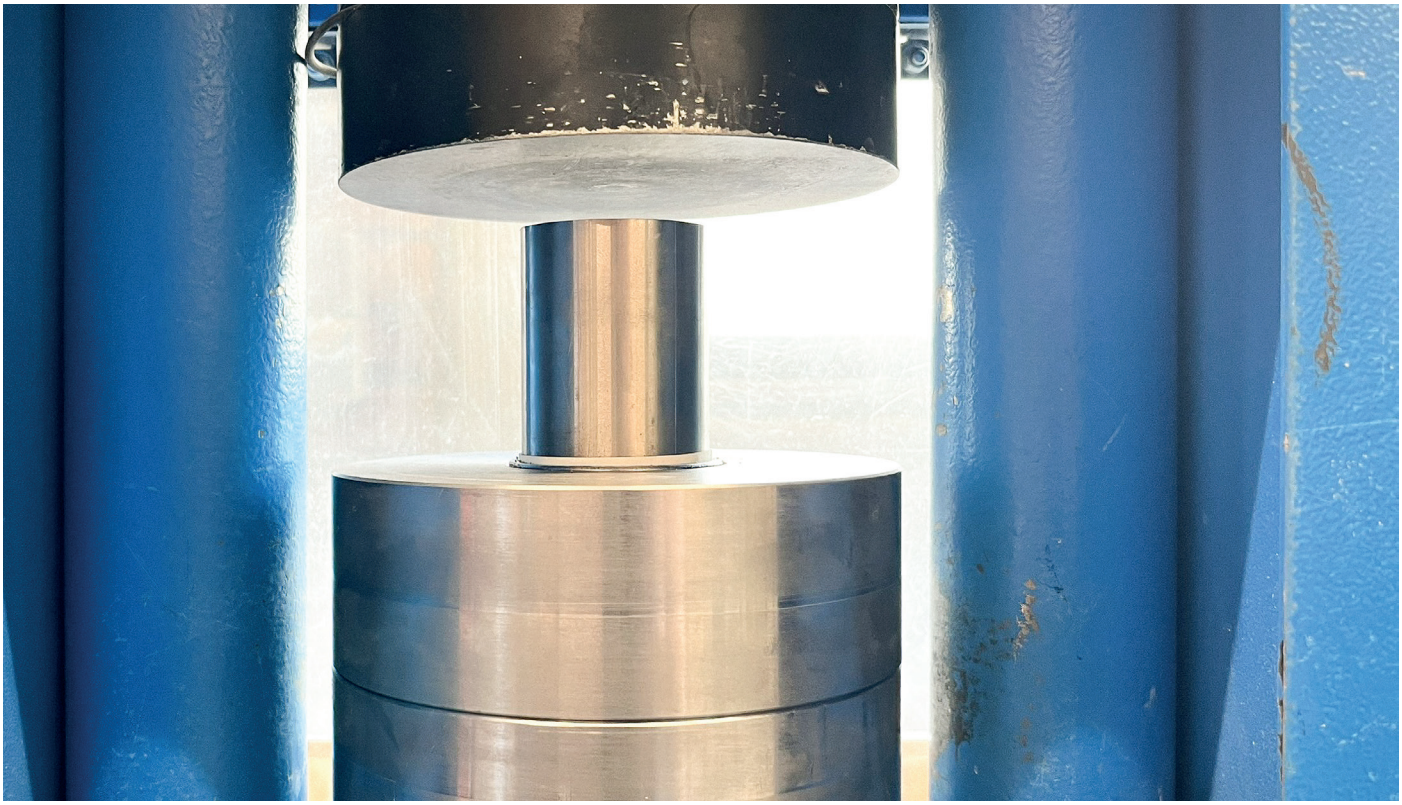

Figure 71: Pressing setup with the closed mould and plunger during compaction.

Figure 72: Inner steel section locally weakened to function as a hinge.

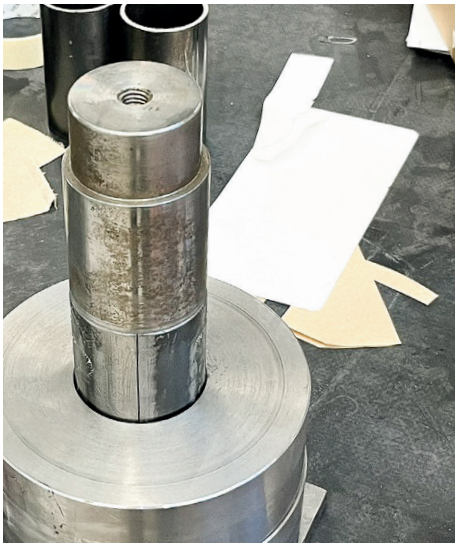

Figure 73: Fitting of the ejection plunger into the inner steel section.

Figure 74: Crack formation at the tube opening.

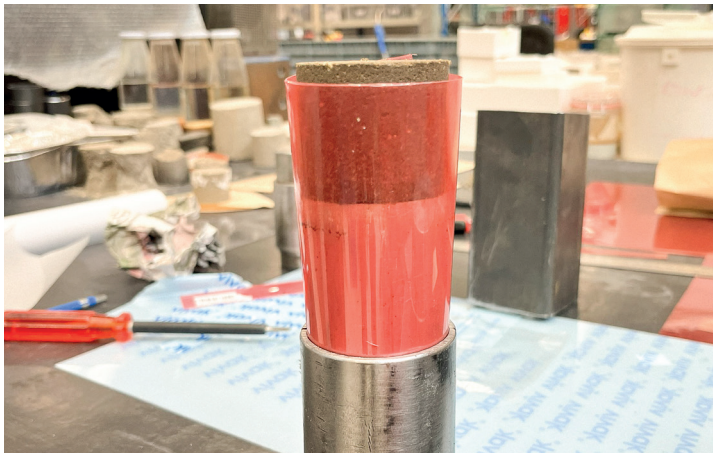

Figure 75: Successful release of the specimen using FPCR inlay.

depth of 1.5 mm to weaken the section locally (Fig. 72). This zone was intended to function as a hinge, allowing the tube to open sufficiently after pressing to release the specimen. Finally, the outer surface of the inner tube was polished using an angle grinder. To enable later removal of the inner ring without the need for additional tools or excessive force, a dedicated ejector piece was fabricated out of stainless steel (Fig. 73). The diameter needed to match the outer dimensions of the inner tube, while a stepped section was machined down to the internal diameter, allowing it to engage 20 mm into the tube.

(4) Test procedure

The test procedure comprised the following steps: (1) preparation of 225 g of mix, (2) placement of a steel base plate in the press, (3) insertion of a filter paper layer, (4) positioning of the first outer-ring cylinder, (5) precise alignment of the second outer-ring cylinder above it, (6) insertion of the pre-greased inner tube, (7) filling of 112.5 g of mix and light manual pre-compaction, (8) roughening of the surface until the earth became loose again, (9) filling of the remaining 112.5 g of mix, (10) manual insertion of the plunger to a depth of 15 mm, and (11) start of the pressing process (Fig. 71).

(5) Limitations

The first compaction trials proceeded smoothly during pressing, and the inner tube could be removed using manual force alone. However, a new problem became apparent during demoulding: As the inner ring was opened and released, the specimen tore from the side of the opening towards the centre because it adhered to the tube wall (Fig. 74).

(6) Mould inserts

Because the use of standard sections left a small clearance between the plunger and the inner tube, the idea emerged to prevent tearing of the specimens by introducing a thin mould liner. Filter paper and 100 g paper were tested for this purpose, each both with and without silicone spray. In all cases, the liners prevented the specimens from tearing during demoulding. However, both materials were repeatedly drawn into the mix by friction during pressing, resulting in surface indentations of varying size. In addition, edge spalling occurred at the underside of the specimens, as the moisture-softened paper was difficult to remove and often tore during separation. A further disadvantage was the instability of the paper inserts. In one instance, the plunger became jammed within the inner tube, and two larger indentations had to be filed out before testing could continue. This made paper-based liners unsuitable for a larger test series. The next idea was therefore to test an insert made from thin acrylic sheet, but this could not be fitted accurately due to the available thickness. The most suitable solution ultimately proved to be a 175 µm FPCR polyester film. This provided sufficient clearance to guide the plunger accurately while still allowing air and water to escape. At the same time, it was stiff enough not to be drawn into the specimen during pressing (Fig. 75).

4.2.5 Evaluation

It became evident that, even with good access to materials and workshop equipment, the development of a test setup suitable for high-compaction experiments required considerably more time and resources than initially anticipated. The main limitations lay in the fabrication of a formwork that was both sufficiently pressure-resistant and openable. Further, the lack of readily available standard components with matching tolerances, and the high friction forces arising during demoulding. At the same time, the setup was constrained by a fundamental geometric trade-off: The mould had to remain small enough for the required compaction pressure to be achieved with a smaller laboratory press, rather than requiring loads in the range of several hundred tones, while still satisfying the available clear heights of the machine. However, the specimen dimensions could not be reduced arbitrarily, as overly small samples would also limit the maximum grain size that could be processed and would therefore no longer represent realistic mix designs adequately. In addition, repeated adjustments were required to prevent specimen damage and reduce wear on the setup. Nevertheless, resolving these constraints was an essential step, as it provided the technical basis for a controlled and reproducible test series under defined compaction conditions.

Figure 76: Specimen series after compression testing.

5. Mechanical optimisation

5.1 Mix design variables

After establishing the soil's suitability, composition, mineral skeleton, and compaction setup, the next step was to develop an appropriate mix composition. The experimental series was therefore designed to identify the composition yielding the highest compressive strength and to isolate the effects of individual processing and mix variables.

5.1.1 Setup and parameter ranges

A first methodological challenge arose from the direct interdependence between clay and moisture content during pressing. In earth mixtures, the optimum water content cannot be defined independently, as it increases with the clay fraction. This is due to the high specific surface area of clay minerals, which must be sufficiently wet to become plastic, and to activate electrochemical attraction between the clay platelets (Minke, 2025; Schroeder, 2016). In theory, an optimum moisture content could be determined for each clay share using the classical Proctor test. This approach was not adopted here, however, because it is highly time-intensive and does not adequately represent the static compaction conditions relevant to CEB production. Given the material and time demands of full-scale block testing, as well as the geometric constraints imposed by the high press loads in the laboratory setup, the experimental strategy employed a constant peak stress-variable stroke approach. This involved testing a range of moisture contents for each clay under constant pressure while recording the resulting varying compaction height.

(1) Selection of clay content range

Because clay acts as the sole binder in unstabilised earth blocks, most literature identifies 10% as the minimum clay content required to ensure sufficient cohesion of the mineral skeleton (Schroeder, 2016). For cement- or lime-stabilised blocks, experimental studies indicate that the technical optimum typically lies within a narrow range of 10-15 % clay content (Reddy, 2022). In unstabilised blocks, however, the upper limit is not controlled by interaction with chemical stabilisers, but primarily by the mineral-specific shrinkage behaviour of the material in combination with packing density and particle-size distribution. The selection of a grading coefficient of n = 0.3 for reconstitution of the laboratory sand resulted in an optimal fine share of 25.12 %, corresponding to a clay content of 11 % for the investigated soil. As this value lies only slightly above the minimum threshold, it was defined as the lower limit for the experimental series. Reddy, (2022) further refers to general earthen construction guidelines and literature, such as Walker et al. (2005), which commonly indicate a theoretical upper limit of up to 20 % clay content for earthen materials. Beyond this range, the risk of volumetric instability increases. This was also supported by the present preliminary tests, in which mixtures with a soil content above 45 % exceeded the critical shrinkage limit of 2 % defined in standards such as DIN 18952. This led to setting the upper limit of the experimental series at 19 % clay, corresponding to 43.18 % soil. The clay content was then varied in increments of 2 %. This interval was chosen to balance methodological efficiency with analytical resolution.

Since specimen preparation and pressing required considerable time and material input, the selected step size allowed the full parameter range to be covered while still making significant trends and correlations identifiable. More targeted refinement within the interval of the identified optima remained possible at a later stage. At the same time, the experimental design assumed that the admixed soil acted only as a fine fraction within the mix. Although the soil itself contained 14.3 % sand, this proportion consisted, as described in the geotechnical classification, only of very fine particles. In addition, milling the soil reduced the material to a fine powder without grain sizes that may significantly contribute to the mineral skeleton.

(2) Definition of moisture content range

According to Schroeder (2016), the optimum moisture range for wet pressing lies between 8 % and 15 %, which corresponds to the common production range for compressed earth blocks under press loads of up to 20 MPa. However, the preliminary mix tests showed that moisture contents of approximately 12-15% could cause severe clump formation and resulted in compositions that were too wet for

Figure 77: Mixture at the processing limit, showing severe clumping during mixing.

Figure 78: Sample weight check after moisture distribution period.

Figure 79: Specimen series oven-dried at 60 °C to avoid alteration of the mineralogical composition.

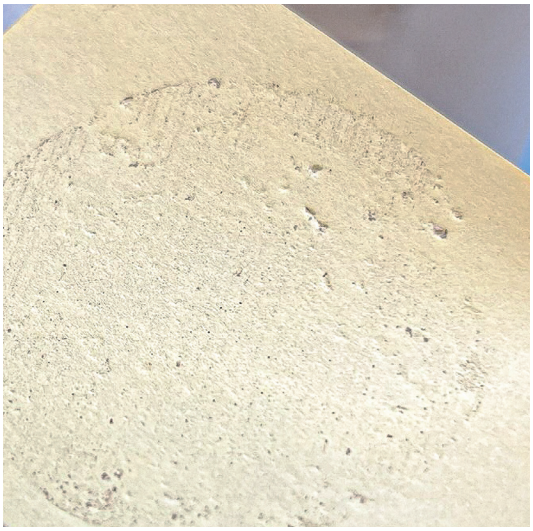

Figure 80: Interlayer absorbing surface irregularities during compression testing.

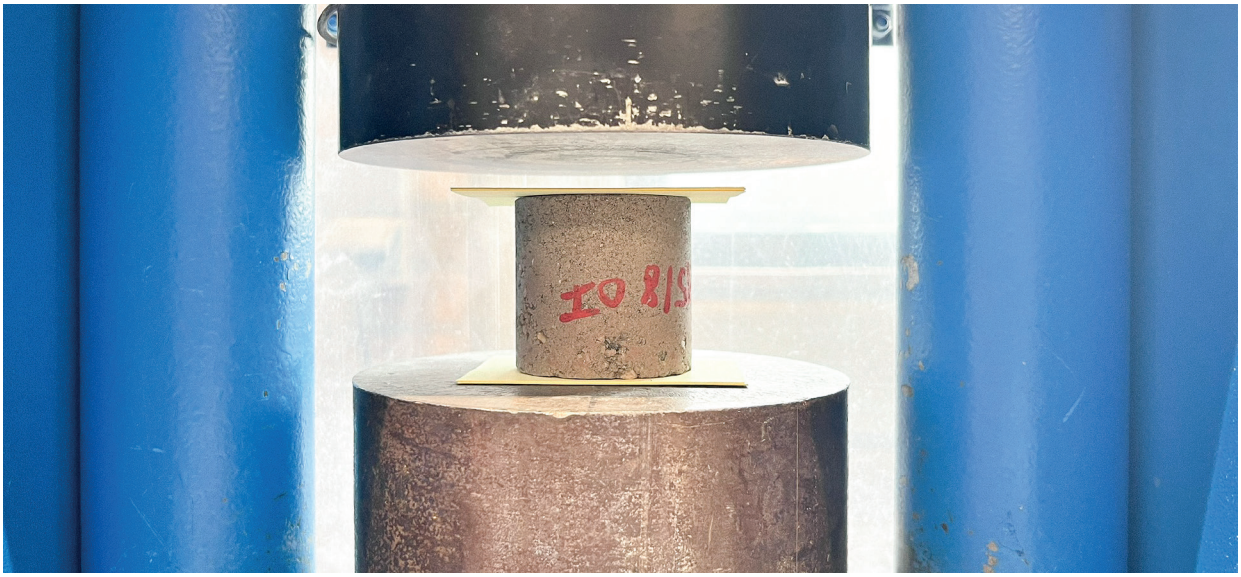

Figure 81: Specimen positioned in the testing press.

effective compaction. The experimental series was therefore started at 8 % moisture for each examined clay content and increased this value in increments of 1 % until the processing limit was reached (Fig. 77). The maximum workable moisture therefore increased stepwise with clay content, reaching 11 %, 12 % and 13 % for the lower, intermediate and highest clay-content compositions.

(3) Mix Preparation

For the first series, a total of 24 specimens were prepared and processed under identical conditions. First, the clay powder was dry mixed with the sieved sand. Secondly, water was added using a syringe. Third, the mixture was blended for 300 s. For each sample, 250 g were transferred into an airtight bag and weighed. Before pressing, the mass was checked again to ensure that no moisture had been lost through leakage. Finally, the mixtures were left to rest for 12 h to allow the moisture to distribute evenly (Fig. 78).

(4) Compaction

After preparation of the mould, 112.5 g of the respective mix was filled in, lightly pre-compacted by hand, and roughened again at the surface before a further 112.5 g was added. Each specimen was therefore pressed from a total mass of 225 g at an initial height of 85 mm. All samples were compacted under a press load of 10 MPa. A compaction rate of 0.1 kN/s was selected to prevent tilting of the plunger and to allow sufficient time for material consolidation. Pressing time, the specimen height after ejection, and the mass after pressing were recorded.

(5) Drying

All specimens were first air-dried for 48 h at laboratory temperatures between 15 and 20 °C. After this period, the moisture content of all samples had already fallen below 5 %. The specimens were then oven-dried at 60°C for 240 min under continuous fresh-air ventilation (Fig. 79). After removal from the oven, they were left in the laboratory for 24 h to re-equilibrate under room temperature.

(6) Compression test

Before each test, the specimen mass was recorded, and three calliper measurements were taken for both height and diameter, from which mean values were derived. In addition, the outer edges were lightly deburred using 250-grit sandpaper. To compensate for minor surface irregularities that could otherwise lead to premature failure, and to reduce friction between the compression plates, a 0.58 mm paper layer was placed on both sides of each specimen. Fig. 80 shows how small surface irregularities were absorbed by the interlayer.

(7) Normalization of strength results

One limitation of the constant peak - stress variable stroke approach was that the resulting specimens differed slightly in height. As all compression tests were carried out in the concrete laboratory, an initial form factor of 0.87 for h/d = 1 was adopted, consistent with the correction setting of the machine used, to estimate shape independent strength. This was considered an appropriate reference, as the earth specimens likewise exhibit brittle failure behaviour. Because the cylindrical specimens nevertheless showed slight geometric variation around a slenderness ratio of 1, the measured compressive strengths were subsequently corrected more precisely by linear interpolation. Following ASTM-based aspect-ratio correction tables, the equivalent compressive strength of a standard cylinder with h/d = 2.0 corresponds to a factor of 1.00. The specimen-specific correction factor, k, was therefore calculated as:

$$k = 0.87 + 0.13\left(\frac{h}{d} - 1\right)$$

The factor was then multiplied by the measured failure stress to obtain the equivalent compressive strength, $f_{c,eq}$.

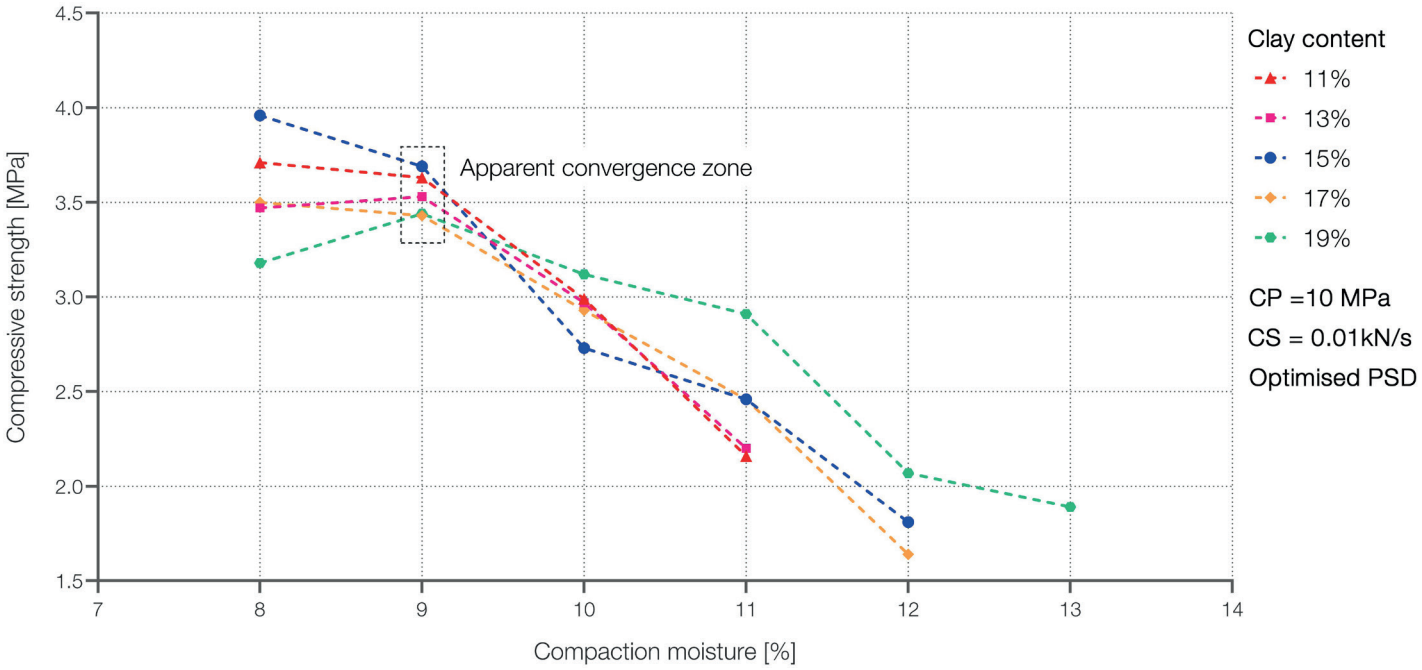

Figure 82: Raw compressive strength over the investigated compaction-moisture range for different clay contents.

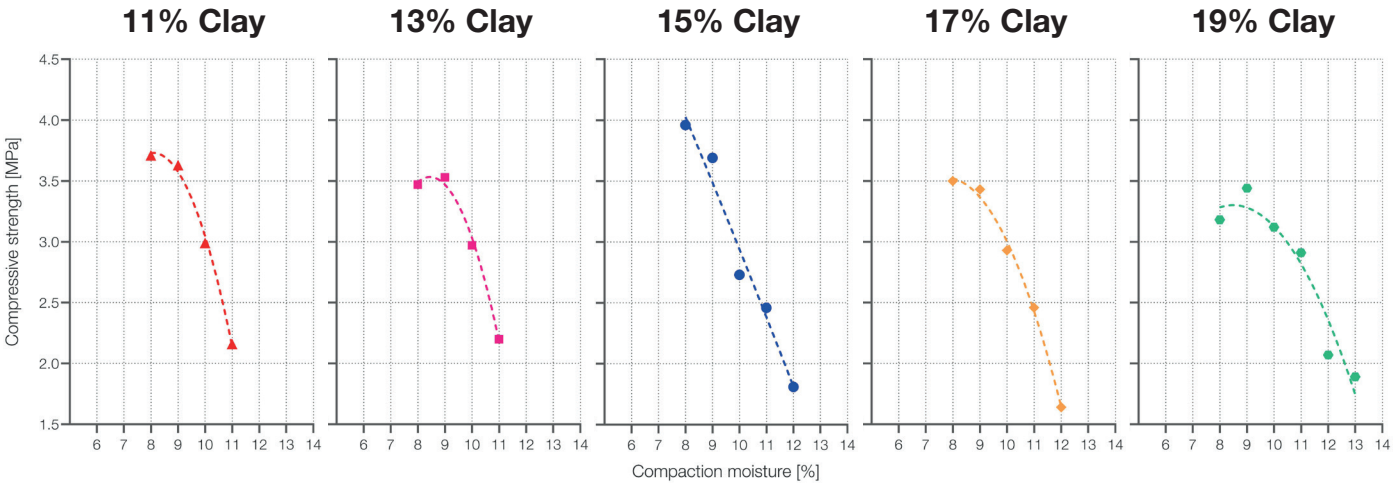

Figure 83: Raw compressive-strength and polynomial fits over the investigated compaction-moisture range for individual clay contents.

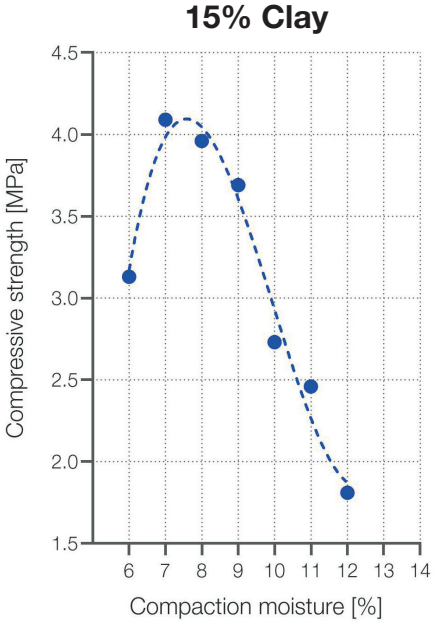

Figure 84: Raw compressive-strength and polynomial fit over the investigated compaction-moisture range for 15% clay content.

5.1.2 Effect of compaction moisture and clay content on compressive strength

To capture initial trends and identify more favourable compositions, the measured raw compressive strength of the first 24 specimens was plotted against their respective moisture during compaction. This was done for each clay-content series, with every data point representing one sample and each curve corresponding to one clay amount (Fig. 82). Given the brittle nature of the material and the use of single data points, the plotted values should be interpreted as indicative and subject to natural scatter. Even so, the data showed a dominant negative effect of compaction moisture on mechanical stability across the entire clay-content range, beginning at the lowest tested level of 8 % and persisting up to 13 %.

The strength maximum of 3.96 MPa was reached at a composition of 15 % clay content and 8 % compaction moisture. A similarly high value of 3.71 MPa was obtained at the same moisture level with a lower clay share of 11 %. While the mix with the highest clay content of 19 % showed the lowest initial strength at 8% moisture, it seemed to exhibit a higher tolerance to increasing water content, reflected in a flatter decline in strength. In addition, a zone of convergence was indicated at 9 % moisture content, where the compressive strengths of all mixes temporarily converged irrespective of clay content. While standard deviation decreased from 0.291 at 8 % to a minimum of 0.115 at 9 % (n = 5), at higher moisture contents, the values diverged again, accompanied by a renewed increase to 0.141 at 10 % and 0.299 at 11 %.

Following this, a second-order polynomial regression model was applied to facilitate visualizing the relationship between compaction moisture and compressive strength within each clay-content series (Fig. 83). This approach was chosen based on the premise that an optimum moisture content exists for compressive strength. As the mix with 15 % clay did not yet indicate a characteristic decline in strength and exhibited the maximum value at 8 % compaction moisture, an additional targeted pressing series was carried out. The experimental range was therefore extended downwards by two further measurements at 6 % and 7 % moisture. With these additional data points, the expected non-linear trend could be reconstructed in the final regression graph (Fig. 84). To capture the underlying asymmetry of the material response more accurately, this specific dataset was modelled using a third-order polynomial. The results confirmed the initial assumption: At 7 % moisture, the measured compressive strength increased further to 4.09 MPa, representing the highest value of the entire experimental series, whereas at 6 % moisture the strength decreased again.

Overall, the results indicated, that optimal compaction moisture was considerably more influential than optimal clay content, provided that the minimum clay threshold is not undershot.

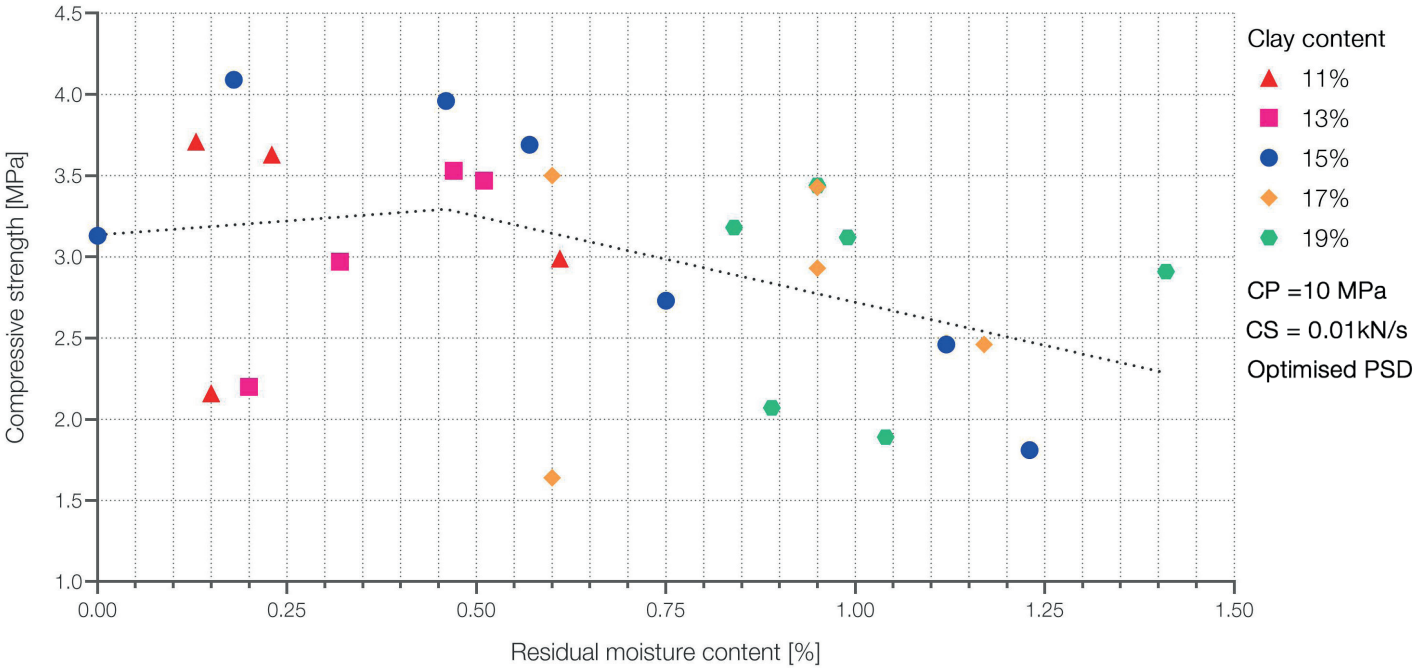

Figure 85: Residual moisture content of samples across the investigated compaction-moisture range for different clay contents.

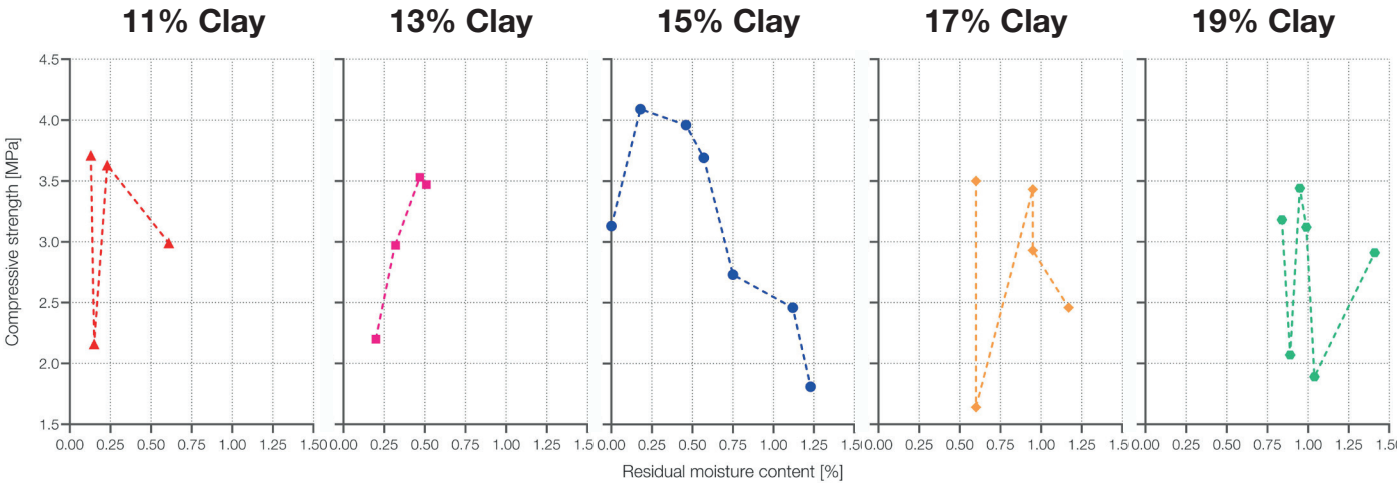

Figure 86: Residual moisture content of samples across the investigated compaction-moisture range for the individual clay contents.

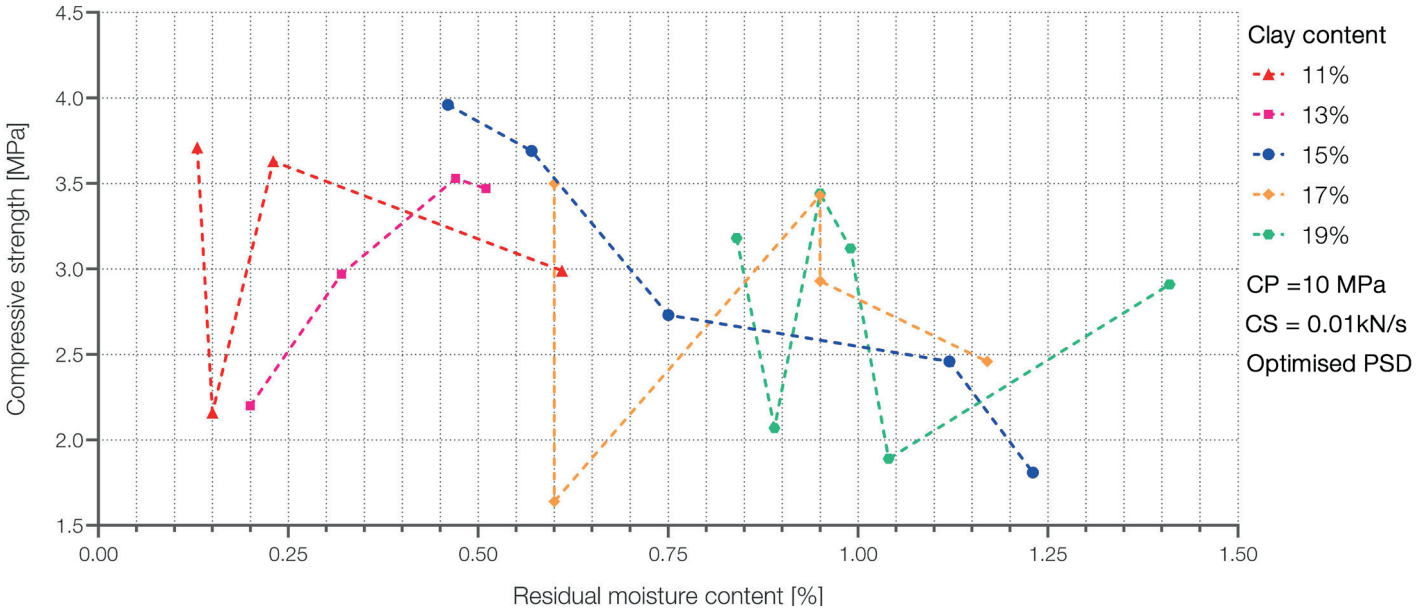

Figure 87: Residual moisture content of samples across the investigated compaction-moisture range for the different clay contents, as connected data points.

5.1.3 Influence of residual pore water

Despite the standardized drying history, with identical exposure time under constant ambient conditions, the different formulations retained distinct residual moisture contents ranging from 0 to 1.41 %. This divergence was consistent with increasing clay contents. When interpreting the raw data, it therefore had to be considered that no uniform zero-moisture state had been reached across all samples and that the influence on compressive strength first had to be assessed.

An initial linear regression across all 26 data points did not yield a statistically significant result. A simple linear model was therefore not sufficient to describe the relationship between residual moisture and compressive strength. This was also evident from the experimental data themselves. In the series with 13 % clay, for example, the specimen with the highest compressive strength, still exhibited a residual water content of 0.47 %. Whereas a specimen retaining only 0.20 % moisture showed a distinct strength decline. A comparable pattern was observed in the other series, where specimens with nearly identical residual moisture contents still exhibited markedly different compressive strengths. In the mix with 17 % clay, one specimen reached 3.43 MPa despite a comparatively high residual moisture content of 0.95 %, while the other sample containing only 0.60 % moisture achieved 1.64 MPa. To test whether a systematic change in behaviour nevertheless occurred beyond a certain residual moisture level, a pooled segmented linear regression analysis was applied. This model suggested an apparent transition point at 0.46 % residual water content (Fig. 85). Below this threshold, the initial slope was not statistically significant, indicating that no reliable increase in strength could be demonstrated. Above 0.46%, by contrast, a statistically significant negative slope was obtained. However, the global explanatory power of the model remained too limited in order to draw meaningful conclusions (R^2=0.1777; Sy.x = 0.6705 MPa).

That is why in the following step, the clay series were examined separately (Fig. 86). This showed that, for clay contents of 11 %, 13 %, 17 %, and 19 %, residual moisture did not exhibit a systematic pattern with respect to compressive strength loss. The trend observed in the 15 % clay series therefore appeared more likely to reflect a localized coincidental anomaly than a universal mechanism within this moisture range. On this basis, no general mathematical correction was applied to the raw dataset at this stage. At the same time, when the series were plotted together, a continuous rightward shift in residual moisture became apparent (Fig. 87), indicating that mixes with higher clay contents retained higher internal moisture after the same drying period. It was therefore be concluded that the physical trend identified in the previous section was not likely to be fundamentally distorted by residual moisture, even though individual values may have still been subjected to natural variation. This was further supported by the 11 % clay series, for which all specimens were dried to constant mass and nevertheless showed the same dependence on compaction moisture as the other curves. In addition, the peak values of the 11 %, 13 %, and 15 % clay series could be compared directly, as all specimens were dried to constant mass. Within this comparison, the composition with 15 % clay and 7 % compaction moisture therefore remained the overall maximum, reaching 4.09 MPa. For the 17 % and 19 % clay series, however, no equally definitive conclusion could be drawn. The peak value of 3.50 MPa at 17 % clay still showed a residual moisture content of 0.60%, while the peak value of 3.44 MPa at 19 % clay and 9 % compaction moisture still retained 0.95 % moisture. It could therefore not be excluded that, if dried to constant mass, these specimens would have reached similar peak strengths. Residual moisture thus appeared insufficient to explain the overall behaviour but remained relevant for the interpretation of individual peak values in the clay-richer series.

It was therefore concluded that remaining pore water may have locally affected individual measurements, leading to limited deviations in compressive strength, but did not fundamentally alter the overall trend.

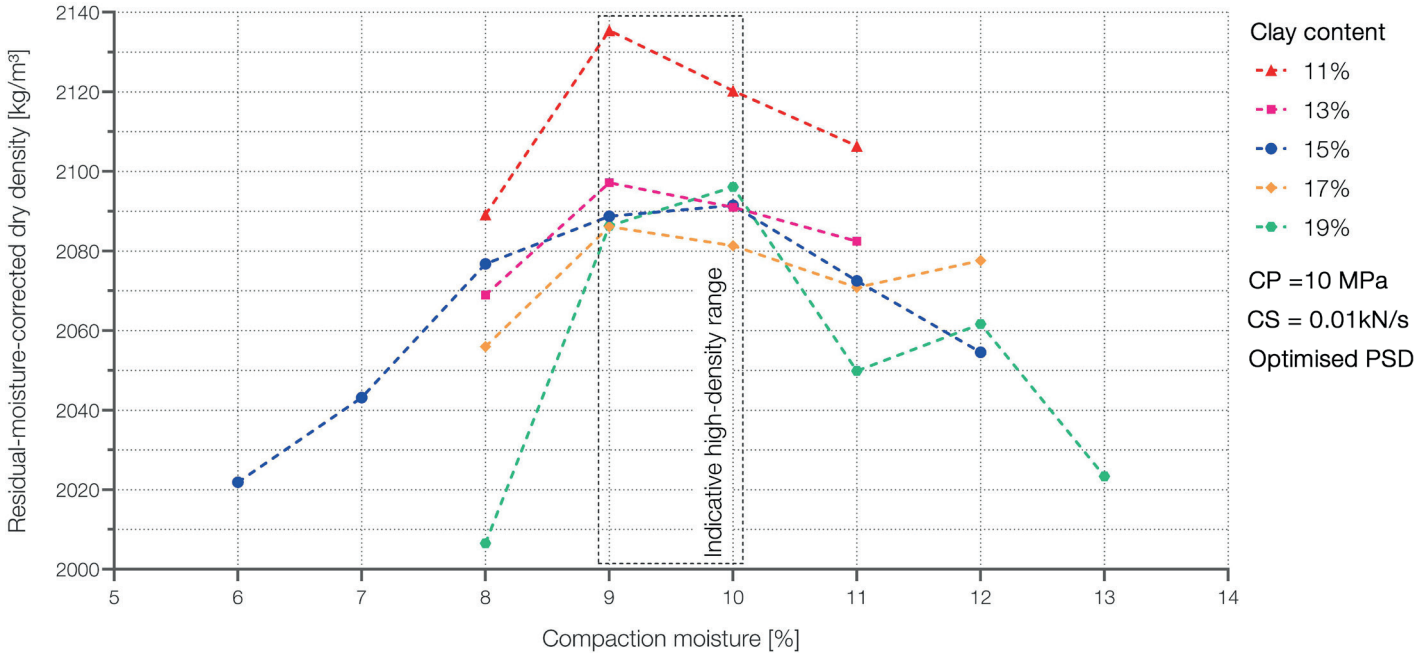

Figure 88: Residual moisture corrected dry density over the investigated compaction-moisture range for different clay contents.

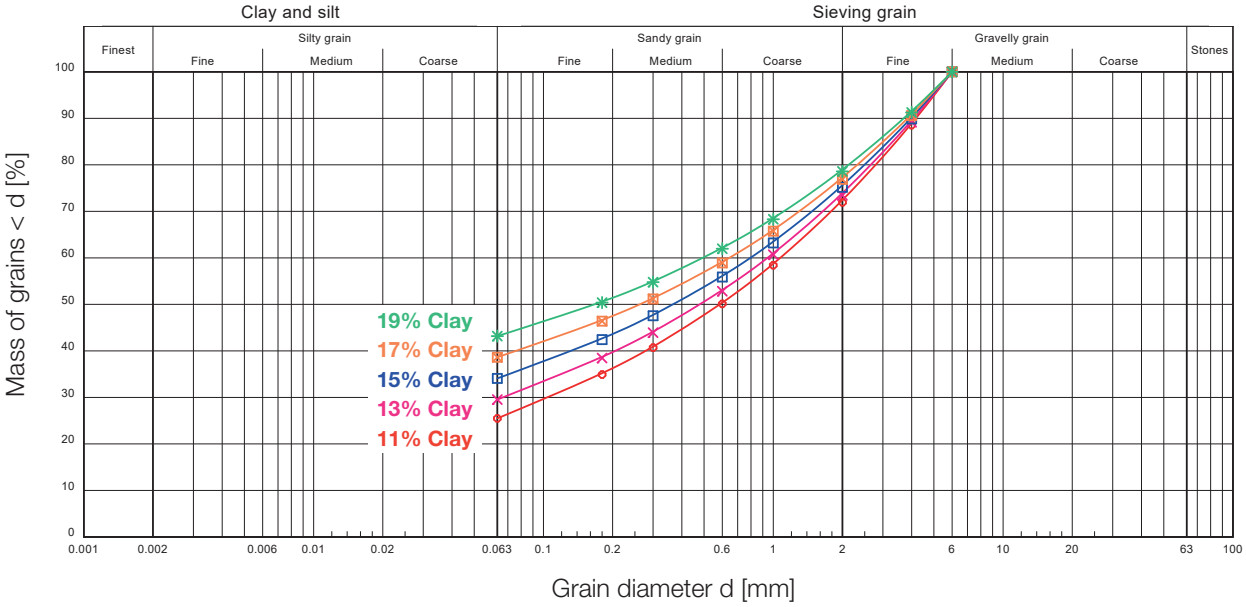

Figure 89: Adapted sand grading curve for different clay contents.

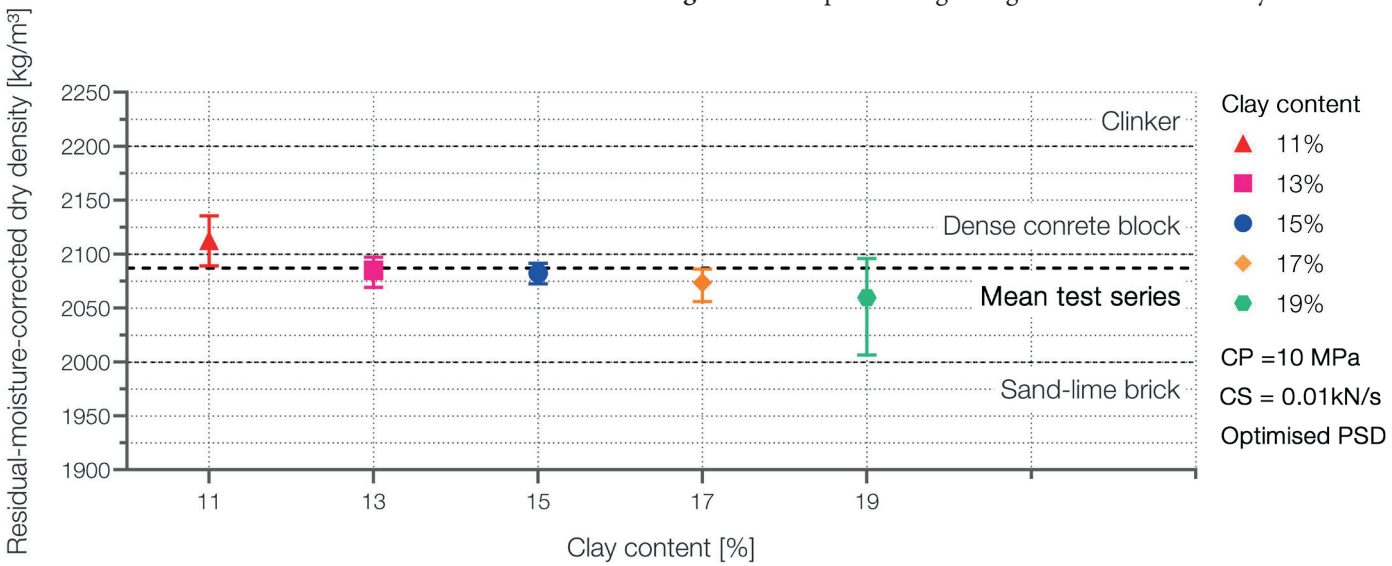

Figure 90: Mean corrected dry density for each clay content with range indication.

5.1.4 Moisture-density relationship

Unlike compressive strength, dry density could be corrected for residual moisture without requiring further assumptions. The following analysis was therefore based on residual-moisture corrected density values to consider variability in the specimens. However, the applied correction remained limited, with a median adjustment of 0.6 % and a maximum adjustment of 1.41 %. Subsequently, the corrected dry density was plotted against compaction moisture.

Across all clay contents, the resulting curves indicated a similar trend, resembling the typical moisture density relationships known from Proctor tests, although the latter are based on dynamic rather than static compaction. Each clay content therefore exhibited a density maximum at a specific moisture level, beyond which dry density decreased on either side of the optimum. For clay contents of 11 %, 13 %, and 17 %, the maximum dry density was reached at 9 % compaction moisture, whereas for 15 % and 19 % clay content it occurred at 10 %. This suggested a common high-density range within a compaction-moisture window of 9-10 % across all tested clay contents.

The highest measured dry density was 2135.46 kg/m³, obtained at 11 % clay content and 9 % compaction moisture. The shared moisture range of 8-11 % further allowed the trends to be compared directly across all formulations. Across this interval, the mean dry density showed a slight decline from 11 % to 19 % clay content (Fig. 88). This could be related to the previously calculated optimum packing state based on the modified Fuller curve, which reached its closest match at 11 % clay content and was progressively exceeded with increasing fine shares (Fig. 89). Since the densities for 13 %, 15 %, 17 %, and 19 % clay remained within a very narrow range, this suggests that similarly high dry densities may be achievable if the grading curve is adjusted more precisely to the respective clay content. Fig. 90 also places the mean dry density of the test series in relation to other conventional construction materials. Across the investigated clay contents, the dry density falls within a range between sand-lime bricks and dense concrete blocks.

The results showed that dry density followed a consistent moisture-dependent optimum across all clay contents, while the narrow variation at high density levels suggested that the optimised particle size distribution and compaction setup produced a uniformly dense packing.

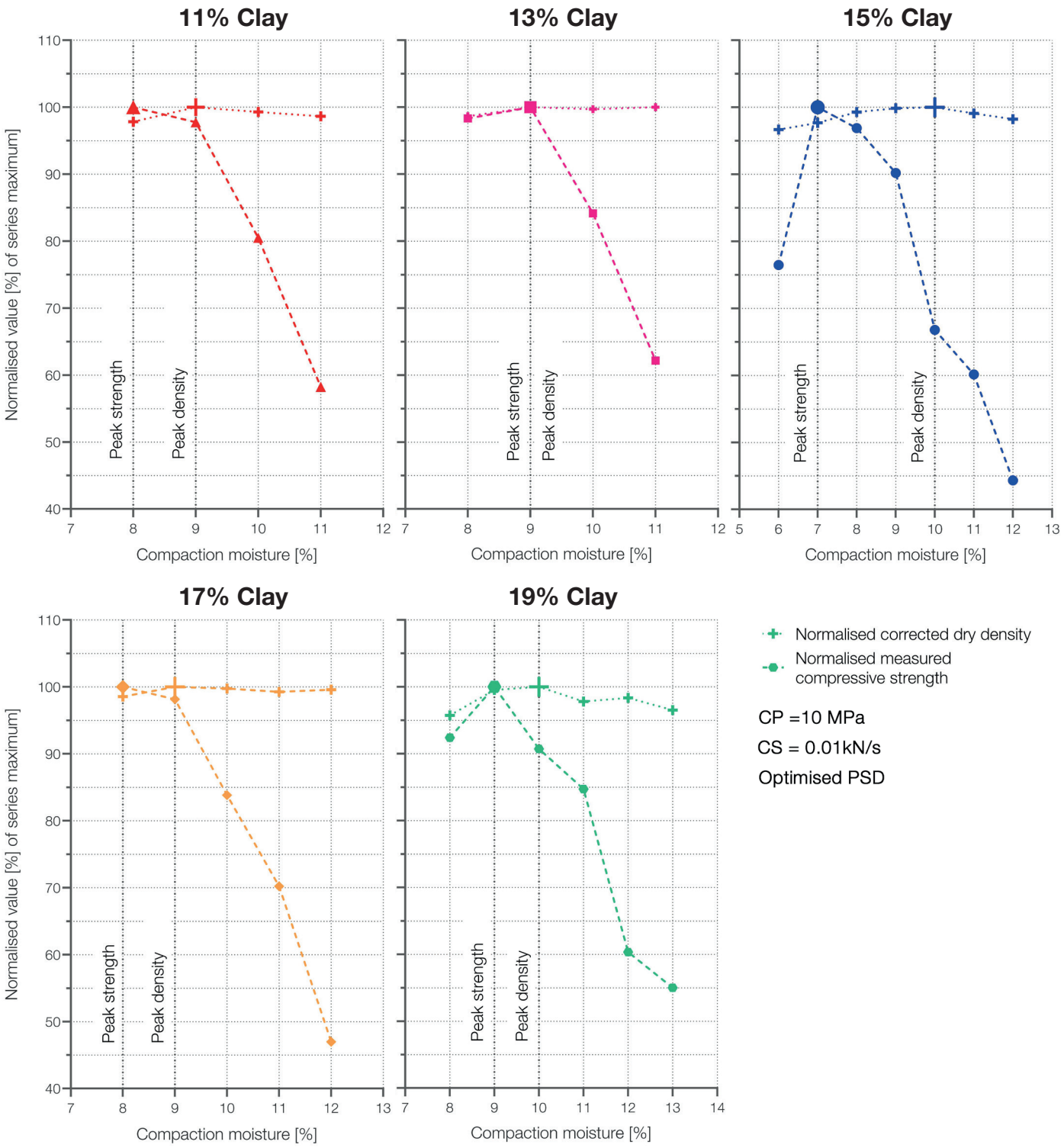

Figure 91: Normalised dry density and compressive strength relative to the series maximum over the investigated compaction-moisture range.

5.1.5 Dry density and compressive strength

The similar plateau formation of peak compressive strength and maximum dry density suggested, that the optimum pressing moisture for both may coincide or overlap closely. It also raised the question of whether specific density levels correlated with corresponding strength values. To compare the moisture-dependent response of dry density and compressive strength despite their different units, both parameters were normalised to the maximum value within each clay content series. Because the tested moisture ranges were not identical for all clay contents, the comparison was carried out in individual series plots (Fig. 91). This approach did not remove the remaining uncertainty associated with residual moisture or material scatter, but it allowed the relative position of the highest measured density and compressive strength to be evaluated.

Direct comparison showed, that the relative variation in dry density remained within a very narrow range across all clay contents, with a maximum deviation of only 4.27 %. By contrast, the corresponding variation in compressive strength was substantially larger, reaching more than 55 % within the 15 % clay series alone. Since this trend was observed across all clay contents, the achieved dry density within this range was seen unlikely to represent the lone controlling factor for the final strength. This showed, for example, in the 19 % clay 12 % compaction moisture composition, which reached 98.36 % of the maximum dry density of its series but only 60.34 % of the corresponding maximum compressive strength. A significant influence of residual moisture could likewise be excluded. In the 11 % clay series, for which all specimens were dried to constant mass, the 11/10 formulation still reached 99.29 % of the maximum dry density of the series, but only 80.50 % of its maximum strength.

Regarding the optimum moisture contents for peak strength and peak dry density, coincidence occurred only in the 13 % clay series, where both maxima were reached at 9 % compaction moisture. In the 11 %, 17 %, and 19 % series, the maximum compressive strength occurred at a moisture content level 1 percentage point lower than that of maximum dry density. In the 15 % series, for which a wider moisture range was tested, the optimum strength range was shifted even further, lying 2 percentage points below the measured peak-density. Given the experimental limitations and the natural scatter of brittle materials, the observed offsets were interpreted with caution.

Nevertheless, the overall results showed that dry density and compressive strength followed a similar moisture-dependent pattern. Their respective optima, however, did not appear to systematically coincide at the same compaction moisture content. Further, dry density showed no consistent correlation with compressive strength, suggesting that, within the narrow density range achieved, compactness alone was insufficient to explain the observed strength development.

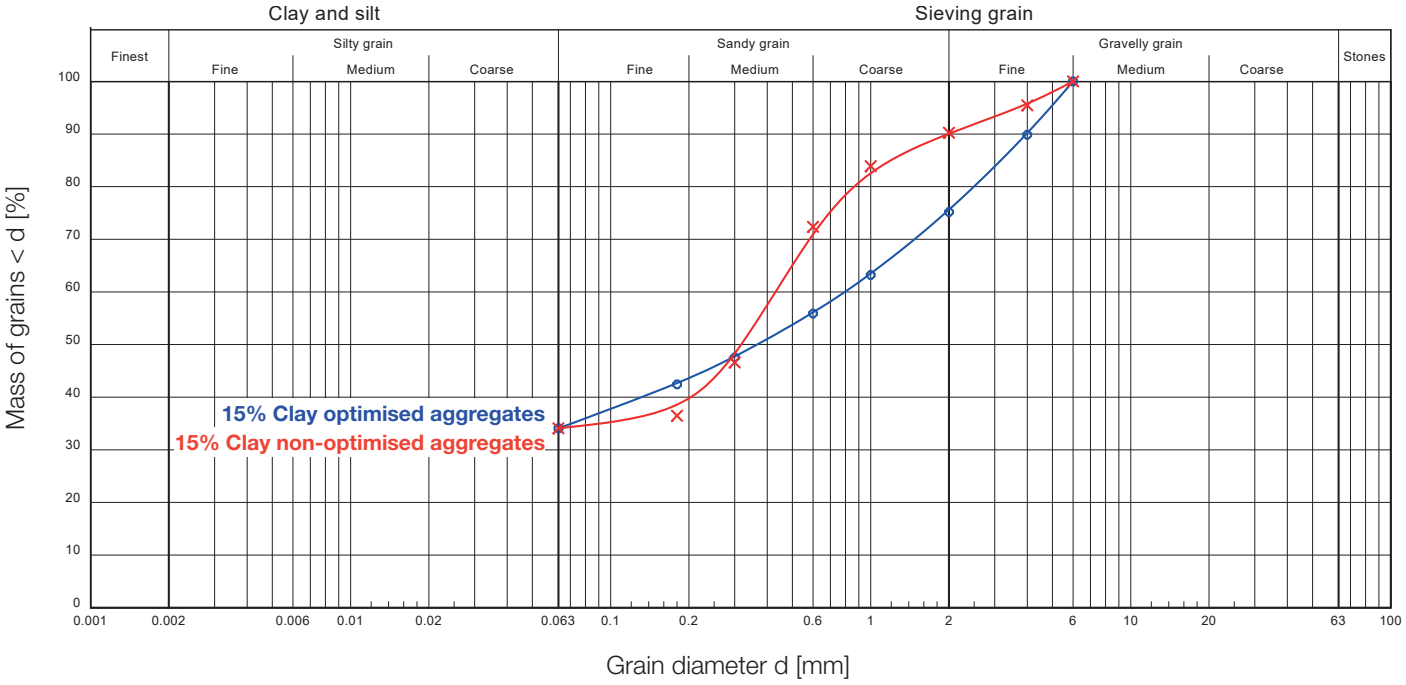

Figure 92: Optimised and unoptimised sand grading curves at 15% clay content.

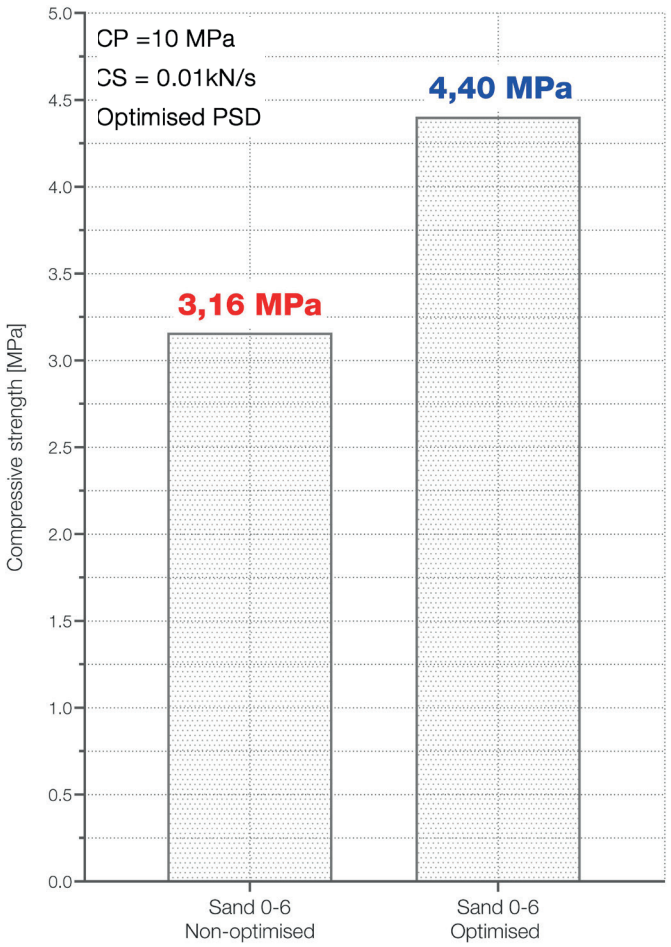

Figure 93: Mean compressive strength of the optimised and unoptimised mixtures at 15% clay content.

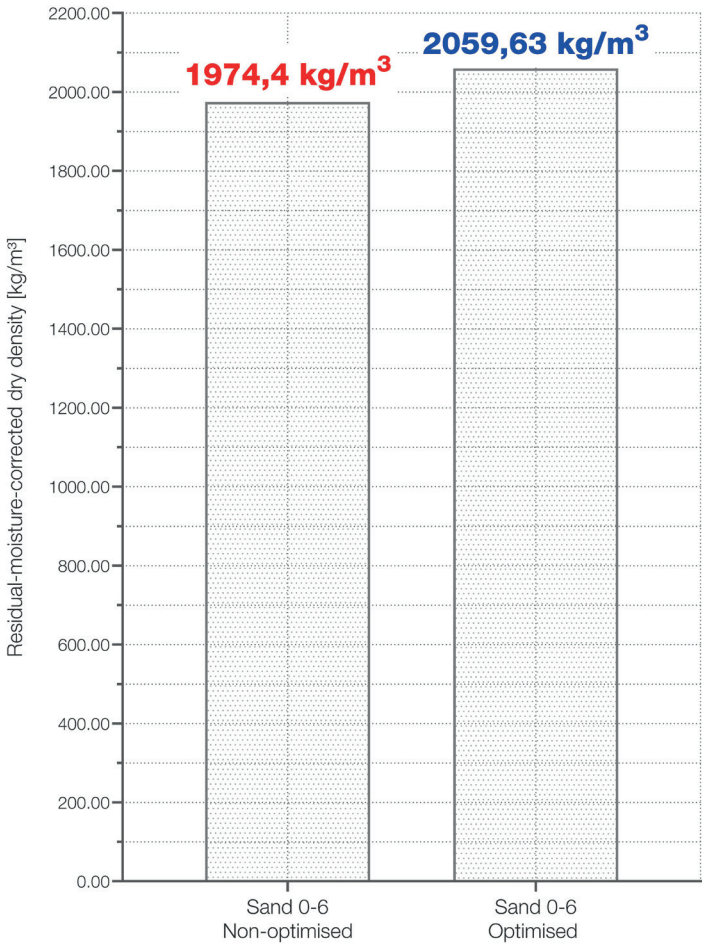

Figure 94: Mean dry density of the optimised and unoptimised mixtures at 15% clay content.

5.1.6 Effect of particle-size optimisation on compressive strength

To assess the effect of PSD optimisation, three optimised specimens with a clay content of 15 % and a compaction moisture content of 8 % were reproduced. Subsequent they were compared with three specimens containing the same composition, but an unoptimized sand skeleton. Since all fractions above 6 mm had been removed for the optimised mix, the same upper grain-size limit was also applied to the unoptimized mixture. The corresponding particle-size distributions are shown in Fig. 92.

Despite the comparatively small sample size of n = 3, the results indicated a clear strength increase through grading optimisation. The unoptimised specimens reached a mean compressive strength of 3.16 MPa with a standard deviation of 0.196 MPa, whereas the optimised specimens achieved a mean strength of 4.40 MPa with a standard deviation of 0.384 MPa. This corresponded to an average increase of 39,2 %. An exploratory unpaired Welch's t-test indicated a statistically significant difference between both groups, with a mean shift of 1.243 MPa. Although brittle materials exhibit a certain degree of scatter, the measured strength ranges remained without overlap, supporting the conclusion that optimization of the PSD had a substantial positive effect on compressive strength. By contrast, comparison of the achieved dry densities showed a much smaller relative difference between (Fig. 94). While the unoptimized specimens reached a mean dry density of 1974.41 kg/m³, the optimised specimens achieved an average of 2059.63 kg/m³. This corresponds to an increase of only 4.3 %. The gain in dry density was therefore comparatively small relative to the increase in compressive strength.

As an additional exploratory check within the optimized PSD setup, two further specimens were compressed at lower loading rates of 0.05 kN/s and 0.025 kN/s instead of the standard 0.1 kN/s. The sample pressed at 0.05 kN/s showed a lower compressive strength of 3.81 MPa while also reaching a comparatively low dry density of 2018.5 kg/m³, whereas the specimen pressed at 0.025 kN/s exceeded the previous strength maximum by a small margin, reaching 4.78 MPa. Given the very limited number of additional tests and the inconsistent direction of the response, these differences were interpreted as experimental scatter rather than as clear evidence of a systematic effect. The parameter was therefore not pursued further in this study, although a possible influence of compaction rate cannot be fully excluded.

Taken together, these results indicated that PSD optimisation substantially increased compressive strength, whereas the accompanying increase in dry density remained comparatively small. No systematic effect of compaction rate could be identified within the supplementary test.

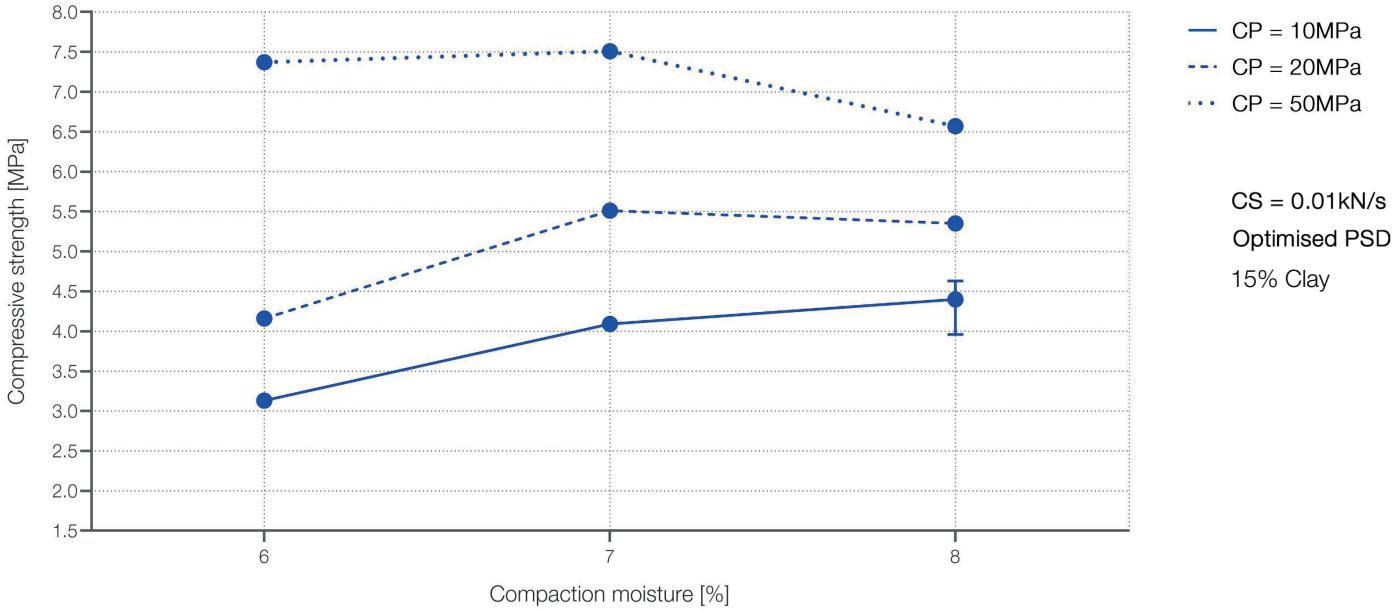

Figure 95: Raw compressive strength over the investigated compaction-moisture range for different moulding pressures.

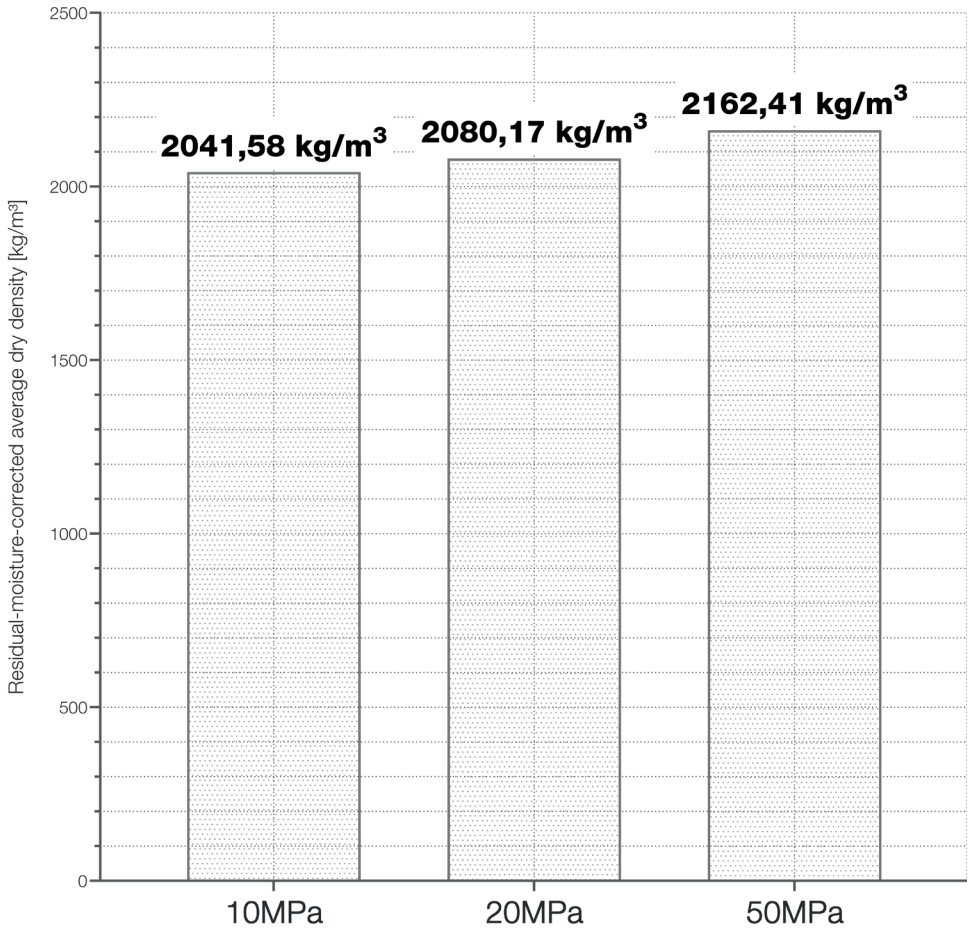

Figure 96: Mean dry densities for different compaction pressures.

5.1.7 Effect of elevated press loads on dry density and compressive strength

Up to this point, all specimens had been compacted at 10 MPa. For CEB production, this already represented a comparatively high-pressure level and was consistent with the upper range of current block pressing practice. This was also reflected in the high mean dry density of 2087 kg/m³ achieved for the optimised grain skeleton. Since compaction pressure is a key parameter in the mechanical performance of CEBs, two additional pressure levels were investigated, with three specimens produced at each level: 20 MPa and 50 MPa. Since moulding pressure also influences the optimum moisture content, tending to decrease with increasing compaction load (Reddy, 2022), a moisture range of 8 %, 7 %, and 6 % was prepared for each series.

Fig. 95 shows the compressive strengths achieved at the respective compaction-moisture levels for all applied compaction loads. For the 10 MPa series at 8 % moisture content, an indicative scatter range is additionally shown, based on previous replicate measurements. The results showed, that increasing the load to 20 MPa led to an average increase in compressive strength of 29.7 % across the tested moisture range. The highest compressive strength was reached at 7 % compaction moisture, with a value of 5.51 MPa. This corresponded to an increase of 35 % relative to the 10 MPa series at the same moisture content and to an increase of 18.9 % compared with the previous peak value obtained at 10 MPa. A further increase in press load from 20 to 50 MPa raised the average compressive strength across the same moisture range by a further 45 %. The peak value was again reached at 7 % moisture content, with a compressive strength of 7.51 MPa. This corresponds to an increase of 36 % relative to the peak value at 20 MPa and to an overall increase of 62 % compared to the 10 MPa series.

Dry density likewise increased systematically with compaction pressure. The mean dry density rose by 1.9 % from 10 to 20 MPa and by a further 3.9 % at 50 MPa. At the same time, the density range remained similar between 10 MPa and 20 MPa, at 37.73 and 39.52 kg/m³, respectively, but narrowed markedly at 50 MPa to only 14.23 kg/m³. A comparable trend was observed for compressive strength, whose spread decreased from 1.27 MPa at 10 MPa and 1.18 MPa at 20 MPa to 0.94 MPa at 50 MPa.

Overall, the findings suggested that higher press loads not only raised the general level of compaction and compressive strength, but also seemed to reduce the sensitivity of both parameters to fluctuations in compaction moisture.

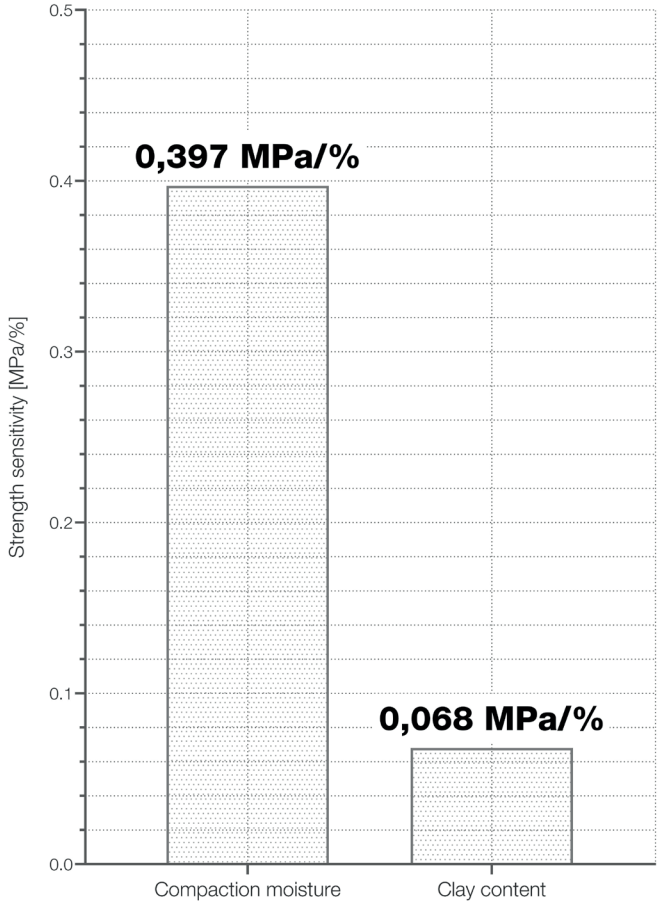

Figure 97: Relative sensitivity of compressive strength to a 1% change in clay content and compaction moisture within the investigated mix range.

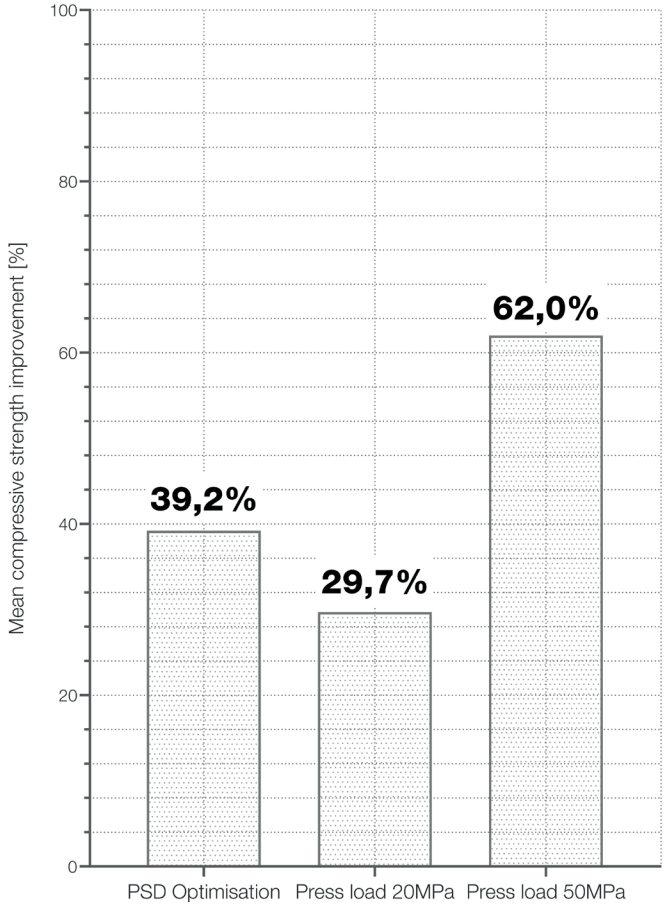

Figure 98: Average strength improvement through PSD optimisation and increased compaction pressure.

5.1.8 Comparative summary of mix and process parameters

In order to conclude the experimental results, the relative influence of the mix variables was evaluated by means of a comparative sensitivity analysis, while the processing parameters were assessed in terms of their resulting strength gains. Starting with the assessment of the compaction moisture influence, the observed strength range was first determined separately within each clay series across the common interval. These range effects were then averaged and related to the global strength range of the full dataset (R_{total} = 1.80 MPa). In this way, the average moisture-driven range effect of 1.19 MPa corresponded to 66,2 % of the total observed strength window. The same procedure was applied to each moisture series. In this way, the average clay driven range effect of 0.54 MPa corresponded to 30.2 % of the total observed strength window.

Since both parameters were varied over different intervals, however, this comparison still reflected only their observed contribution to the global response window and did not yet allow a direct sensitivity comparison per percentage point. For this reason, both effects were normalized by their respective tested parameter ranges. This yielded a moisture sensitivity of 0.397 MPa per percentage point and a clay sensitivity of 0.068 MPa per percentage point (Fig. 97). On this basis, compaction moisture showed an approximately 5.8 - fold stronger effect on compressive strength per tested percentage point than clay content.

As a complementary measure, the practical optimisation potential within the shared experimental window was also considered (Fig. 98). For compaction moisture, the relative strength gain between the minimum and maximum value within each clay series was evaluated across the common moisture range of 8-11 %. This showed that the achievable strength gain decreased systematically with increasing clay content, from 71.7 % at 11 % clay to 18.0 % at 19 % clay. Thus, although moisture exerted the stronger overall influence, its optimisation potential became progressively smaller in the clay-richer formulations. By contrast, the corresponding gains associated with clay variation remained smaller and less systematic, ranging from 7.5 % to 34.6 % across the tested moisture levels, without a clear pattern. Beyond these mix variables, the processing parameters showed that substantial strength gains could be achieved through targeted intervention. PSD optimisation increased mean compressive strength by 39.2 %. Likewise, increasing the press load from 10 to 20 MPa raised the average compressive strength across the tested range by 29.7 %, while a further increase to 50 MPa produced an additional gain of 45 %. In relation to the original 10 MPa reference series, the peak compressive strength at 50 MPa was thus increased by 62%.

These observations showed that, despite experimental limitations, material heterogeneity and inherent scatter, systematic tendencies associated with the investigated parameters became visible and could not be explained by random variation alone. These limitations were mainly related to the restricted sample size, manual production tolerances, the natural variability of the raw material as well as the limited parameter range covered by the test series. As a result, the available data did not allow for a fully predictive mathematical model or a definitive separation of all individual influencing factors. Nevertheless, the comparison of specimen groups and the series based average values provided a framework for assessing the relative magnitude of the observed effects. On this basis, process-oriented recommendations could be derived for clay content, compaction moisture, particle-size distribution and applied compaction pressure.

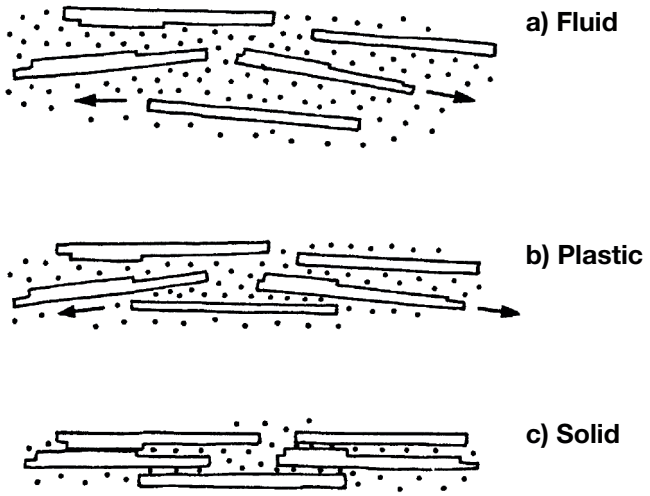

Figure 99: Consistency of clay particles depending on water content. Adapted from Hamer (1975).

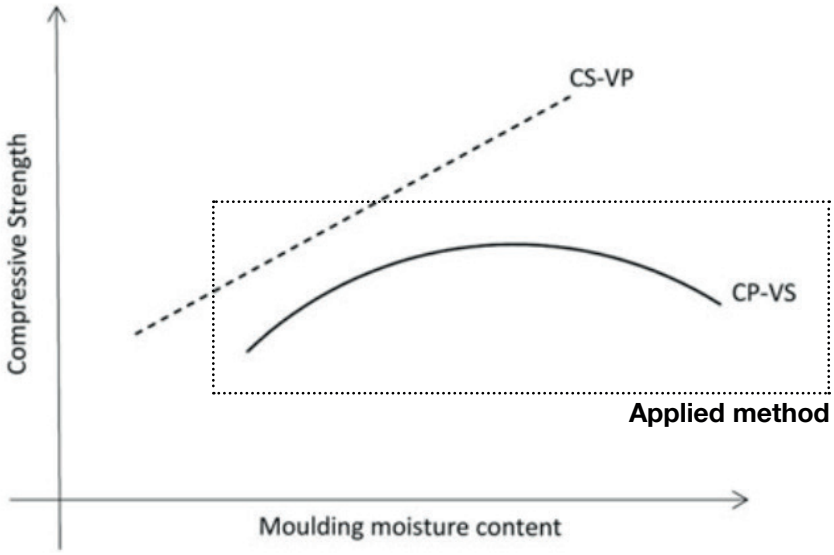

Figure 100: Typical strength–moulding moisture relationships for cement-stabilised CEBs produced using different static compaction methods. Adapted from Reddy (2022).

5.1.9 Interpretation of the experimental findings and methodological limitations

(1) General methodological constraints

The following section interprets the experimental findings in relation to existing literature and revisits the methodological constraints identified above, focusing on how they affect the interpretation and transferability of the findings. Since most formulations were represented by single specimens, the discussion distinguishes between robust patterns observed across the experimental matrix and mechanisms that remain plausible but not directly verified. Attention is therefore given to material scatter, residual moisture variation and the absence of direct microstructural evidence where these factors affect the interpretation of individual results.

(2) Compaction moisture - strength plateau

Because compaction moisture proved to be a critical parameter throughout the experimental series, the observed patterns required closer interpretation. Within the first test series, the data already suggested that strength did not decrease in a purely monotonic manner, but that a plateau-like optimum might be forming across the investigated clay contents. At that stage, however, this pattern could not be considered conclusive, given the experimental limitations. In the extended series for 15 % clay content, this plateau formation became much more distinct. This, in turn, supported the interpretation that the trend was not solely an artefact of scatter. Reddy, (2022) likewise using a constant-pressure, variable-stroke approach, describes a comparable effect in the relationship between moisture content and compressive strength (Fig. 100). In that study, however, the behaviour was demonstrated for cement-stabilized CEBs. Owing to the additional interaction between cement and water, as well as the soil-specific nature of earth materials, these results could not be transferred directly. In order to better understand this behaviour, the mechanisms acting on either side of the optimum, that is, at lower and higher pressing moisture contents, were therefore considered separately.

(3) Lower compaction moisture

On one hand, the binding capacity of clay is activated only through water, in combination with particle movement. Only when the soil becomes plastic at an appropriate moisture content, the clay minerals rearrange into a denser, more parallel structure and thereby develop greater binding capacity (Minke, 2025), (Fig. 99). This means that, if insufficient water is available for activation, even high a clay content remains largely ineffective. This effect was illustrated by the 15 % clay series, in which the maximum strength of 4.09 MPa was reached at 7 % moisture, whereas a reduction of only 1 percentage point in pressing moisture lowered the strength to 3.13 MPa. Given the underlying binding mechanism, this behavior was unlikely to be attributable primarily to measurement error, although experimental scatter may have amplified the apparent steepness of the strength drop.

(4) Higher compaction moisture

At the same time, even a modest increase in moisture content of 2-3 percentage points led to a marked reduction in compressive strength. While the same limitations remained, both the magnitude of the observed strength reduction and its consistency across all 24 measurements made it unlikely that the negative trend could be attributed to these factors alone. One possible explanation was that compaction efficiency decreased at higher water contents, since water itself is essentially incompressible. In the present setup, however, excess water could escape through the mould assembly, and visible water loss increased markedly in the wetter mixes. A direct rebound of the compaction tool, as described by (Schroeder, 2016), could not be observed. At the same time, because the mould was not optimized for efficient drainage, it remained possible that part of the observed effect was attributable to water not being expelled sufficiently during compaction.

Further explanation is given by (Reddy, 2022), who describes that, under static compaction, an increasing share of the applied energy is consumed by drainage rather than by particle rearrangement. Since all specimens were pressed under the same compaction speed of 0.1kN/s resulting in a median press duration of 3:24 min, the drier mixes could possibly use a greater proportion of this period

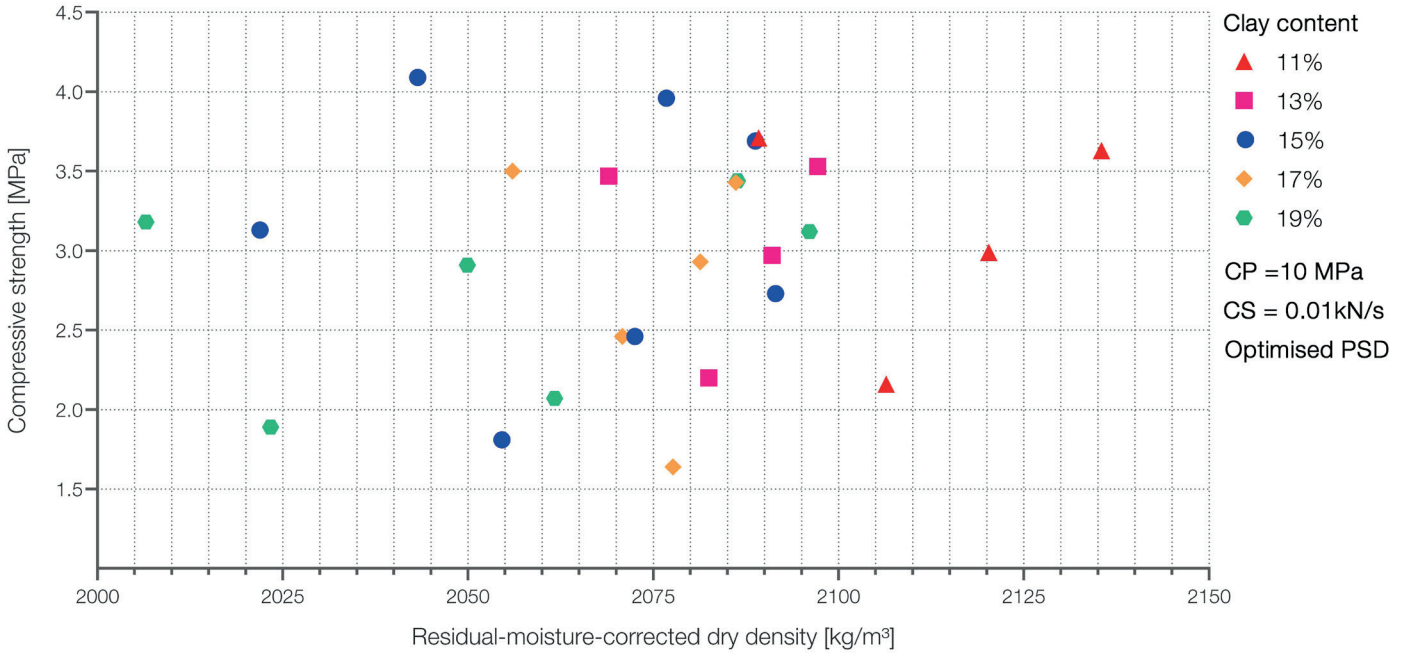

Figure 101: Relationship between compressive strength and residual-moisture-corrected dry density

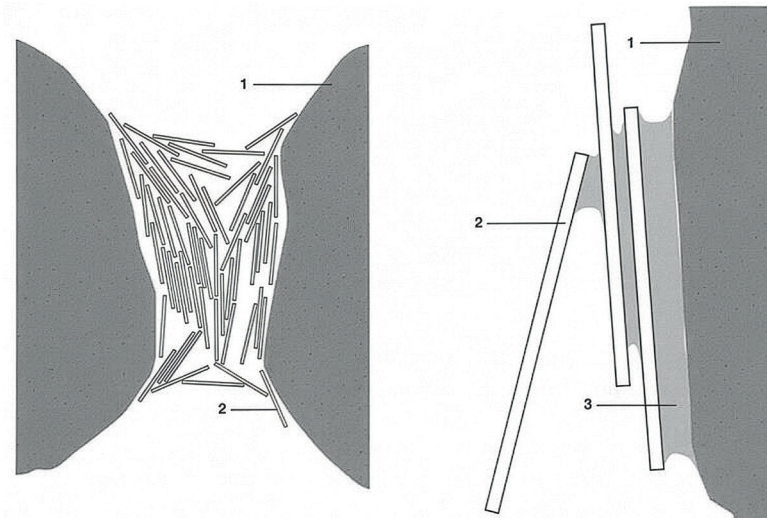

Figure 102: Clay platelets and water forming cohesive bridges between silt and sand grains. 1 sand grain, 2 clay platelet, 3 water. Reproduced from Hebel et al. (2024).

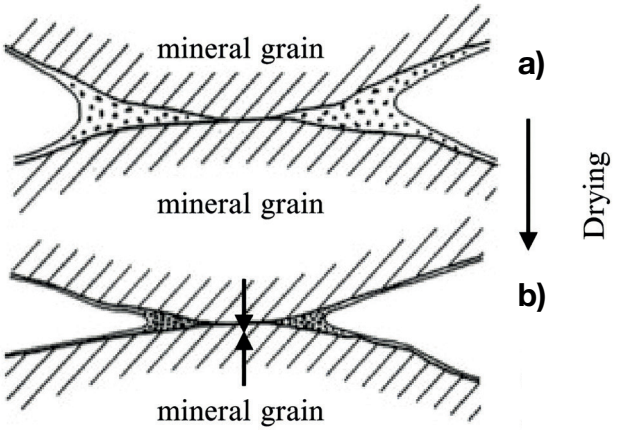

Figure 103: Very fine particles in pore spaces: a) freely suspended in the pore water; b) crowded in pore corners where coarser grains meet, increasing grain-to-grain tension. Adapted from Schroeder (2016).

for actual consolidation of the soil skeleton. It was therefore likely that specimens pressed at higher water contents developed less efficient particle packing and retained more residual voids after unloading and drying, resulting not only in lower dry density but also in reduced compressive strength.

(5) Dry density-strength relationship

If a reduction in dry density were the dominant explanation, a clear correlation between dry density and compressive strength would have been expected. However, when the measured data was plotted in a diagram (Fig. 101), no such trend could be identified. At the same time, this graph had to be interpreted considering the experimental tolerances affecting dry-density determination. The reported values were based on residual moisture corrected densities. Although this correction reached up to 1.41 %, the corresponding specimen volumes could not be corrected for any further shrinkage that might have occurred during complete drying. A specimen retaining residual moisture may therefore still have undergone a slight reduction in volume. This source of error was, however, considered limited, as all mixtures showed a general linear shrinkage well below 2 % and the residual moisture contents remained within a narrow range of 0 to 1,41 %. This was further supported by the 11 % clay-content series, in which all specimens were dried to constant mass and nevertheless exhibited the same general density trend. Uncertainty in the original volume measurement was additionally reduced by taking three calliper measurements each of diameter and height and calculating mean values, although minor errors cannot be excluded.

Given their limited magnitude, these uncertainties were not considered sufficient to alter the overall interpretation, which in any case did not suggest a clear or systematic relationship between the achieved dry density and compressive strength within the observed window. Although compressive strength is highly sensitive to changes in dry density (Reddy, 2022), Minke, (2025) likewise shows that, in earthen construction, maximum dry density does not necessarily coincide with maximum strength. By separating individual process parameters, including clay activation through kneading and different compaction methods, he demonstrates that strength depends also on the way the clay matrix is activated and rearranged during processing. In this context, he also refers to Boemans (1990), who similarly observed that the water content yielding maximum dry density does not generally coincide with maximum compressive strength.

(6) Microstructural interpretation

If the strength reduction could not be explained by dry density and the compaction process alone, microstructural effects also had to be considered. Within the limitations of this study, the reduction in compressive strength above the optimum compaction moisture could therefore possibly be interpreted in relation to the internal organisation of the clay matrix and the granular skeleton. As described in the preceding section, wetter mixtures may still have reached high dry densities because water reduced inter-particle friction and facilitated rearrangement during pressing. In the drier mixtures, however, the applied pressure was less affected by pore-water displacement and could therefore contribute more directly to grain contact and mechanical interlocking.

Schroeder (2016) describes a comparable effect in relation to dry compression, where mechanical action contributes to local particle deformation and breakdown. The comparatively high compaction pressure of 10 MPa was important in this context, as it likely provided sufficient mechanical input for dry compression effects. At the microstructural level, drying may have been relevant for the formation of clay bridges (Fig. 103). According to Schroeder (2016), clay minerals are initially suspended in the pore water and as drying progresses, accumulate in the pore corners where they form cohesive bridges between coarser particles (Fig. 102). These clay bridges provide the matrix cohesion of unstabilised earth but remain weaker than the individual mineral grains themselves. Failure may therefore occur through the rupture of these bridges rather than through the crushing of the grains. Following this interpretation, wetter mixtures may have formed a more continuous clay matrix after drying, whereas drier mixtures, despite potentially retaining a slightly higher pore volume, may have achieve more effective grain-to-grain contact and

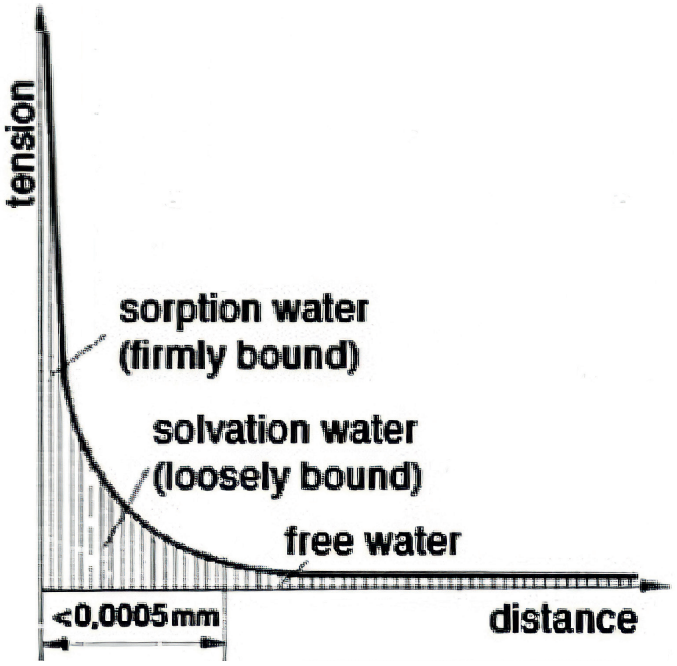

Figure 104: Attractive forces between mineral particles and water as a function of distance. Adapted from Schroeder (2016).

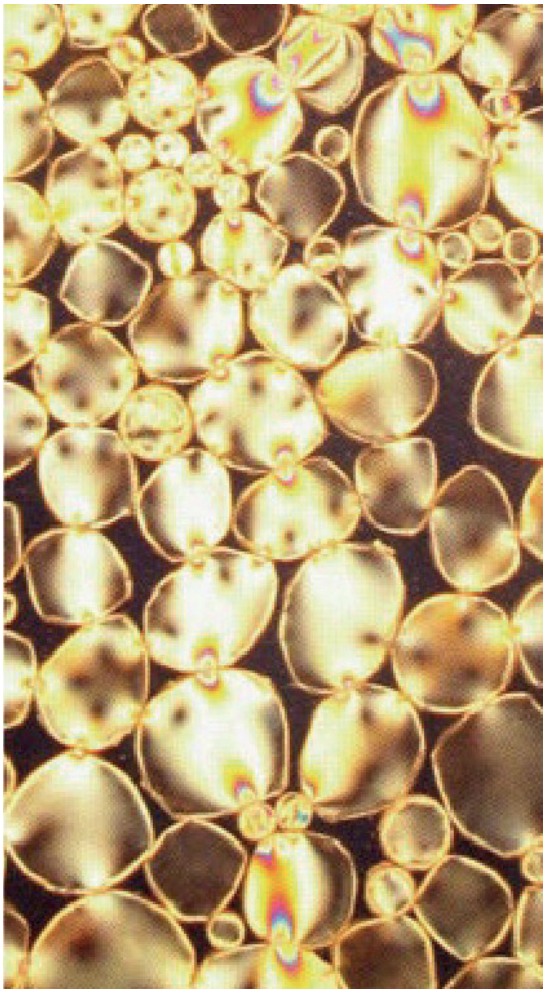

Figure 105: Principle of load transmission in earth building elements through grain-to-grain contact, polarised-light image. Reproduced from Schroeder (2016).

mechanical interlocking during compaction (Fig. 105). This could have explained why similar dry densities did not necessarily result in comparable compressive strengths. Furthermore, the expected improvement in strength through better alignment of laminar clay minerals also appeared limited under the given experimental framework. Minke (2025) emphasises that both water and movement, such as kneading or vibration, are required for the effective orientation of clay platelets and the resulting increase in electrostatic attraction. Since the specimens in this study were produced by static compaction, higher water contents alone were unlikely to produce optimal platelet alignment. This may further explain why additional moisture did not increase strength, despite achieving high dry densities.

(7) Moisture sensitivity at higher clay contents
The reduced moisture sensitivity observed at higher clay contents may be explained by the specific surface area of the particles. Whereas sand has a specific surface area of approximately 23 cm^2/g and silt around 450 cm^2/g, clay minerals such as Montmorillonite can reach values on the order of 1000 m^2/g (Minke, 2025). Schroeder (2016) describes that water directly bound to mineral surfaces may behave almost like a solid phase due to the high surface-tension at the solid-water interface (Fig. 104). Excess water that would remain as free, incompressible pore water in a leaner mixture may therefore be partly absorbed as water films around the clay lamellae in clay-richer mixtures. As a result, the water was less likely to act as disruptive incompressible phase within the granular skeleton. However, this interpretation should be considered against the background of the methodological limitations. A more robust verification would require repeated specimen series under identical conditions, combined with methods capable of assessing porewater distribution, particle arrangement, and interparticle bonding after compaction.

(8) Clay content influence and sensitivity comparison
As shown by the results, the variation in clay content did not produce a substantial effect on compressive strength. Within the shared compaction-moisture window, the highest mean strengths were generally recorded at 15 % clay, except at 10 % moisture content, where the maximum occurred at 11 % clay share. However, the differences between the series remained marginal. For example, the mean compressive strength decreased only slightly from 3.21 MPa at 15 % clay to 3.08 MPa at 17 %. Given these observations, no preferred clay content could be identified with confidence. The apparent convergence at 9 % moisture content should therefore also be interpreted with caution, as it may have reflected coincidental clustering rather than a systematic material response. These findings showed that, within the tested range, clay content was no longer the primary controlling parameter. Its influence was likely reduced because all mixtures already exceeded the minimum clay and moisture thresholds required for cohesion and clay activation. This was consistent with the criteria used to define the experimental range, as the optimum clay content was not determined by quantity alone, but also by shrinkage behaviour, clay mineralogy, and the distribution of fines within the granular skeleton. Further, shrinkage was kept well below 2 % for all mixtures, and the particle-size distribution had already been optimized. Since these factors were therefore largely controlled, clay content itself only showed a marginally independent effect. This interpretation is further supported by Minke (2025), who shows that a higher clay content and the associated increase in binding capacity does not necessarily result in higher compressive strength. Referring to a BRI study, he reports that a silty loam with a binding force of 80 g/cm^2 achieved a compressive strength more than 2,5 times higher than that of a silty clay with a binding force of 390 g/cm^2.

In the reviewed literature, no directly comparable sensitivity analysis was identified that quantifies the relative influence of clay content and compaction moisture on compressive strength within one combined experimental matrix. Both parameters are widely described as fundamental to the performance of compressed earth materials, but their effects are usually investigated in separate test series. This is partly due to their mutual dependency, as outlined previously, but also to the material-specific nature of earthen construction. Since compaction

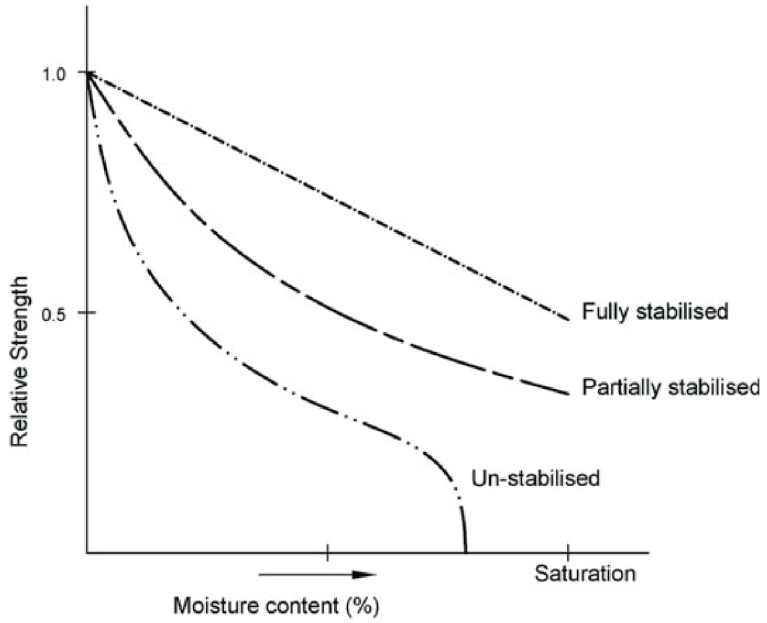

Figure 106: Generic representation of the relationship between compressive strength and internal moisture content during testing of compressed earth products. Reproduced from Reddy (2022).

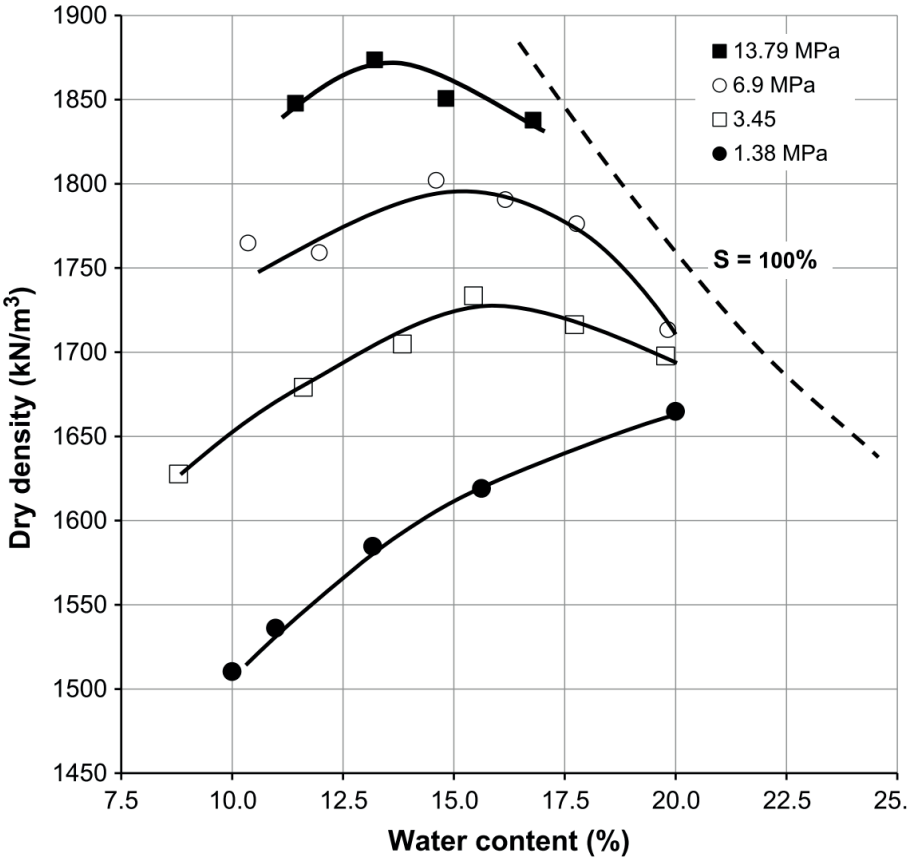

Figure 107: Typical compaction curves for compressed earth products under constant peak stress and variable stroke length. Reproduced from Reddy (2022).

moisture follows an optimum-based response rather than a linear trend, its influence depends on the selected moisture window. The sensitivity analysis presented in this thesis should therefore be understood as a material-specific evaluation within the experimentally investigated processing window. Further, the absolute magnitude of this effect should be interpreted with regards to the underlying experimental uncertainties.

(9) Residual moisture as methodological limitation
Given the central role of compaction moisture in compressive-strength development and clay-mineral bonding, the absence of a clear correlation between residual moisture content and strength reduction required clarification. Since unfired earth materials are hygroscopic, even in a dried state, clay minerals adsorb water molecules from the surrounding air. Under normal indoor conditions, at approximately 20 °C and 40-70 % relative humidity, unstabilised earth materials do not remain completely dry but stabilize at an internal equilibrium moisture content. Schroeder (2016) places this typically around 2-3 % of the component mass, although the exact value depends on the mineralogical composition, particularly the type and amount of clay minerals, and may therefore be higher for more moisture active soils. He also notes that this moisture state is considered part of the material behaviour when determining properties such as thermal conductivity and compressive strength.

While Fig. 106 illustrates the general decline in compressive strength with increasing residual moisture in unstabilised earth blocks, no comparable negative trend was observed in this study. This was likely because the measured residual moisture contents remained well below the equilibrium moisture range reported by Schroeder (2016). Differences from the reported trend may further be related to the re-equilibration time, the specific material composition and the mineralogical characteristics of the investigated soil. Nevertheless, local effects on individual strength measurements cannot be excluded, since the remaining moisture was not uniform across all specimens. This should also be considered when interpreting absolute strength values and is one contributing reason why no definitive preferred clay content was identified. A more controlled assessment would require an extended test series under climate-chamber conditions, with longer conditioning periods and a dedicated measurement of the water absorption capacity associated with the specific mineralogy of the material.

(10) Moisture-dependent density optimum
The observed compaction-moisture-dependent density optimum across all clay contents was consistent with the typical curve formation described by Reddy (2022) for the applied constant peak stress-variable stroke method. Referring to earlier experimental work by Turnbull (1950), Fitzmaurice (1958), and Olivier and Mesbah (1987), Reddy describes a relationship similar to a classical Proctor-type curve (Fig. 107). Despite the scatter and the limited resolution of individual data points, the same pattern was visible across the test series and was consistent with the underlying compaction mechanisms: At lower moisture contents, the added water acts as a separating and lubricating film between particles. As described by Minke (2025), this reduces the mechanical resistance between rough grains and allows denser particle rearrangement under constant pressure. Consequently, dry density increases with rising compaction moisture until an optimum is reached. Beyond this point, additional water no longer primarily supports particle rearrangement. As already discussed in relation to the strength plateau, a larger share of the applied press energy was then likely consumed by pore-water expulsion rather than by further densification of the particle skeleton. If this excess water was not fully displaced under constant pressure, it occupied volume within the compacted specimen and reduced the efficiency of particle packing. After drying, this resulted in a lower dry density, which in turn provided a plausible explanation for the observed decline beyond the moisture optimum.

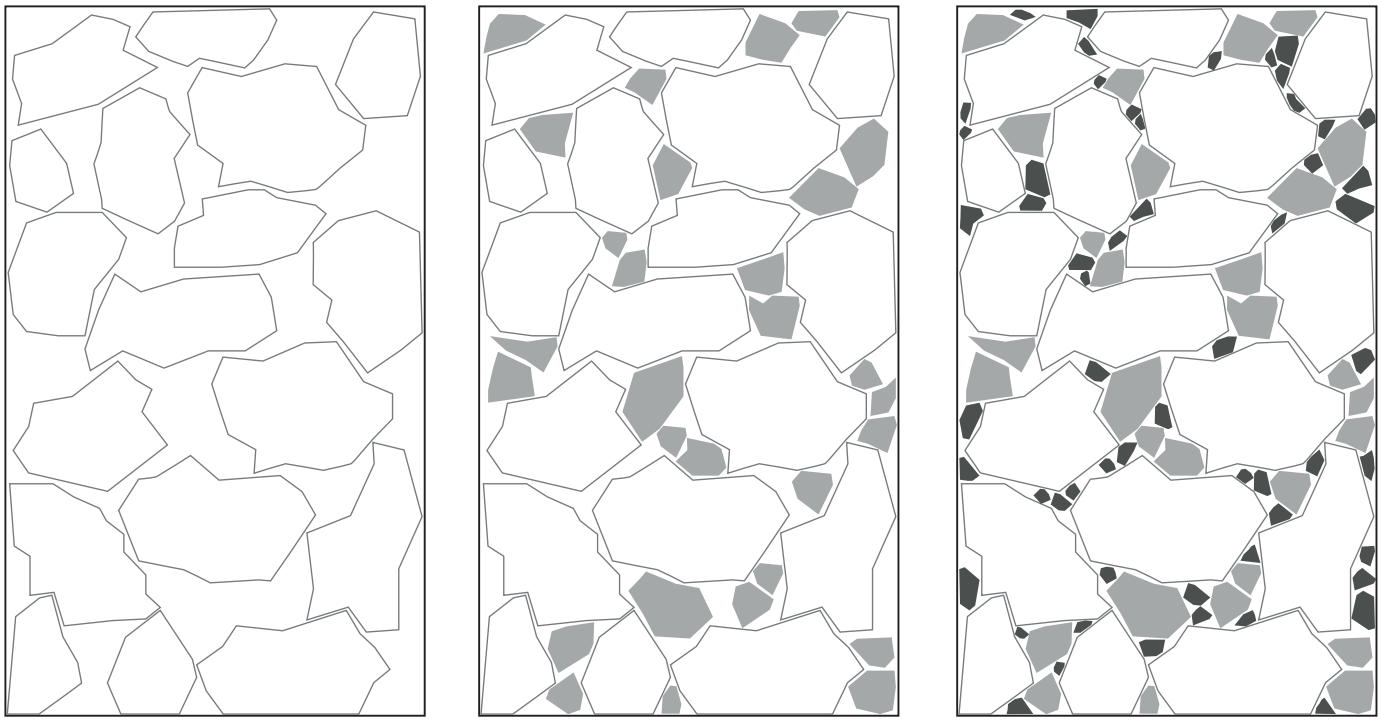

Figure 108: Conceptual representation of particle packing, showing the progressive filling of voids between coarse particles by increasingly finer particles. Adapted from Kumar and Santhanam (2003, Fig. 1), after Andersen and Johansen (1991).

(11) PSD optimisation

The observed 39.2% increase in compressive strength through PSD optimization remained quantitatively constrained by measurement uncertainty. Nevertheless, the result was consistent with the mechanism described by Minke (2025), who explicitly notes that the effect of grain-size optimization on strength is often underestimated. In practical terms, a better-balanced granular skeleton allows finer fractions to occupy voids between coarser grains more effectively (Fig. 108). This reduction in pore volume and improvement in particle contact was also consistent with findings of Schroeder (2016) and Reddy (2022), who both emphasise the role of void structure and compaction quality in the mechanical performance of compressed earth materials. In the present test series, it provided a plausible explanation for why the optimised mixture achieved substantially higher strength under otherwise unchanged clay content, compaction moisture, and press load.

(12) Elevated compaction load

The strength increase achieved by raising the compaction load from 10 to 20 MPa, and further to 50 MPa, could be interpreted through the combined effects of densification, pore-water expulsion, and improved grain contact. Higher static pressure generally increased direct contact between particles and reduced pore volume, which was reflected in the measured dry densities (Reddy, 2022; Schroeder, 2016). The mean dry density thereby increased by 1.9 % from 10 to 20 MPa and by a further 3.9 % at 50 MPa. At first sight, this appeared to contradict the previous observation that, within the moisture-optimisation series, dry density did not correlate directly with compressive strength. However, this earlier finding appeared to apply only within the narrow density range of the moisture-optimisation series in which variations in pore-water behaviour and clay-matrix bonding were more decisive. In the elevated-pressure series, the mixtures were already tested close to their previously identified optimum moisture content. Under these conditions, even a moderate additional reduction in pore volume, combined with stronger grain-to-grain contact and local particle deformation, could have plausibly contributed to a substantial increase in strength. This interpretation is consistent with (Bruno et al., 2015), who shows that consolidation under static pressure depends not only on the applied load, but also on the duration of loading and the ability of excess pore water to drain from the mould. This finding also points to a limitation of the mould design, as longer pressing durations did not lead to a measurable improvement, potentially due to the limited drainage capacity of the setup. A comparable relationship is further described by Reddy (2022) who also observes that the optimum water content decreases with increasing compaction pressure. The present results follow the same tendency: Higher loads enabled substantially higher strength values but also shifted the system towards a lower moisture demand and greater dependence on effective pore-water release. This became particularly clear in the exploratory peak-load test. While the highest compressive strength in the initial series was 7.51 MPa at 15 % clay, 7 % compaction moisture, and 50 MPa press load, compacting the same mixture at 120 MPa increased strength only to 8.46 MPa. Moreover, the specimen pressed at 50 MPa was released from the mould in a dry condition, whereas the 120 MPa specimen still showed a visible water film between the sample and the loading piston. This suggested that, beyond a certain pressure level, further strength gains may be limited less by the applied load itself than by the capacity of the mould system to expel excess pore water. Future tests should therefore not only increase compaction pressure but also optimise the formwork for controlled drainage. Repeated specimens would also be required to reduce the uncertainty associated with the experimental limitations.

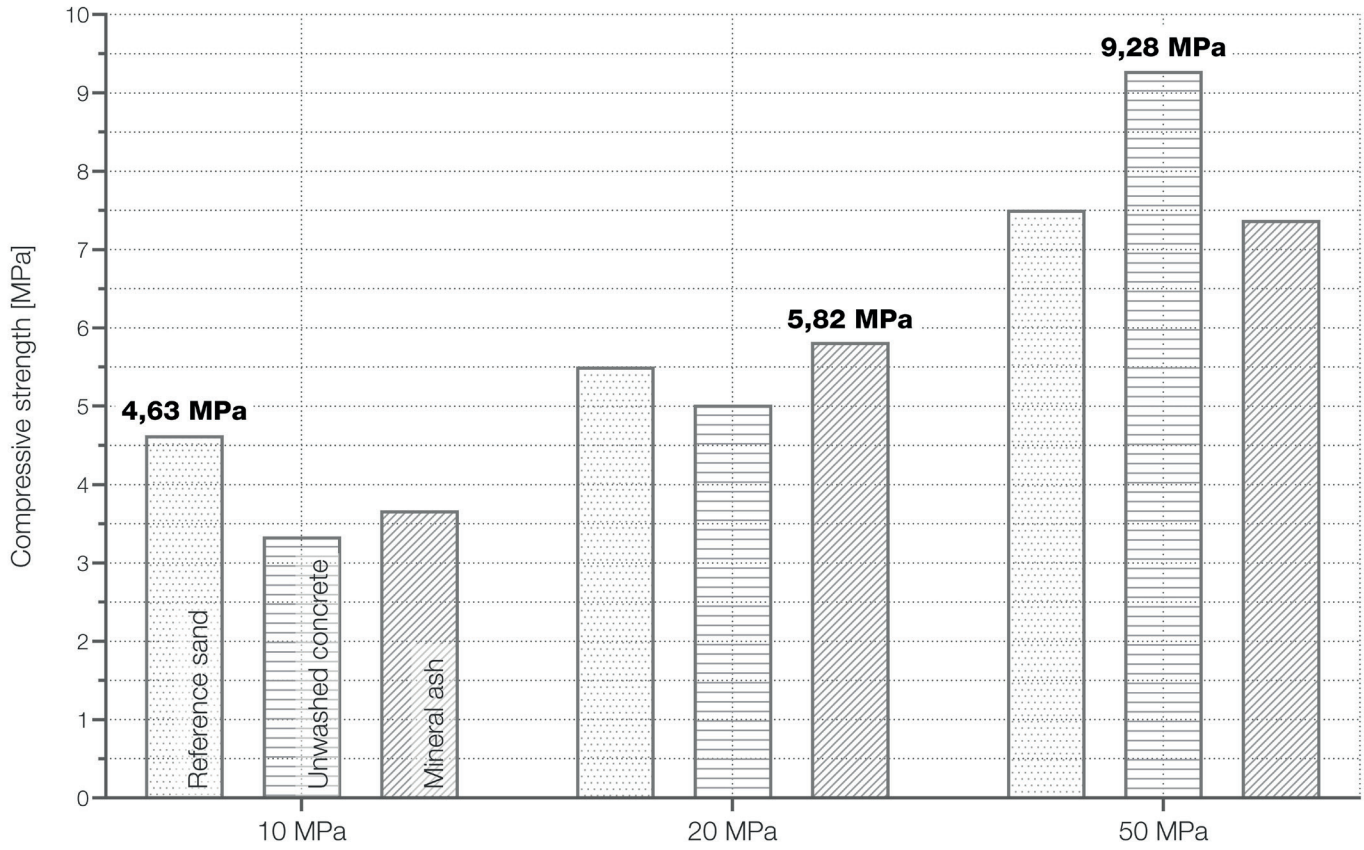

Figure 109: Compressive strength of mixtures with reference sand, unwashed concrete and mineral ash at different compaction pressures; recycled aggregates were tested one percentage point above the corresponding reference moisture.

5.2 Recycled aggregate trials

Following the material-specific processing implications, two previously introduced secondary aggregates, unwashed concrete sand and mineral ash, were examined as an exploratory extension of the experimental series. The aim was not to establish a fully optimized mix design, but to assess their initial processability and performance potential within the developed workflow.

(1) Experimental framework

All preparation, mixing, and compaction procedures were kept consistent with the previously established workflow. The specimens were also tested using the same compression setup, including paper inlay and the conversion from measured failure load to compressive strength followed the identical form-factor correction used for the reference sand series. In addition, the grading curve of each recycled aggregate was adjusted according to the same procedure. The material was dry sieved, and missing grain-size fractions were supplemented using the same aggregate material. However, the initial compaction moisture was set 1 percentage point above the optimum identified for the conventional sand mixture, as both recycled aggregates showed higher water demand during mixing. This behaviour was likely related to differences in material composition and surface characteristics. Accordingly, all recycled-aggregate mixtures were prepared with a clay content of 15 %. For the 10 MPa test series, the specimens were compacted at 9 % moisture content. For the 20 MPa and 50 MPa series, the compaction moisture was set to 8 %.

(2) Observations

At 10 MPa compaction pressure, the reference sand mixture achieved the highest compressive strength, with a peak value of 4.63 MPa. The unwashed concrete sand reached approximately 72 % of this value, while the mineral ash mixture reached about 79 %. At 20 MPa, the highest strength was measured for the mineral ash mixture, with 5.82 MPa. The reference sand reached 94 % of this value, while the unwashed concrete sand reached 86 %. At 50 MPa, the highest compressive strength measured in the entire experimental series was achieved with unwashed concrete sand, reaching 9.28 MPa. This corresponds to a strength increase of 23.5 % compared with the reference sand and 25.7 % compared to the mineral ash mixture at the same compaction pressure.

(3) Interpretation and limitations

Despite the limited number of specimens, expected material scatter, and the absence of empirically determined optimum moisture contents for the alternative aggregates, the exploratory series provided an important indication. The results showed that recycled aggregates can achieve compressive strength levels comparable to, and in some cases higher than, those obtained with the reference sand (Fig. 109). They could therefore represent a realistic alternative to conventional sand, depending on the intended application, available material streams, and production conditions. Further experiments would be required to quantify scatter, optimize the moisture and grading conditions for each recycled aggregate, and evaluate their behaviour in full-scale block specimens, including processing, demoulding, drying, shrinkage, and edge stability. Future work could also investigate whether these recycled aggregates provide additional performance benefits beyond strength, particularly regarding water resistance and durability under wetting drying conditions.

6. Conclusion

6.2.1 Answers to the sub-questions

(1) Which physical, mineralogical, and environmental properties characterise the locally excavated soil and how do they determine its suitability for CEB production?

The investigated material stream, likely originating from marine to estuarine deposits of the Naaldwijk Formation, represents a characteristic regional excavation soil, resulting in a distinct set of physical, mineralogical and environmental properties. It can be described as a fine-grained mineral soil: clay, slightly sandy and highly silty. It is characterised by strong cohesion, high dry strength and pronounced shrinkage.

Mineralogically, quartz, feldspars and muscovite form the non-plastic framework, while vivianite and biogenic fragments support the interpretation of a marine origin. This geological setting is associated with a clay mineral assemblage mainly consisting of illite, smectite, kaolinite and minor chlorite. The observed physical behaviour is therefore largely governed by the binding and swelling capacity of these minerals, particularly the smectites. Their high reactivity and swelling potential argue against cement stabilisation and support the decision to develop unstabilised CEBs. In contrast, the high calcite content may contribute to structural stability while reducing water susceptibility. Low organic contents and contamination levels allowed unrestricted use, while ion chromatography showed that chloride, nitrate, sulphate and total salt contents were below harmful thresholds. The remaining uncertainty concerns possible future sulphate or gypsum formation from pyrite oxidation. However, due to aggregate addition and high compaction, this risk is considered limited, although it should be reassessed depending on the final application and exposure conditions. Overall, the soil is not suitable as an untreated CEB material. Its potential lies in the application as clay-rich binder fraction within a well-graded and shrinkage-controlled composition.

(2) What soil-specific process is required to translate the identified material behaviour into a reproducible CEB mix design and production workflow?

The identified material behaviour requires a dry-processing workflow that converts the plastic, clay-rich raw soil into a controllable fine binder fraction. This involves drying, pre-crushing and pulverization before it is combined with the selected coarser grain fractions. Reproducible production strongly depends on dry binder-aggregate blending followed by staged water addition to achieve a defined compaction moisture. Laboratory trials showed that uncontrolled addition of water and insufficient mixing cause immediate clumping, moisture loss or poor homogenization. For full-scale production, mixing intensity and water dosing must therefore be precisely coordinated to ensure consistent workability. The compaction workflow further showed that quality depends not only on the mix itself, but on the test setup. A closed mould caused high friction and specimen damage, making larger series unreliable. For a reproducible workflow, an openable, high-pressure-resistant and low-friction mould setup is required that allows consistent compaction and reliable demoulding. The required process can be summarized as:

(1) Drying

(2) Pre-crushing

(3) Pulverizing

(4) Binder-aggregate blending

(5) Staged moisture adjustment

(6) Airtight resting and moisture equalisation

(7) Static compaction

(8) Low friction demoulding

(9) Controlled drying

(3) How do material behaviour, composition and production parameters influence the compressive strength of CEB specimens, and which variables are most decisive?

Within the investigated processing window, compressive strength is strongly influenced by the moisture-dependent behaviour of the fine binder fraction throughout mixing, compaction and drying. Water enables clay activation and denser particle rearrangement during pressing, but only within a narrow range. Insufficient moisture limits matrix formation, while excess moisture reduces compaction efficiency through pore-water displacement and may affect individual strength values as residual moisture during testing. This is reflected in the sensitivity analysis, where compaction moisture showed an approximately 5.8 times stronger influence on compressive-strength variation than clay-content adjustment. Under the investigated compaction setup, the most favourable compressive-strength values were generally reached at 7-8 % compaction moisture, while maximum dry density occurred slightly higher, most consistently between 9 % and 10 %. Dry density therefore supports the interpretation of compaction behaviour but does not directly predict peak strength. Within the narrow density range achieved, strength appears to depend more on moisture-controlled microstructural mechanisms.

In terms of composition, compressive strength is influenced by both the binder fraction and the grading of the mineral skeleton. A clay content above approximately 10 % is required to form a cohesive matrix, while the most favourable results were generally obtained around 15 % clay content, corresponding to approximately 34.09% of the processed soil. Since shrinkage remained below 2 % even up to 19 % clay content, higher shares of clay are technically possible but do not appear to provide clear advantage regarding elevated compressive strength. Their main benefit may instead lie in buffering small deviations in compaction moisture. By contrast, particle-size-distribution optimization increased compressive strength by 39.2 %, showing that a well-graded mineral skeleton is a strong compositional lever.

Further, production parameters are decisive for how well the adjusted mix can be compacted. Higher compaction pressure improves particle contact, reduces pore volume and substantially increases compressive strength. Increasing the press load from 10 to 20 MPa raised compressive strength by approximately 29.7 %, while 50 MPa resulted in an increase of approximately 62 %. This confirms elevated compaction pressure as a major optimization potential. At the same time, higher press loads shift the system towards lower moisture demand and require advanced mould drainage and low-friction set-ups.

Within the investigated processing window, precise control of compaction moisture should be prioritised over fine adjustment of clay content, as its influence on compressive strength was approximately six times greater.

At the same time, the results indicate that higher clay contents may partly buffer the sensitivity to compaction moisture when the target value cannot be achieved exactly.

Across the investigated press-load range, compaction-moisture contents of 7-8 % defined the most favourable window for achieving peak compressive strength.

By contrast, peak dry density was generally reached at slightly higher moisture contents, most consistently between 9 % and 10 % across the investigated press loads.

Particle-size-distribution optimisation should be treated as a critical processing step, as it increased compressive strength by nearly 40 % under otherwise identical material and production conditions.

Although 20 MPa, and especially 50 MPa, exceed conventional CEB compaction loads, the results showed that these higher pressures can provide substantial strength gains, particularly for load-bearing masonry applications.

How can locally excavated soils from Rotterdam be translated into reproducible compressed-earth blocks by understanding how material behaviour, composition and production parameters influence their mechanical performance?

6.2.3 Main research synthesis

Locally excavated soils from Rotterdam can be translated into reproducible compressed-earth blocks when they are no longer treated as undefined bulk material for low-value reuse, but as functional material fractions within a circular construction value chain. Clay-rich fine fractions can act as local binders, while suitable sandy or granular fractions may contribute to the mineral skeleton if their grading, cleanliness and mechanical behaviour are compatible. Where the excavated material itself does not provide a sufficient granular skeleton, as in the investigated soil, additional sand or recycled mineral aggregate fractions are required to complete the composition.

This translation requires early suitability assessment to be integrated into existing soil-handling workflows. Subsurface models can provide first indications of expected soil types before excavation, while simple field tests allow rapid on-site screening of plasticity, cohesion, shrinkage tendency, organic indications and granular content. For clay-rich marine or estuarine mineral soils, this must be followed by targeted laboratory assessment of particle-size distribution, shrinkage behaviour, organic content, contamination status, soluble salts and pyrite-related risks. While the Dutch Besluit bodemkwaliteit can provide the environmental basis for verifying safe reuse, CEB production also requires a technical qualification of the material's performance.

Consistent CEB quality is therefore achieved through coordinated control of material behaviour, composition and production parameters rather than through a universal mix recipe. For the investigated soil, this means drying, pre-crushing and pulverising the clay-rich fraction, blending it with a suitable granular skeleton, applying controlled moisture adjustment and defining the compaction window through representative specimen testing. Reproducibility further depends on batch control, as natural variation requires repeated verification. The decisive controls for compressive strength are compaction moisture, grading and compaction pressure, while clay content mainly defines the minimum binder threshold. The final transfer to full-scale blocks should be validated according to the intended application. This includes block geometry, mould filling, pressure distribution, demoulding, drying behaviour, edge stability and water resistance.

Category	Class	Criterion	Required testing	Requirement	Study classification
Application class	AC Ia	Plastered external masonry in exposed truss-framed walls	Immersion, contact, absorption, frost	≤5% mass loss; 24 h absorption; 15 frost cycles	Additional tests required
Application class	AC Ib	Externally plastered masonry exposed to the elements	Immersion, contact, absorption, frost	≤5% mass loss; 3 h absorption; 5 frost cycles	Additional tests required
Application class	AC II	Weather-protected external masonry or internal masonry	Immersion, contact, absorption	≤20% mass loss; 0.5 h absorption	Additional tests required
Application class	AC III	Dry applications, such as ceiling infill or partition walls	None	No additional requirements	Possible within this study
Bulk density class	2.2	Mean dry block density	None	2,010–2,200 kg/m^3	Highest density class possible under all press loads
Compressive strength class	3	Dry compressive strength	Compression test	Mean ≥3.8 N/mm^2; lowest ≥3.0 N/mm^2	Possible at 10 MPa press load
Compressive strength class	4	Dry compressive strength	Compression test	Mean ≥5.0 N/mm^2; lowest ≥4.0 N/mm^2	Possible at 20 MPa press load
Compressive strength class	5	Dry compressive strength	Compression test	Mean ≥6.3 N/mm^2; lowest ≥5.0 N/mm^2	Possible at 50 MPa press load

Figure 110: Reduced overview of the relevant application, density and strength classes for unstabilised compressed earth blocks, adapted from DIN 18945.

7. Outlook

Against the background of the identified limitations and the need to test and validate the results through full-scale prototypes, including extended assessments of water resistance, erosion and frost behaviour, this final chapter provides an architectural application perspective on the study. It attempts to outline which opportunities could emerge from the further development of the material and its process logic, which application fields may already be within reach, and how compressed-earth systems could evolve beyond conventional masonry systems.

7.1 Application potential

In order to relate the experimental findings to possible application fields, DIN 18945 is used again as an indicative benchmark. As discussed earlier, no directly comparable Dutch standard currently defines product requirements for unstabilised compressed-earth blocks. Although DIN 18945 is a German standard and does not address mortar-free or interlocking systems, it remains useful for defining performance requirements for industrially manufactured earthen masonry units bound solely by clay.

7.1.1 Load bearing masonry

To be used as load-bearing masonry, DIN 18945 requires at least strength class 2, corresponding to a mean compressive strength of 2.5 N/mm², with no individual unit below 2.0 N/mm². The experimental results showed that considerably higher strength values were already achieved at 10 MPa compaction pressure. This indicates that load-bearing masonry could potentially be produced even with pressing systems that generate lower compaction pressures than those used in the test series. Beyond compressive strength, the possible field of application also depends on the exposure class of the block. The standard distinguishes between application classes related to moisture and weather resistance. A full classification would therefore require additional tests, particularly erosion testing and, where relevant, frost-resistance testing. Only after these tests wall dimensioning could be carried out with the corresponding moisture-related reduction factors. Nevertheless, reaching strength class 2.0 already indicates plausible protected applications. AC III would cover dry indoor uses, such as internal walls or ceiling infill. AC II could also be considered for heated office or industrial buildings, where the blocks are conventionally laid with mortar and protected from direct weather exposure.

7.1.2 Target application

However, against the background of this thesis, the intended application was defined as:

A low-rise industrial hall with a maximum height of 6m, constructed as self-supporting masonry, protected from direct weather exposure but uninsulated and therefore exposed to outdoor temperature conditions.

For this use case, strength class 4 was initially defined as the target, requiring a mean compressive strength of 5.0 N/mm² and a minimum individual value of 4.0 N/mm². At a compaction pressure of 10 MPa, however, the lowest value within the best-performing series was 3.96 N/mm², while the mean value of 4.4 N/mm² would be also insufficient for classification in strength class 4. Nevertheless, strength class 3 was reached without difficulty at this compaction pressure. In conventional mortared masonry, this would theoretically allow load-bearing buildings up to 13 m in height. For internal walls thicker than 240 mm, the simplified design approach does not define a restriction on wall height. If the compaction pressure is increased to 20 MPa, the application target becomes more realistic. Assuming, as an indicative extrapolation, the same relative scatter observed in the 10 MPa series, the material could reach strength class 4, with a measured minimum value of 4.71 N/mm² and a mean value of 5.24 N/mm². The next step towards validating this application target would therefore be the required moisture- and frost-related performance tests. If the compaction pressure could be increased to 50 MPa, the same assumption suggests that even strength class 5 could be reached. This class is no longer included in the standard simplified design tables, but such strength levels would provide greater flexibility for structural design and increase robustness against local stress

Figure 111: AI-generated visualisation illustrating the possible appearance of standard compressed earth blocks produced from the investigated Rotterdam excavation material.

concentrations and moisture-related reduction factors. Further, the highest dry density class of 2.2 was achieved throughout all compaction pressures. It may be favourable for future water-resistance testing, as a denser pore structure can reduce the rate of water ingress. However, this remains to be confirmed through dedicated tests.

7.1.3 Use of recycled aggregates

The use of recycled mineral aggregates is explicitly addressed in the regulatory framework. Brick chippings from production waste are mentioned as one possible example, provided that the origin and contamination status of the materials are clearly documented. For the recycled aggregates used in this study, however, a distinction must be made between inert mineral fractions and cementitious residues. This is particularly relevant for the unwashed recycled concrete fraction. Since concrete consists of cement, fine crushed particles or dust is likely to contain reactive cementitious phases. If introduced in significant amounts, these fines contribute to hydraulic reactions within the mix and act as an additional chemical binder. While the resulting block could no longer be considered a purely unstabilised earth block and would fall outside the conventional framework for clay-bound earthen masonry, the hydraulic reaction could also open up additional application fields through improved water resistance and compressive strength.

7.2 The standard block

The laboratory results showed that the investigated soil can achieve considerable compressive strength in unstabilised compressed-earth specimens. This makes the standard CEB the most immediate application pathway, as it relies on an established product format, available pressing technology and well-known masonry practice. Rather than suggesting a one-to-one substitution of conventional construction materials, the results point towards a more application-specific allocation of materials: Energy-intensive materials where their performance is indispensable, and standard earth blocks where their local availability, low-temperature production and moisture-regulating properties can be fully exploited. A further practical advantage of smaller standard block formats is their compatibility with higher compaction pressures. Since the required press force depends directly on the loaded area, pressures in the range of 20 MPa, and potentially even 50 MPa, are more realistic to achieve industrially with smaller units than with larger block formats. The required press capacity is not only a technical parameter, but also affects investment cost, machine availability, maintenance requirements and the possible location of production. Smaller formats may therefore provide a feasible starting point for transferring the laboratory findings into practical manufacturing.

Applied to a Rotterdam industrial context, standard CEBs could be used for compartment walls between office, production and storage areas, internal zoning walls, and structural or non-structural infill in framed buildings. Further, low-tech service or storage buildings appear particularly suitable, as they allow monolithic wall approaches and visible material expression without requiring strict visual homogeneity. More exposed applications, such as fully load-bearing outer walls, remain possible development fields. Their feasibility strongly depends on further assessing capillary water uptake, erosion resistance and frost behaviour. At the same time, their application also becomes a matter of architectural detailing, where earth materials must be protected through appropriate plinths, joints, roof edges and façade interfaces. This detailing requirement also reveals the main limitation of the conventional block format: In industrial buildings, small-format masonry has to compete with faster, less labour-intensive and more space-efficient construction systems. Although future resource and carbon pressures may improve its competitiveness, standard CEB construction still depends on specific material knowledge, suitable mortar systems and careful execution. While earth mortar can support reversibility, it also adds more complexity. This reduces the simplicity that is often associated with dry or easily demountable circular systems. It also relates back to the perception problem introduced at the beginning of this thesis. When earth blocks are used in a conventional brick format, they are almost inevitably compared with fired masonry products or associated with pre-industrial building traditions. They may therefore appear as the lower-

Figure 112: Exploratory interlocking earth brick prototypes developed by T. Jorgensen within the framework of extrusion-based manufacturing. Reproduced from Jorgensen (2023).

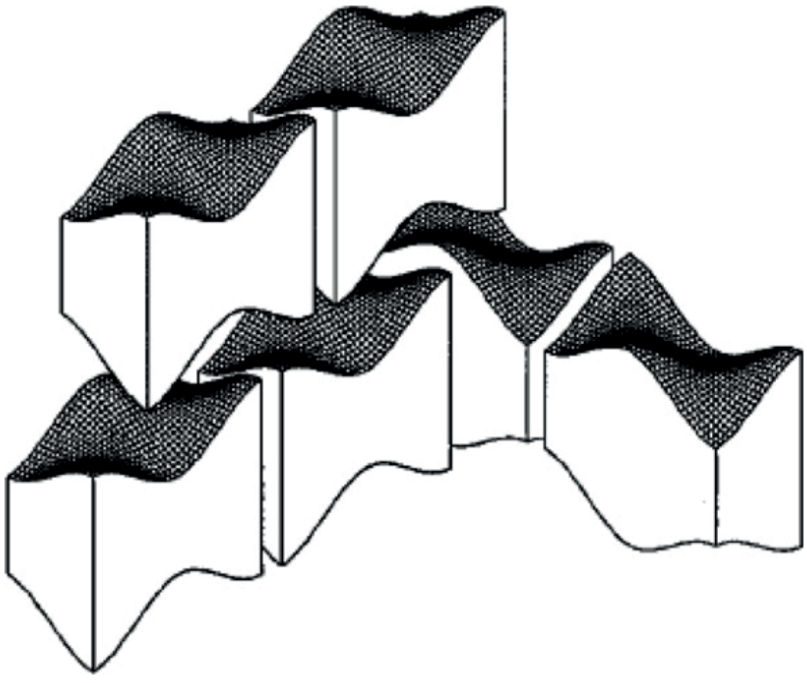

Figure 113: Osteomorphic block assembly illustrating a topological interlocking system. Reproduced from Djumas et al. (2007).

performance alternative, even though their value lies in a different material logic. A next step could therefore be to develop an interlocking principle that follows the material properties of compressed earth. In this sense, the connection could become not only a technical assembly strategy, but also a way to reposition compressed earth architecturally: As a material system with its own structural logic, expression and construction culture.

7.3 The simple interlock

To and disassembly, and improve competitiveness in industrial construction contexts, larger block formats combined with a dry assembly system appear more effective than conventional small-format masonry. A possible direction for such an interlocking mechanism is illustrated by the exploratory design experiments of Jorgensen (2023). The research investigated innovative earth brick geometries intended to facilitate rapid earth construction, although under the specific premise of extrusion-based manufacturing. Within this process, several interlocking prototypes were developed, as shown in (Fig. 112). While these geometries were initially not developed for compressed earth block production, they may still provide a relevant starting point for adapting similar principles to a compression-based production system. Static compaction offers a specific opportunity in this regard, as both the mould base and the pressing plate could theoretically be adapted to produce such an interlocking geometry during compaction. The main challenges are likely to concern force flow, the uniform introduction of load during pressing and the development of a geometry that remains robust despite production tolerances, edge defects or minor dimensional deviations. Even in a dry assembly system, a strategy for levelling and tolerance compensation may be required. As shown in the laboratory tests, damage-free de-moulding becomes a critical challenge, especially under higher compaction pressures. If the pressing plates are adapted, the contact area between soil and tooling would increase further, particularly during release of the piston. For such a system, low-friction surfaces, multi-sided de-moulding and slightly tapered interlocking forms could become central design requirements. For larger block formats, staged layer-by-layer compaction could also be explored. By combining sequential material placement, intermediate surface roughening and repeated static pressing, the process could possibly reduce required press capacity while improving interlayer bonding and production continuity. In this context, a two-piston press could also be considered in order to reduce one-sided density gradients. Thereupon, the question arises whether geometry could also be used as part of the material strategy itself, improving not only assembly and reversibility, but also load transfer, positional stability and failure behaviour of the system.

7.4 The topological interlock

One such approach could be through topological interlocking. Here, the geometry of individual building blocks and the topology of their assembly are configured so each element is mechanically constrained by its surrounding components. This prevents removal through kinematic interdependence rather than using mortars or fasteners (Dyskin et al., 2012). More recent work by (Prasad et al., 2025) shows, that improvements in structural performance can be achieved through geometric optimization alone, without adding extra cementitious materials. Another key advantage of these systems can be their damage tolerance. Cracks are prevented from spreading through the entire structure because they are stopped at the interfaces between individual blocks, confining damage to localized regions. Numerical simulations by Djumas et al. (2007) showed that, in osteomorphic block assemblies (Fig 113.), nearly one quarter of the blocks must fail before the percolation limit is reached and collapse occurs. For earth-based materials, where material variability and comparatively high scatter in mechanical performance are difficult to eliminate, such damage tolerance could offer a particular advantage. The absence of rigid mortar joints also allows relative movement between blocks. This controlled mobility lets structures dissipate dynamic and vibrational energy (Tan et al., 2025). These properties may be particularly relevant for industrial applications, where recurring vibrations and dynamic operational loads can place additional demands on masonry systems. Furthermore, however, these systems are also

Figure 114: Examples of structures that can be assembled from osteomorphic blocks. Reproduced from Dyskin et al. (2012).

Figure 115: AI-assisted visualisation of exploratory osteomorphic-inspired compressed earth blocks based on the investigated excavation material.

inherently reversible. Once external confinement is removed, the structure can be disassembled, and individual blocks can be reused or reconfigured in new assemblies (Fig. 114) (Dyskin et al., 2012). Beyond its technical potential, this reversibility also opens up a new architectural dimension. A visible interlocking logic could become part of the spatial and material expression of CEB blocks, rather than remaining a purely functional connection principle.

7.5 Further research

Future research should build on the established material understanding and move from specimen-level optimisation towards product-level validation. The next step would not be to simply develop a more complex block geometry, but to test how the selected mix performs in full-scale prototypes, particularly regarding capillary water uptake, erosion resistance, frost behaviour, shrinkage, dimensional tolerances and long-term durability. In parallel, the production process would need to be scaled and refined through suitable high-compaction systems and improved moulding and demoulding strategies. Only on this basis interlocking or topological geometries can be developed in a meaningful way: Not as a transferred brick or Lego-like principle, but as a product logic that responds to the actual behaviour of compressed earth. This could include the further exploration of block principles inspired by osteomorphic systems, as well as suitable manufacturing methods for producing such geometries in compressed earth. Future research should also examine material-specific durability strategies, including natural admixtures or surface treatments such as linseed oil, and potentially through localised thermal surface treatment during pressing to harden or densify only the outer surface of the block. However, such approaches would only be meaningful if it required substantially less energy than conventional firing and remained compatible with the low-energy, material-specific principle. Future research should therefore connect durability testing, low-energy process engineering, geometry development and architectural application.

Figure 116: AI-assisted visualisation, illustrating the possible appearance of compressed earth blocks produced from Rotterdam-Delft excavation soil in a wall assembly.

8. Reflection

For me, one of the main outcomes of this work was that it made the development of a compressed earth block within a local context much more tangible. Already during the literature review, I found extremely valuable references from India and southern Germany, which showed a very deep understanding of earth construction. At the same time, it was not always clear to me how these findings could be translated into the actual development of one specific block from one particular soil. More importantly, I wanted to understand which decisions actually matter in this translation: What improves the block, what only changes it slightly, which parameters have the greatest influence on its structural performance, and which practical problems only appear when the knowledge is translated into practice.

This was partly because the literature often works on very different levels: Some sources discuss earth construction in a broad and general way, while others go very deeply into specific material mechanisms, tests or local practices. Through the thesis, it became much more clear why this is the case. The local origin of the soil, its individual composition and its specific behaviour make these blocks so difficult to standardise. For me, this is also where the research gap became most visible. The challenge was therefore not only to generate new findings, but to translate existing knowledge from geotechnics, policy context, material testing, mechanical engineering and architectural requirements into a reproducible process.

To me, this reflects, what Building Technology is about: Working within the tension of different disciplines. The thesis showed me once again that new solutions and approaches do not always mean inventing everything from scratch. At the beginning, I sometimes asked myself what I could still contribute to a building material that has already been used for thousands of years. However, I realised once more, that there are always new perspectives that can emerge from different disciplines, backgrounds and ways of thinking. What I found motivating is that, even after this intense time, the topic never felt completely closed. Instead, I could now identify more clearly which questions remain open and where further approaches could still be developed.

On a broader level, I think it is always valuable to question how we can use our resources in a more careful, intelligent and responsible way. The geopolitical and climate-related challenges of recent years should make this clear. Since the Netherlands does not have a strong contemporary tradition of earth construction, I would be glad if this thesis contributed, even within my own small sphere of influence, to making a few more people interested in the topic or motivated to invest further time in it. At the same time, the work also made the limitations of earth construction very clear. It is not a universal solution, and it should not be treated as one. Nevertheless, this thesis has hopefully shown how much potential still lies in excavation soil as a material stream that is often underused or not yet considered at building-product level.

It is also important to me, that the potential of compressed earth could also lie in the possibility of moving beyond the image of conventional masonry. Architecturally, earth already has a strong quality, which can be seen in the appreciation of rammed earth walls. Through new shapes, interlocking principles and application-specific geometries, CEBs could become less of a repeated traditional technique and more of a contemporary product that follows its own material logic. I would have liked to develop this direction further within the thesis, beyond presenting it mainly as an outlook. However, the laboratory work also showed me how demanding and time-intensive this step really is. Before moving towards a more developed product, the material first has to be understood in detail - and for the investigated material, I would now allow myself to say that this foundation has been built.

9. References

Aboziada, Y., Abdelrahman, M., AbdelRahman, B., & Galal, K. (2025). Behavior of Dry-Stacked Interlocking Masonry: State of the Art. Lecture Notes in Civil Engineering, 681 LNCE, 83–95. https://doi.org/10.1007/978-3-031-96763-4-7

AlJaber, A., Martinez-Vazquez, P., & Baniotopoulos, C. (2024). Developing Critical Success Factors for Implementing Circular Economy in Building Construction Projects. Buildings, 14(8). https://doi.org/10.3390/buildings14082319

André Weijenberg, I. B. F. van K. K. de V. (2012). Rotterdamse grondstromen eng.

Attri, G. K., Gupta, R. C., & Shrivastava, S. (2022). Comparative Environmental Impacts of Recycled Concrete Aggregate and Manufactured Sand Production. Process Integration and Optimization for Sustainability, 6(3), 737–749. https://doi.org/10.1007/s41660-022-00244-4

Augarde, C. E., Beckett, C. T. S., Smith, J. C., & Corbin, A. J. (2016). Challenges in treating earthen construction materials as unsaturated soils. https://doi.org/10.1051/03002

Batjes, N. H., & Van Oostrum, A. J. M. (2023). World Soil Information Service (WoSIS)— Procedures for standardizing soil analytical method descriptions. https://doi.org/10.17027/isric-1dq0-1m83

Bauwesen, D.-N. (2024). DIN 18945, Lehmsteine –Anforderungen, Prüfung und Kennzeichnung. www.din.de

Borkovec, M., De Paris, W., & Peikert, R. (1994). THE FRACTAL DIMENSION OF THE APOLLONIAN SPHERE PACKING. In Appeared in Fractals (Vol. 2, Number 4).

Bruno, A. W., Gallipoli, D., Perlot, C., Mendes, J., & Salmon, N. (2015). First International Conference on Bio-based Building Materials MECHANICAL PROPERTIES OF UNSTABILIZED EARTH COMPRESSED AT HIGH PRESSURES.

Cristóbal, J., Foster, G., Caro, D., Yunta, F., Manfredi, S., & Tonini, D. (2024). Management of excavated soil and dredging spoil waste from construction and demolition within the EU: Practices, impacts and perspectives. Science of the Total Environment, 944. https://doi.org/10.1016/j.scitotenv.2024.173859

Dan Gavriletea, M. (2017). Environmental impacts of sand exploitation. Analysis of sand market. In Sustainability (Switzerland) (Vol. 9, Number 7). MDPI. https://doi.org/10.3390/su9071118

Diko-Makia, L., & Ligege, R. (2020). Composition and technological properties of clays for structural ceramics in limpopo (South Africa). Minerals, 10(8), 1–11. https://doi.org/10.3390/min10080700

Djumas, L., Molotnikov, A., Simon, G. P., & Estrin, Y. (2016). Enhanced Mechanical Performance of Bio-Inspired Hybrid Structures Utilising Topological Interlocking Geometry. Scientific Reports, 6. https://doi.org/10.1038/srep26706

Drozdz, M., Appert, M., & Harris, A. (2018). High-Rise Urbanism in Contemporary Europe. In BUILT ENVIRONMENT (Vol. 43).

Dyskin, A. V., Pasternak, E., & Estrin, Y. (2012). Mortarless structures based on topological interlocking. Frontiers of Structural and Civil Engineering, 6(2), 188–197. https://doi.org/10.1007/s11709-012-0156-8

ETH Zürich. (2025). Nachhaltig bauen Wie sich die ETH Zürich für eine klimafreundliche Architektur engagiert.

European Commission. (2020). A new Circular Economy Action Plan. https://www.un.org/sustainabledevelopment/sustainable-consumption-production/

European Commission. (2021). EN. https://www.eea.europa.eu/data-and-maps/dashboards/land-take-statistics#tab-based-on-data

Finamore, M., & Oltean-Dumbrava, C. (2024). Circular economy in construction - findings from a literature review. In Heliyon (Vol. 10, Number 15). Elsevier Ltd. https://doi.org/10.1016/j.heliyon.2024.e34647

García, C., Caro, J., Gallo, G., & Tonini, F. (2024). Techno-economic and environmental assessment of construction and demolition waste management in the European Union Status quo and prospective potential. https://doi.org/10.2760/721895

Gemeente Rotterdam. (2019). Hoogbouwvisie-2019.

Gharbage, I., Benmahiddine, F., & Sebaibi, N. (2025). Mechanical, thermal and hydric properties of compressed earth blocks: A review. In Journal of Building Engineering (Vol. 104). Elsevier Ltd. https://doi.org/10.1016/j.jobe.2025.112387

Goncikowski, M. (2020). TYPOLOGY OF ARCHITECTURE OF INDUSTRIAL BUILDINGS AT THE TURN OF THE 20 TH AND 21ST CENTURY. Space&FORM, 2020(43), 41–54. https://doi.org/10.21005/pif.2020.43.B-02

Griffioen, J., Klaver, G., & Westerhoff, W. E. (2016). The mineralogy of suspended matter, fresh and Cenozoic sediments in the fluvio-deltaic Rhine-Meuse-Scheldt-Ems area, the Netherlands: An overview and review. In Geologie en Mijnbouw/Netherlands Journal of Geosciences (Vol. 95, Number 1, pp. 23–107). Cambridge University Press. https://doi.org/10.1017/njg.2015.32

Hale, S. E., Roque, A. J., Okkenhaug, G., Sørmo, E., Lenoir, T., Carlsson, C., Kupryianchyk, D., Flyhammar, P., & Žlender, B. (2021). The reuse of excavated soils from construction and demolition projects: Limitations and possibilities. Sustainability (Switzerland), 13(11). https://doi.org/10.3390/su13116083

Hanaor, D. A. H. (Ed.). (2025). Sustainable Materials for the Built Environment (Vol. 352). Springer Nature Switzerland. https://doi.org/10.1007/978-3-031-97818-0

Hongu, H., Yoshiasa, A., Kitahara, G., Miyano, Y., Han, K., Momma, K., Miyawaki, R., Tokuda, M., & Sugiyama, K. (2021). Crystal structure refinement and crystal chemistry of parasymplesite and vivianite. Journal of Mineralogical and Petrological Sciences, 116(4), 183–192. https://doi.org/10.2465/JMPS.200904

Jansen, M., Brandellero, A., & van Houwelingen, R. (2021). Port–city transition: Past and emerging socio–spatial imaginaries and uses in Rotterdam's makers district. Urban Planning, 6(3), 166–180. https://doi.org/10.17645/up.v6i3.4253

Jorgensen, T., & Lightfoot, S. (2024). PLEA 2024: (RE)THINKING RESILIENCE The book of proceedings PLEA 2024: (RE)THINKING RESILIENCE Proceedings of 37 th PLEA Conference, Sustainable Architecture and Urban Design Digital Toolmaking for Earth Building Components The use of low-cost extruder and 3D printing to develop new fabrication approaches for cob and light earth bricks. http://www.oficyna.pwr.edu.pl

Kumar, S., & Santhanam, M. (2003). Particle packing theories and their application in concrete mixture proportioning: A review.

Masuda, K. (2020). Frictional properties of anorthite (feldspar): implications for the lower boundary of the seismogenic zone. Earth, Planets and Space, 72(1). https://doi.org/10.1186/s40623-020-01271-6

McGowan, G., & Prangnell, J. (2006). The significance of vivianite in archaeological settings. Geoarchaeology, 21(1), 93–111. https://doi.org/10.1002/gea.20090

Ministerie van Infrastructuur en Waterstaat. (2023). Afvalverwerking in Nederland, gegevens 2021 Datum februari 2023. www.afvalcirculair.nl

Minixhofer, P., Scharf, B., Hafner, S., Weiss, O., Henöckl, C., Greiner, M., Room, T., & Stangl, R. (2022). Towards the Circular Soil Concept: Optimization of Engineered Soils for Green Infrastructure Application. Sustainability (Switzerland), 14(2). https://doi.org/10.3390/su14020905

Minke, G. (2025). Birkhäuser Basel Design and Technology of a Sustainable Architecture Fifth and revised edition.

Mishra, A., Das, S. K., & Reddy, K. R. (2023). Life cycle assessment of processing alternate sands for sustainable construction: Coal mine overburden sand versus manufactured sand. Journal of Building Engineering, 75. https://doi.org/10.1016/j.jobe.2023.107042

Molotnikov, A., Estrin, Y., Dyskin, A. V., Pasternak, E., & Kanel-Belov, A. J. (2007). Percolation mechanism of failure of a planar assembly of interlocked osteomorphic elements. Engineering Fracture Mechanics, 74(8), 1222–1232. https://doi.org/10.1016/J.ENGFRACMECH.2006.07.012

Olaf Merk, & Theo Notteboom. (2013). The Competitiveness of Global Port-Cities: The Case of Rotterdam/Amsterdam, the Netherlands: 2013/08 (OECD Regional Development Working Papers). https://doi.org/10.1787/5k46pghnvdvj-en

Pelicaen, E., Novais Passarelli, R., & Knapen, E. (2023). Challenges to upscale earth block masonry in Western Europe from a life cycle perspective. IOP Conference Series: Earth and Environmental Science, 1196(1). https://doi.org/10.1088/1755-1315/1196/1/012062

Port of Rotterdam. (2019). Portvision Rotterdam.

Prasad, H. G. V., Nirmala, D. B., Keshava, M., & Jagadish, K. S. (2025). Behavior of interlocking compressed stabilized earth masonry under flexure and shear. Innovative Infrastructure Solutions, 10(10). https://doi.org/10.1007/s41062-025-02262-w

Reddy, B. V. V. (2022). Compressed Earth Block & Rammed earth structures. https://link.springer.com/bookseries/13593

Ritzema, H. P., & Stuyt, L. C. P. M. (2015). Land drainage strategies to cope with climate change in the Netherlands. Acta Agriculturae Scandinavica Section B: Soil and Plant Science, 65, 80–92. https://doi.org/10.1080/09064710.2014.994557

Röhlen, U., & Ziegert, C. (2020). Lehmbau-Praxis.

Schroeder, H. (2016). Sustainable Building with Earth.

Schützenhofer, S., Kovacic, I., Rechberger, H., & Mack, S. (2022). Improvement of Environmental Sustainability and Circular Economy through Construction Waste Management for Material Reuse. Sustainability (Switzerland), 14(17). https://doi.org/10.3390/su141711087

Shiferaw, A. T. (2025). Carbon Conscious Construction: Evaluating Compressed Stabilized Earth Blocks. Buildings, 15(23), 4362. https://doi.org/10.3390/buildings15234362

Tan, S. K., Ma, H., & Ma, Q. (2025a). A Review of Interlocking Earth Block: Material Modification, Block Structural System, and Seismic Performance. In Iranian Journal of Science and Technology - Transactions of Civil Engineering (Vol. 49, Number 4, pp. 3275–3291). Springer Science and Business Media Deutschland GmbH. https://doi.org/10.1007/s40996-024-01704-2

Tan, S. K., Ma, H., & Ma, Q. (2025b). A Review of Interlocking Earth Block: Material Modification, Block Structural System, and Seismic Performance. In Iranian Journal of Science and Technology - Transactions of Civil Engineering (Vol. 49, Number 4, pp. 3275–3291). Springer Science and Business Media Deutschland GmbH. https://doi.org/10.1007/s40996-024-01704-2

Tan, S. K., Ma, H., & Ma, Q. (2025c). A Review of Interlocking Earth Block: Material Modification, Block Structural System, and Seismic Performance. In Iranian Journal of Science and Technology - Transactions of Civil Engineering (Vol. 49, Number 4, pp. 3275–3291). Springer Science and Business Media Deutschland GmbH. https://doi.org/10.1007/s40996-024-01704-2

Tasellari, A., & Kaiku, E. (2012). Conference of Civil Engineering (Vol. 2012).

Tavoosi Gazkoh, M., Lin, X., & Zhou, A. (2024). Advancing Topological Interlocking Structures: Recent Developments, Applications, and Challenges in Civil Engineering. In International Journal of Concrete Structures and Materials (Vol. 18, Number 1). Springer Nature Korea. https://doi.org/10.1186/s40069-024-00735-3

van der Veer. (2006). 2 Concise description of the soils in the Netherlands. www.esri.com

Van Eijk, F., Breukelman, H., Keesman, B., & Prummel Joan. (2022). Waste Management as a catalyst to a Circular Economy 3 Content.

van Es, H. (2017). A New Definition of Soil. CSA News, 62(10), 20–21. https://doi.org/10.2134/csa2017.62.1016

Waseda, Y., Matsubara, E., & Shinoda, K. (2011). X-Ray Diffraction Crystallography X-Ray Diffraction Crystallography Introduction, Examples and Solved Problems.

Wiehle, P., Baier, J., & Thiele, M. (2025). Structural Design of Earth Masonry in Accordance with Eurocode 6 – Considering Moisture Content and E / f k Ratio . Ce/Papers, 8(1), 9–21. https://doi.org/10.1002/cepa.3287

Yin, X., Guo, C., Sun, B., Chen, H., Wang, H., & Li, A. (2023). The State of the Art in Digital Construction of Clay Buildings: Reviews of Existing Practices and Recommendations for Future Development. In Buildings (Vol. 13, Number 9). Multidisciplinary Digital Publishing Institute (MDPI). https://doi.org/10.3390/buildings13092381

Supervised by
Dr. ir. Telesilla Bristogianni
Dr. Ing. Marcel Bilow